The role of caseinolytic mitochondrial matrix peptidase proteolytic subunit (CLPP) in regulation of mitochondrial ribosome biogenesis in mammals

Inaugural–Dissertation

zur

Erlangung des Doktorgrades

der Mathematisch-Naturwissenschaftlichen Fakultät

der Universität zu Köln

vorgelegt von

Priyanka Maiti

aus Kolkata, India

Köln 2015

Berichterstatter: **Prof. Dr. Aleksandra Trifunovic**

Prof. Dr. Thomas Langer

Tag der mündlichen Prüfung: 15.06.2015

To My Beloved Family and Friends…

Table of Contents

List of Figures

List of Tables

Abbreviations

3’	three prime end of DNA sequence
5’	five prime end of DNA sequence
2D	two-dimensional
A	adenosine
ADP	adenosine diphosphate
ATP	adenosine triphosphate
BAT	brown adipose tissue
bp	base pairs
BN	blue native
C	cytosine
cDNA	complementary DNA
Ci	Curie
Cre	bacteriophage P1 derived site-specific recombinase
COX	cytochrome c oxidase
CLPP	caseinolytic mitochondrial matrix peptidase proteolytic subunit
Cyt	cytochorome
Da	Dalton
DAPI	4,6-diamidino-2-phenylindole
ddH_2O	double distilled water
DNA	desoxyribonucleic acid
dNTP	desoxyribonucleotide-triphosphate
ECL	enhanced chemoluminiscence
EDTA	ethylendiamine tetraacetate
EF-$G1_{mt}$	mitochondrial elongation factor G1
EGTA	ethylene glycol tetraacetic acid
ERAL1	Era G-protein like 1
EtBr	ethidium bromide
ETC	Electron transport chain
ETS	Electron transfer system
EtOH	ethanol

g	gram
G	guanine
H_2O_2	hydrogen peroxide
HCl	hydrochloric acid
HEPES	N-2-hydroxyethylpiperazine-N-2-ethansulfonic acid
i.e.	*id est*
IMM	inner mitochondrial membrane
IMS	inter membrane space
k	kilo
KCl	potassium chloride
KOH	potassium hydroxide
l	liter
L	loxP flanked
LSU	large subunit
m	milli
M	molar
MAD	mitochondria associated degradation
$MgCl_2$	magnesium chloride
mtDNA	mitochondrial DNA
mRNA	messenger RNA
MQC	mitochondrial quality control
MTERF	mitochondrial transcription termination factor
MTS	mitochondrial targeted sequence
nDNA	nuclear DNA
NLS	nuclear localization signal
NaCl	sodium chloride
NaF	sodium fluoride
NAH_2PO_4	monosodium phosphate
$NaHCO_3$	sodium bicarbonate
NaOH	sodium hydroxide
OMM	outer mitochondrial membrane
OXPHOS	oxidative phosphorylation
PAGE	polyacrylamide gel electrophoresis

PBS	phosphate buffered saline
PCR	polymerase chain reaction
PINK1	PTEN-induced putative kinase 1
P_i	Phosphates
RC	respiratory chain
RNA	ribonucleic acid
rRNA	ribosomal RNA
RNase	ribonuclease
ROS	reactiove oxygen species
Rpm	revolutions per minute
RT	room temperature
rtPCR	reverse transcription polymerase chain reaction
RQ	respiratory quotient
SDS	sodiumdodecylsulfate
SEM	standard error of the mean
SSU	small subunit
TBE	tris-borate-EDTA buffer
TE	tris-EDTA buffer
TFAM	mitochondrial transcription factor A
TFB1M	mitochondrial transcription factor B1
TFB2M	mitochondrial transcription factor B2
Tris	2-amino-2-(hydroxymethyl)-1,3-propandiole
tRNA	transfer RNA
TWEEN	polyoxethylene-sorbitan-monolaureate
U	units
UPR_{mt}	mitochondrial unfolded protein response
V	volt
v/v	volume per volume
w/v	weight per volume
β-me	β-mercaptoethanol
µl	microliter

Abstract

CLPP (caseinolytic mitochondrial matrix peptidase proteolytic subunit) is a highly conserved serine protease. Molecular and structural studies in *E. coli* and other prokaryotes have revealed CLPP specific substrates and the mechanisms underlying their identification and subsequent degradation. These studies showed that ClpXP is involved in DNA damage repair, stationary-phase gene expression, and ssrA-mediated protein quality control. Similarly, diverse roles for the eukaryotic CLPP have been suggested. In the filamentous fungus *Podospora anserine Clpp* depletion promotes longevity. In *Caenorhabditis elegans* it has been demonstrated that CLPP have a central role in mediating the UPR^{mt} signals. Loss of function CLPP mutations in humans cause Perrault syndrome that results in ovarian failure and sensorineural hearing loss accompanied with shorter stature. Despite this we still have a very limited knowledge about the functional role of eukaryotic CLPP, its specific substrates and underlying molecular mechanism.

In order to decipher the *in vivo* role of CLPP in mammals we have developed a CLPP deficient mouse model ($Clpp^{-/-}$). Interestingly, only about half of *Clpp* knockout mice according to Mendelian proportion (12,5%) are born from intercrossing of *Clpp*+/- mice. These mice are infertile and born ~ 30% smaller than littermates. CLPP deficient mice faithfully replicate the phenotypes observed in human patients. On the molecular level CLPP deficiency leads to an early specific decrease in Complex I activity, followed by a decrease in Complex IV activity later in life. Furthermore, we observed a decrease in mitochondrial translation, which is compensated for by upregulation of mitochondrial transcription. This suggests a direct or indirect role of CLPP in the process of mitochondrial protein synthesis. Gradient sedimentation analysis demonstrates an increase in the steady state levels of small ribosomal subunits, while large ribosomal subunits and monosomes are present in almost normal levels. We also observed an impairment of 12S rRNA assembly into monosomes leading to lower loading of mt-mRNAs. This indicates complications in the function of monosomes. Search for CLPXP substrates and interactors revealed two candidates that are likely to be involved in this process. We show that ERAL1 is one of the substrates of CLPP that is likely causing defective 12S rRNA assembly into the small ribosomal subunit. Additionally, p32, a CLPP interactor is permanently bound to the mitoribosomes. We believe that through

interaction with CLPXP, these proteins are involved in resolution of stalled ribosomes. We are currently working further on elucidating the molecular mechanism underlying impaired mitochondrial translation.

Zusammenfassung

Die Casein abbauende Peptidase P (*caseinolytic mitochondrial matrix peptidase proteolytic subunit*, CLPP) ist eine hoch konservierte Serinprotease. Molekulare und strukturelle Untersuchungen in *E. coli* und anderen Prokaryoten haben CLPP-spezifische Substrate identifiziert und die zugrunde liegenden Mechanismen der nachfolgenden Degradierung dieser Substrate aufgezeigt. Diesen Studien zufolge ist ClpXP bei der Reparatur von DNA-Schäden, in der Genexpression der stationären Phase sowie in der ssrA-vermittelten Proteinqualitätskontrolle involviert. In ähnlicher Weise wurden verschiedene Rollen für die eukaryotische CLPP postuliert. Im filamentösen Pilz *Podospora anserine* förderte die Depletion von CLPP die Langlebigkeit. In *Caenorhabditis elegans* wurde gezeigt, dass CLPP eine zentrale Rolle in der Vermittlung der Signale in der mitochondrialen ungefalteten Proteinantwort (*mitochondrial unfolded protein response*, UPR^{mt}) spielt. Mutationen, die den Verlust der Funktion von CLPP zur Folge haben, verursachen beim Menschen das Perrault Syndrom, das durch Gonadendysgenesie und Innenohrschwerhörigkeit, assoziiert mit Minderwuchs, charakterisiert ist. Trotz dieser Bemühungen ist unser Wissen über die funktionelle Rolle der eukaryotischen CLPP, deren Substrate und über die zugrunde liegenden Mechanismen ihrer Regulation nur sehr begrenzt.

Um die *in vivo* Rolle von CLPP in Säugern zu entschlüsseln, haben wir ein CLPP-defizientes Mausmodell (*Clpp-/-*) entwickelt. Interessant ist, dass nur etwa die Hälfte *Clpp* Knockout-Mäuse nach den Mendelschen Regeln (12,5%) nach der Kreuzung von heterozygoten *Clpp* +/- Mäuse geboren wird. Diese Mäuse sind unfruchtbar und etwa 30% kleiner ist als die nicht betroffenen Wurfgeschwistern. CLPP-defiziente Mäuse replizieren getreu die bei den menschlichen Patienten beobachteten Phänotypen. Auf molekularer Ebene führt der Verlust von CLPP zu einer spezifischen Abnahme der Komplex I-Aktivität im frühen Alter, gefolgt von einer Abnahme der Komplex IV-Aktivität in späteren Lebensabschnitten. Ferner beobachteten wir eine Abnahme in der mitochondrialen Translation, die durch eine Hochregulation der mitochondrialen Transkription kompensiert wird. Dies lässt auf eine direkte oder indirekte Rolle von CLPP im mitochondrialen Proteinsyntheseprozess vermuten. Die Gradientensedimentationanalyse zeigt einen Anstieg der kleinen ribosomalen

Untereinheiten, während die großen ribosomalen Untereinheiten und die Monosomen in fast normalen Werten vorhanden sind. Wir beobachteten auch eine Beeinträchtigung der Assemblierung der 12S rRNA in das Monosom, was zu einer verringerten Beladung der mitochondrialen mRNAs führt. Dies weist auf Komplikationen in der Funktion der Monosomen hin. Die Suche nach den ClpXP-Substraten und möglichen Interaktionspartnern ergab zwei Kandidaten, die wahrscheinlich in diesem Prozess involviert sind. Wir konnten zeigen, dass ERAL1 eines der Substrate von CLPP ist, das wahrscheinlich die defekte Assemblierung der 12S rRNA in die kleine ribosomale Untereinheit verursacht. Ferner scheint p32 ein CLPP-Interaktionspartner zu sein, der fest an den mitochondrialen Ribosomen gebunden ist. Wir glauben, dass diese Proteine durch die Interaktion mit ClpXP bei der Auflösung der ins Stocken geratenen Ribosomen beteiligt sind. Zurzeit arbeiten wir weiter an der Aufklärung der molekularen Mechanismen, die die mitochondriale Translation beeinträchtigen.

1. Introduction

1.1. Mitochondria

Mitochondria are small, highly specialized membrane enclosed organelles present in most eukaryotic cells. The word mitochondrion is derived from Greek words mitos (thread) and chondros (granule) and known as the "energy powerhouse of the cell" [1,2].

Mitochondria possess its own genome and this is explained by the widely accepted endosymbiotic theory [3]. The endosymbiotic hypothesis ('endo-' for internal, and 'symbiont' as in a partner in a mutually beneficial relationship) postulates that mitochondrion evolved from within the bacterial phylum a-proteobacteria via symbiosis within a eukaryotic host cell that happened over two billion years ago. Further phylogenetic reconstruction pointed specifically towards the Rickettsiaceaea family to be most closely related to mitochondria [4]. These phylogenetic studies have revealed that a number of ancestral bacterial genes have been transferred to nuclear genome (endosymbiotic gene transfer) resulting in reduction and compaction of mitochondrial genome [5]. However recent genomics, proteomics and energy metabolism studies have suggested two endosymbiotic models for the origin of mitochondria. The first model "archezoan scenario" states, "the host of the proto-mitochondrial endosymbiont was amitochondrial eukaryote, termed archezoan" [6,7]. The archezoan scenario is most closely related to the widely accepted endosymbiont hypothesis of mitochondrial origin [3,8]. The second model "symbiogenesis scenario" states, "a single endosymbiotic event took place that involved the uptake of an a-proteobacterium by an archaeal cell leading to generation of mitochondria," subsequently followed "by the evolution of the nucleus and compartmentalization of the eukaryotic cell" [6,7].The "hydrogen hypothesis" which is the best example of symbiogenesis scenario states that eukaryotes evolved "through symbiotic association of an anaerobic, strictly hydrogen-dependent, strictly autotrophic archaebacterium (the host) with a eubacterium (the symbiont) that was able to respire, but generated molecular hydrogen as a waste product of anaerobic heterotrophic metabolism. The host's dependence upon molecular hydrogen produced by the symbiont is proposed to be the selective principle that forged the common ancestor of eukaryotic cells [6,9]. This hydrogen hypothesis postulates that the origins of the eukaryotic lineage and that of the

symbiont are identical and the features of eukaryotic cell evolved after the symbiosis of the eubactieruim [6]. Whereas archezoan scenario hypothesize that endosymbiosis of a-proteobacterium giving rise to proto-mitochondrion happened after the formation of amtiochondriate eukarytic cell that served as the host. However the question still remains open regarding the nature of the cell that served as the host for the endosymbiont and evolved into mitochondria. With time more comparative genomics data will gradually refine the current ideas regarding the origin of eukaryotes and mitochondrial evolution.

Mitochondria are known as intracellular "power plants" generating ATP for the sustenance of life. They form a dynamic network that is regulated by constant fusion and fission. A typical eukaryotic cell contains about 2000 mitochondria, which comprises about one fifth of its total volume [1].

Mitochondria are characterized by two specialized membranes, the outer (OMM) and inner mitochondrial membrane (IMM) forming two compartments, the inter membrane space (IMS) and the mitochondrial matrix. The outer membrane is permeable to small molecules and ions that pass through transmembrane channels comprising of integral membrane proteins called porins. Larger molecules are brought across the outer membrane by the translocase of outer membrane (TOM). The inner membrane is highly impermeable to H^+ ions and this property of IMM forms the basis of mitochondrial energy transduction [10]. Compounds, ions and molecules cross inner membrane through translocase of inner membrane (TIM). The inner membrane is further folded to form cristae (Latin for *crest* or *plume*) providing an increase amount of surface area harboring the respiratory complexes and the ATP synthase complex, which control the basic rates of cellular metabolism [1,10]. The innermost space that is enclosed by inner membrane is known as mitochondrial matrix. Various metabolic processes like the b oxidation and tricarboxylic acid (TCA/Krebs cycle) take place in the mitochondrial matrix. In addition this compartment also contains several copies of mitochondrial genome (mtDNA), ribosomes, transfer RNAs (tRNAs), and various proteins and enzymes required for proper mitochondrial function.

Mitochondria produces energy currency ATP by the oxidative phosphorylation system (OXPHOS) situated in the inner mitochondrial membrane. In addition to energy production, mitochondria are involved in various important processes such as the first step of iron-sulfur (Fe-S) cluster biosynthesis, b oxidation of fatty acids and biosynthesis of pyrimidines, amino acids, nucleotides, phospholipids and haem, regulation of cellular

metabolism, programmed cell death (apoptosis), calcium homeostasis and reactive oxygen species (ROS) formation.

1.2. Mitochondrial Genetics

Mitochondria are the only organelles besides nucleus that possess their own independent genome (mtDNA) located in mitochondrial matrix. Each somatic mammalian cell contain between 1000-10,000 copies of mtDNA. mtDNA molecules are packaged into DNA-protein complexes known as nucleoids. Nucleoids contain essential maintenance proteins including the mitochondrial transcription factor A (TFAM) that plays an important role in mtDNA maintenance [11]. Mammalian mtDNA is maternally inherited where mtDNA nucleoids represents the unit of inheritance. During mammalian zygote formation, sperm mitochondria are destroyed thereby blocking the transmission of paternal mtDNA [12]. Inside the cytoplasm of the fertilized oocyte the sperm mitochondria are removed by ubiquitination and later subjected to proteolysis during preimplantation development [13]. However there has been a single report of paternal transmission in humans thereby suggestion this block against transmission of paternal mtDNA can be bypassed [14]. Human mtDNA is a circular double stranded molecule ~16.6 kb that encodes 13 essential polypeptides of oxidative phosphorylation system (OXPHOS) (Figure 1.1). In addition to mRNA molecules, the mitochondrial genome also encodes 2 ribosomal RNAs and 22 transfer RNAs for translation of mtDNA transcripts (Figure 1.1). Around 1500 different proteins are required for the proper functioning of mitochondria, out of which ~ 90 proteins are essential components of oxidative phosphorylation (OXPHOS) system. In addition nuclear encoded proteins are required for maintenance and expression of mtDNA. Hence it is evident that majority of the proteins are encoded by nuclear DNA (nDNA), synthesized in cytosol and imported into mitochondria by its specialized import machineries. Therefore a proper co ordination and communication is needed between the two genomes to maintain the homeostasis. The two strands of mtDNA are distinguished on the basis of their nucleotide composition that results in different densities in alkaline cesium chloride gradients. They are denoted as heavy strand (H) that is guanine rich and light strand (L), which is cytosine rich. mtDNA contains 37 genes, out of which the heavy (H) strand harbors 28 genes, 12 mRNAs, 2 rRNAs and 14 tRNAs whereas the light (L) strand harbors 9 genes, single polypeptide (ND6 subunit of Complex I) and 8 tRNAs (Figure 1.1). Mammalian mtDNA is extremely economic in terms of organization of its

genetic material that is densely packed with genes lacking introns. mtDNA contains only one major non coding region known as the displacement loop (D-loop) (Figure 1.1).

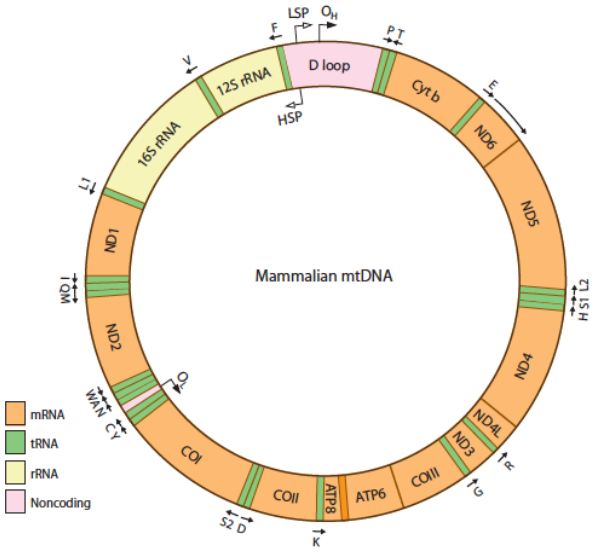

Figure 1.1 Map of human mitochondrial DNA (mtDNA).

The two strands are denoted the heavy (H) and light (L) strand. The only noncoding region, the displacement loop (D loop) contains the promoters for transcription of the H and L strand (HSP and LSP) and the origin of replication of the leading strand of mtDNA (OH). The origin of replication of the lagging strand (OL) is located in a cluster of tRNA genes. Transcription from HSP produces 2 rRNAs (12S and 16S rRNA), 12 mRNAs (ND1–5, ND4L, Cyt b, COI–III, ATP6, and ATP8), and 14 tRNAs (F, V, L1, I, M, W, D, K, G, R, H, S1, L2, T). Transcription from LSP has a dual function. First, it produces RNA primers needed for initiation of replication at OH. Second, it is needed to produce 1 mRNA (ND6) and 8 tRNAs (P, E, S2, Y, C, N, A, Q) [15].

Primers generated by transcription from LSP perform initiation of mtDNA replication at O_H. However, this DNA replication often stops at the end of the D loop thereby resulting in a three-stranded structure containing a nascent H strand. This 1.1 kb control region is a short nucleic acid strand which is complementary to L strand and displaces H strand. The D-loop contains important regulatory elements of mtDNA expression such as the promoters for transcription of the L and H strands (LSP and HSP1) and the origin of replication of the H strand (O_H) (Figure 1.1).

1.3. Oxidative Phosphorylation (OXPHOS) system

As stated earlier, one of the major functions of mitochondria is to generate energy in the form of ATP through a process called oxidative phosphorylation. The mitochondrial respiratory chain consists of five protein complexes (Complex I-V) that are embedded

into the lipid bilayer of the inner mitochondrial membrane (Figure 1.2). Out of the 92 identified structural OXPHOS subunit genes, 79 are encoded by nuclear genome and 13 are encoded by mtDNA genome which are the building blocks for the formation of the five OXPHOS complexes [12]. The subunits of Complex I and Complex III-V are encoded by both nuclear DNA and mitochondrial DNA (mtDNA) whereas subunits of Complex II is exclusively encoded by nuclear genome. ATP is generated in a two-step process. In the first step electrons from NADH (reduced nicotinamide adenine dinucleotide) and $FADH_2$ (flavin adenine dinucleotide), produced by the oxidation of nutrients such as glucose and fatty acids, are passed along a series of carrier molecules called the electron transport chain to molecular oxygen to form water (Figure 1.2) [16]. This generates an electrochemical gradient that allows Complex I, III and IV to pump protons across the inner membrane. This creates a proton gradient across the membrane, which is used by Complex V to produce ATP in the second step.

Complex I or NADH dehrdrogenase (NADH: ubiquinone oxidoreductase) is the largest complex of the respiratory chain consisting of 44 subunits (14 core subunits - 7 from mtDNA and 7 from nDNA) and another 30 nDNA accessory subunits including a FMN-containing flavoprotein and 6 iron-sulfur centers proposed to maintain the stability of the complex [10,12]. Complex I is L-shaped comprising of a long and short arm. The long arm forms the hydrophobic integral membrane protein and the hydrophilic short arm contains the flavin mononucleotide (FMN) and the NADH active center extending into the matrix [10]. In this complex, oxidation of NADH allows the transfer of two electrons from NADH to FMN thereby reducing it to $FMNH_2$. The electrons are further transferred to ubiquinone (Q) via iron sulfur cluster of Complex I. This electron transport is coupled with the transfer of four protons from mitochondrial matrix into the intermembrane space thereby creating the proton gradient (Figure 1.2).

Complex II or succinate dehydrogenase (succinate: ubiquinone oxidoreductase) is the only complex consisting of 4 subunits that are encoded entirely by nDNA [12]. This is another point where electrons can enter the electron transport chain besides Complex I. Complex II catalyzes the oxidation of succinate via flavin adenine dinucleotide (FAD) to form fumarate during which electrons travel from $FADH_2$ through iron sulphur clusters to ubiquinone (Figure 1.2) [16].

Ubiquinone is a lipid soluble benzoquinone that diffuses in the phospholipid bilayer of the inner membrane thereby assisting in shutting electrons between membrane proteins

(Figure 1.2) [10].

Complex III or cytochrome bc_1 (ubiquinol: cytochrome c oxidoreductase) is a complex comprising of 11 subunits; out of which 1 (cytochrome b) is encoded by mtDNA and 10 are encoded by nDNA [12]. This complex catalyzes the transfer of electrons from ubiquinols to cytochrome c that resulted in the translocation of four protons across the inner membrane (Figure 1.2) [16].

Cytochrome c is a peripheral protein facing the intermembrane space and transfers electrons from complex III to complex IV (Figure 1.2) [10].

Complex IV (cytochrome c oxidase) is the last enzyme of the electron transport chain consisting of 3 subunits encoded by mtDNA and 11 subunits encoded by nDNA [12]. This complex transfers four electrons from reduced cytochrome c to O_2 thereby producing two molecules of water. This electron transfer further resulted in the translocation of four protons across the inner membrane (Figure 1.2) [16].

Complex V (F0F1-ATP synthase) consists of 19 subunits where 2 subunits are encoded by mtDNA and the remaining 17 subunits are encoded by nDNA [12]. The electrochemical gradient is utilized by Complex V to drive the synthesis of ATP from ADP and Pi. Powered by the translocation of three protons into the mitochondrial matrix, Complex V synthesizes one molecule of ATP, which is the energy currency of cell that is finally transported outside mitochondria by adenine nucleotide translocase (ANT1) (Figure 1.2) [16].

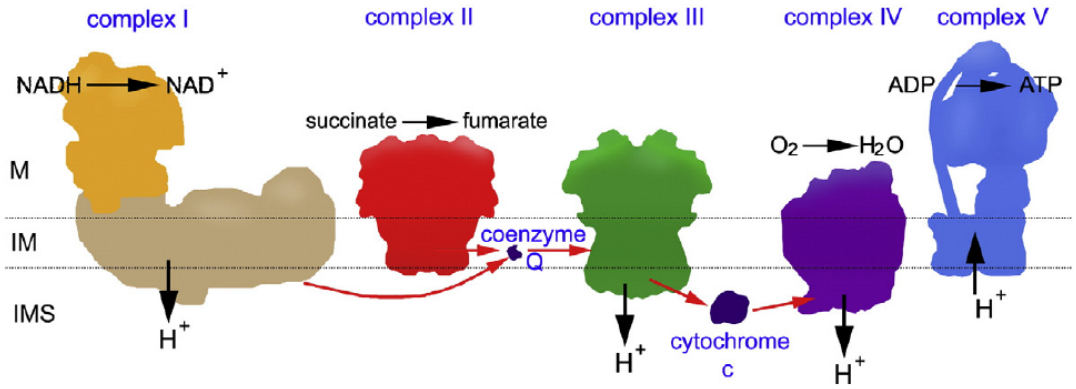

Figure 1.2 OXPHOS system.

Schematic representation of the OXPHOS system showing its individual components. The position of the matrix (M), the intermembrane space (IMS) and cristae or inner membrane (IM) has been indicated [17].

Two models have been proposed describing the supramolecular organization of these five complexes that together form the OXPHOS system. (i) The "fluid state" model postulates that the respiratory chain complexes diffuse freely in inner mitochondrial membrane and the electron transfer is based on random collisions of the single complexes [17,18]. This is supported by the fact that all five complexes of the OXPHOS system can be purified to homogeneity in an enzymatically active form using isolated mitochondrial membranes [17,19]

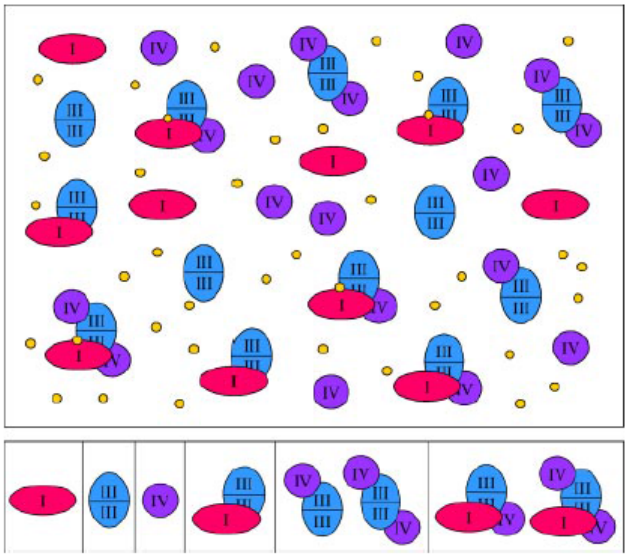

Figure 1.3 Model of the supramolecular structure of the OXPHOS system.

Single complexes co-exist with supramolecular assemblies. Complex I (red) can associate with complex III_2 (blue). Complex III_2 can associate with one or two copies of complex IV (purple). The largest assemblies include complex I, dimeric complex III, and one or several copies of complex IV. (Yellow circles, ubiquinol, which either freely diffuses within the inner mitochondrial membrane or might form part of the $I+III_2$ supercomplex. For simplicity, complex II was omitted from the figure because it is not known to form part of OXPHOS supercomplexes. Furthermore, cytochrome c, alternative oxidoreductases, and the ATP synthase complex are omitted from the figure) [19].

.

(ii) The "solid-state" model proposes stable interactions between the OXPHOS complexes within entities named supercomplexes or respirasomes [17]. Several evidences has been reported in support of this model:(a) Supercomplexes including more than one type of OXPHOS complex are resolved by blue native polyacrylamide gel electrophoresis (BN-PAGE) and are shown to be active by *in-gel* activity experiments [20,21]; (b) Single particle electron microscopy studies revealed defined associations of OXPHOS complexes within the isolated respiratory supercomplexes [22,24]; (c) Studies showed that point mutations in genes encoding one of the subunits of one OXPHOS

complex affect the stability of other OXPHOS complexes [25]; (d) Flux control experiments indicate that respiratory chain operates as one functional unit [26,27]; (e) Various reconstitution experiments showed that different OXPHOS complexes when present at defined stoichiometries generated highest electron transfer activities [19;28]; (f) Cardiolipin seems to assists the formation of some supercomplexes [29,30].

Complex I, III, IV has been shown to form supercomplexes with defined stoichiometric composition (Figure 1.3). Electron microscopy studies have revealed interaction between complexes I and III, among complexes I, III and IV and in a dimeric form of complex V, between two ATP synthase monomers. The $I+III_2+IV_{1-2}$ supercomplex is known as respirasome that can autonomously carry out respiration in the presence of ubiquinone and cytochrome c (Figure 1.3) [17]. Complex II in general, seems to maintain its singular state due to its direct involvement in the citric acid cycle and does not take part in formation of the respiratory chain supercomplexes [17]. However one study reported Complex II containing supercomplexes [31].

Although the debate on the membrane state of OXPHOS system is still ongoing, it is clear that many experimental observations cannot be explained only with "fluid state" model whereas other observations do not indicate only towards a "solid state" model. Hence this arise a possibility where the membrane state of OXPHOS system is of dynamic nature where respiratory supercomplexes may co-exist within the inner mitochondrial membrane with single OXPHOS complexes (Figure 1.3) [17,19].

1.4. Replication of mtDNA

mtDNA replication occurs randomly throughout the cell cycle and is independent of nuclear DNA replication. mtDNA replication machinery and proteins for maintaining its integrity are encoded by nuclear genome and subsequently imported into mitochondria. In eukaryotes, mtDNA replication takes place in a 'replisome' by mtDNA polymerase g (Pol g) which is a heterotrimeric protein consisting of a catalytic subunit (Pol g A) and a dimeric accessory subunit (Pol g B) (Figure 1.4). This heterotrimeric protein has three activities: DNA polymerase activity, 3'-5' exonucleolytic proofreading activity and a 5'dRP lyase activity that is required for enzymatic DNA repair [12]. The additional components included in the replisome are mitochondrial single stranded binding protein (mtSSB) and TWINKLE which is a 5'-3'DNA helicase (Figure 1.4). Moreover mitochondrial transcription factor A (TFAM), RNA polymerase (POLRMT), RNA

processing enzymes (RNaseH1) and topoisomerase (mtTOP1) are required for the mtDNA replication. During mtDNA replication the TWINKLE helicase forms a hexamer that unwinds mtDNA in the 5'-3'direction facilitating mtDNA synthesis. The resulting single stranded region of mtDNA at replication fork is stabilized by mtSSB, which further stimulates the TWINKLE dependent mtDNA unwinding and enhancement of polymerase gamma activity (Figure 1.4) [12,13]. POLRMT act as a primase to provide primers required for the initiation of lagging-strand DNA synthesis [15]. RNaseH1 is involved in removing the short RNA primers required for the initiation of H and L strand DNA synthesis. mtTOP1 is proposed to have a role in relaxing negative supercoils and removing positive supercoils at the replication fork generated by DNA helicase [13]. Finally TFAM plays a role in the maintenance of mtDNA integrity by actively participating in bending and packaging of mtDNA into nucleiods [32].

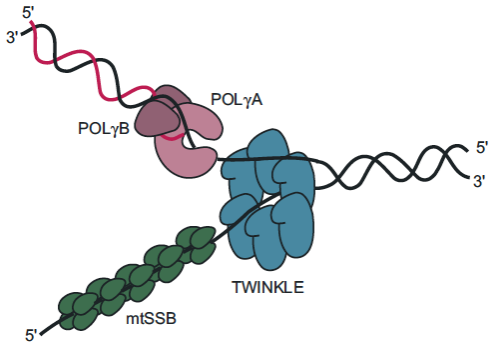

Figure 1.4 The mtDNA replication machinery.

The TWINKLE helicase has 5'to 3'directionality and unwinds the duplex DNA template. The mtSSB proteinstabilizes the unwound conformation and stimulates DNA synthesis by the POLγ holoenzyme [13].

1.5. Mitochondrial transcription

mtDNA transcription generates the RNA primers for initiation of mtDNA replication at O_H along with mtDNA expression. The principal mitochondrial transcription machinery consists of the mitochondrial RNA polymerase (POLRMT), mitochondrial transcription factor B2 (TFB2M), and mitochondrial transcription factor A (TFAM) [33]. Recent studies have shown that TFB1M, which is a paralog of TFB2M, has no direct role in mtDNA transcription. However, TFB1M functions as a 12S rRNA methyltransferase that stabilizes the small subunit of the mitochondrial ribosome [34]. Mitochondrial transcription is a bidirectional process that is initiated in the D-loop region where light-strand transcription starts from the light-strand promoter and heavy-strand transcription initiates

from two heavy strand promoters: HSP1 and HSP2 (Figure 1.1). TFAM is important for transcription initiation, as it preferentially binds the mtDNA upstream of the promoters thereby regulating RNA transcription. mtDNA transcription that is initiated from HSP1 promoter terminates at the tRNALeu (UUR), thereby transcribing tRNAVal, tRNAPhe and 2 ribosomal RNA (12S and 16S) whereas transcription initiated from HSP2 promoter transcribes the full-length mtDNA [35]. Moreover, mtDNA transcription that is initiated from LSP promoter can either proceed through entire mtDNA or can terminate prematurely to prime mtDNA replication. There are additional factors that modulate the activity of basal mitochondrial transcription machinery thereby affecting both transcription initiation and termination. POLRMT plays a role in elongation of transcription, which is also enhanced by mitochondrial transcription elongation factor (TEFM) [12]. Termination of both H and L strand transcription has been proposed to be carried out by the mitochondrial transcription termination factor 1 (MTERF1) that binds downstream of the rRNA genes [12,15,36]. In mammals, there is a family of four MTERF proteins (MTERF1–4) [15,37], where MTERF1-3 has been proposed to bind to the promoter region thereby modulating mtDNA transcription [35]. Recent studies have shown different roles of the MTERF family proteins: MTERF2 has been shown to regulate oxidative phosphorylation by modulating mtDNA transcription [38]. MTERF3 is shown to be a negative regulator of mtDNA transcription [39] and also plays a role in regulating mitochondrial ribosome biogenesis [40]. MTERF4 is reported to regulate mitochondrial translation and ribosomal biogenesis by targeting RNA methyltransferase NSUN4 to the large ribosomal subunit [41].

1.6. Mitochondrial translation

Mitochondrial protein synthesis is an important process for all mammals since it produces thirteen polypeptides that are key components of the OXPHOS complexes. Despite of a 50-year period of research where many factors critical for mitochondrial translation have been identified, the molecular details underlying the mitochondrial translation process remains incomplete. One of the major reasons behind this is the absence of an *in vitro* reconstituted system established from mammalian mitochondria that is capable of correct initiation and synthesis of a mitochondrial encoded protein. However studies in the past years have provided valuable information on specific features of mammalian mitochondrial protein synthesis where a number of the individual steps of protein

synthesis have been successfully carried out *in vitro*. Mitochondrial ribosome or mitoribosome is the key component of the mitochondrial protein synthesis process. Studies have shown that mammals possess a distinct set of ribosomes which sediment as 55S particles and comprise 2 subunits, a 28S small subunit (mt-SSU) and 39S large subunit (mt-LSU) [42,43]. Only two rRNA species has been identified in each subunit of mammalian mitoribosomes, 12S rRNA in small subunits and 16S rRNA in large subunit. In addition, ribosomes may also carry a 5S rRNA has been reported [44]. Mammalian mitoribosomes have lower sedimentation coefficient (55S) compared to prokaryotes (70S) and cytosolic (80S) counterparts. This is due to the change in protein to RNA ratio. For prokaryotes/eukaryotic cytosolic ribosomes the protein:RNA ratio is 1:2 whereas for mammalian mitoribosome it is 2:1 suggesting a relatively low RNA content thereby compensated by a large number of mitoribosomal proteins, reviewed in [43]. The small subunit comprises of 29 proteins out of which 14 are homologues of prokaryotic ribosomes whereas the large subunits is composed of 48 proteins and 28 of them are homologues of bacterial ribosomal proteins [45]. There are four steps (phases) for the protein synthesis in mammalian mitochondria: Initiation, elongation, termination and ribosomal recycling.

(i) Translation initiation of mammalian mitochondria:

The translation initiation process of mammalian mitochondria is different from that in prokaryotes and eukaryotic cytoplasm. It is still unclear how the mitoribosomes are directed to the initiation codon since mitochondrial mRNAs are not capped and lack any upstream leader sequences [46]. Till date only two mitochondrial initiation factors have been identified, mitochondrial initiation factor 2 ($IF2_{mt}$) and mitochondrial initiation factor 3 ($IF3_{mt}$). According to a recent study it was shown *in vitro* that with $IF2_{mt}$ and $IF3_{mt}$ it was possible to assemble an initiation complex on 55S mitoribosomes with fMet-tRNA correctly positioned at the start codon of a mitochondrial mRNA [42]. Based on various studies a current working model has been proposed for the initiation of translation (Figure 1.5). In the first step, $IF3_{mt}$ interacts with 55S ribosome thereby loosening the interaction between the two subunits, releasing the 39S subunit and forming a transient 28S:$IF3_{mt}$ complex in the second step (Figure 1.5). This is followed by the binding of $IF2_{mt}$: GTP to the small subunit in the third step. In the fourth step, it has been shown that the mRNA feeds into the 28S subunit via an mRNA entrance gate (Figure 1.5) [47].

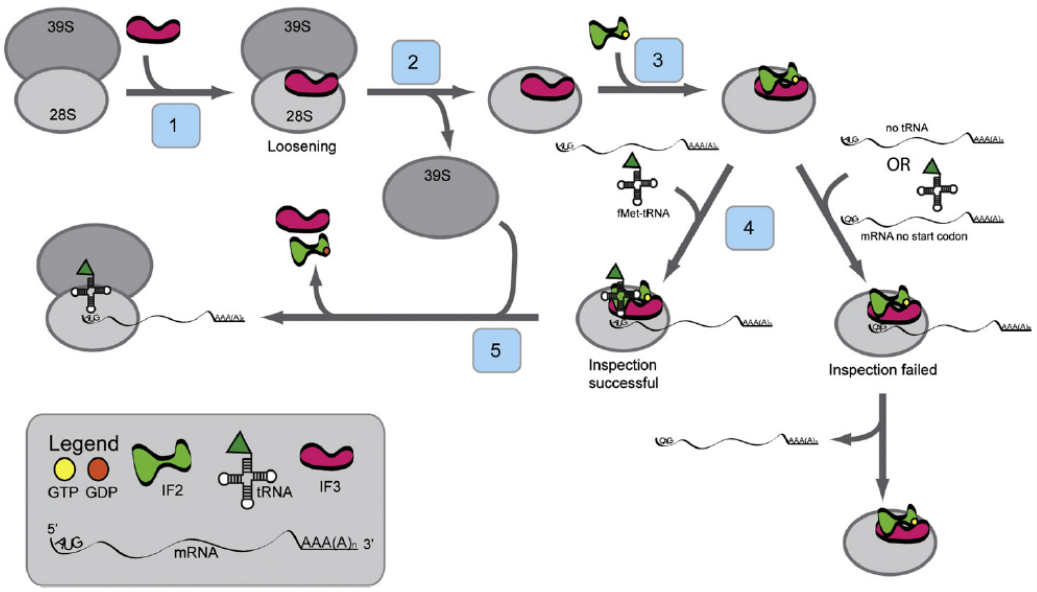

Figure 1.5 Model for the initiation phase of mitochondrial translation.

In the current model for the initiation of protein synthesis, mitochondrial initiation factor 3 ($IF3_{mt}$) actively dissociates 55S ribosomes, forming a transient [$IF3_{mt}$:55S] complex (Step 1) and leading to the formation of an $IF3_{mt}$:28S complex (Step 2). Mitochondrial initiation factor 2 ($IF2_{mt}$) bound to GTP binds to the small subunit (Step 3), followed by the fMet-tRNA and mRNA (Step 4), although the exact order of binding is not clear. Once the 28S initiation complex has formed, the large subunit joins, and along with the hydrolysis of GTP to GDP, the initiation factors exit (Step 5) leaving a 55S:fMet-tRNA:mRNA complex that is ready for the elongation phase of protein synthesis [42].

After the first 17 nucleotides of mRNA enters the ribosome the 5'end of mRNA pauses at the P-site of the ribosome. During this time, inspection is carried out by 28S subunit at the 5' end of mRNA for the start codon. At this time, $IF2_{mt}$: GTP may promote the binding of fMet-tRNA to the ribosome. If correct start codon in present in the P-site of mitoribosomes, a stable 28S initiation complex is formed via the codon:anticodon interactions between the fMet-tRNA and the 5'AUG start codon (Figure 1.5). However, if the inspection fails, when fMet-tRNA binds without mRNA or mRNA lacks a proper 5' start codon, the mRNA slides through the small subunit and finally dissociates (Figure 1.5). But once the inspection succeeds and 28S initiation complex is formed, the large subunit joins the complex followed by hydrolysis of GTP to GDP by $IF2_{mt}$ in the fifth step. The initiation factors are released and 55S:fMet-tRNA:mRNA complex is formed that is ready for the elongation phase of protein synthesis (Figure 1.5) [42].

(ii) Translation elongation of mammalian mitochondria:

Three mitochondrial elongation factors, EF-G_{mt}, EF-Ts_{mt} and EF-Tu_{mt} are involved in the process of polypeptide chain elongation. This elongation phase in mammalian mitochondria has many similarities to the process in prokaryotes [48], as compared to initiation and termination phases. The tRNA containing the growing polypeptide chain is located in the P-site of the mitoribosome. In the first step, GTP bound elongation factor Tu (EF-Tu_{mt}) that is the active form, binds aminoacyl-tRNA (aa-tRNA) to form a ternary complex (EF-Tu_{mt}-GTP-aa-tRNA) and enters the A-site of mitoribosome (Figure 1.6) [42]. In the second step, once the codon:anticodon interactions take place, the ternary complex is selected triggering the hydrolysis of GTP to GDP by EF-Tu_{mt}, thereby releasing EF-Tu_{mt}-GDP from the ribosome.

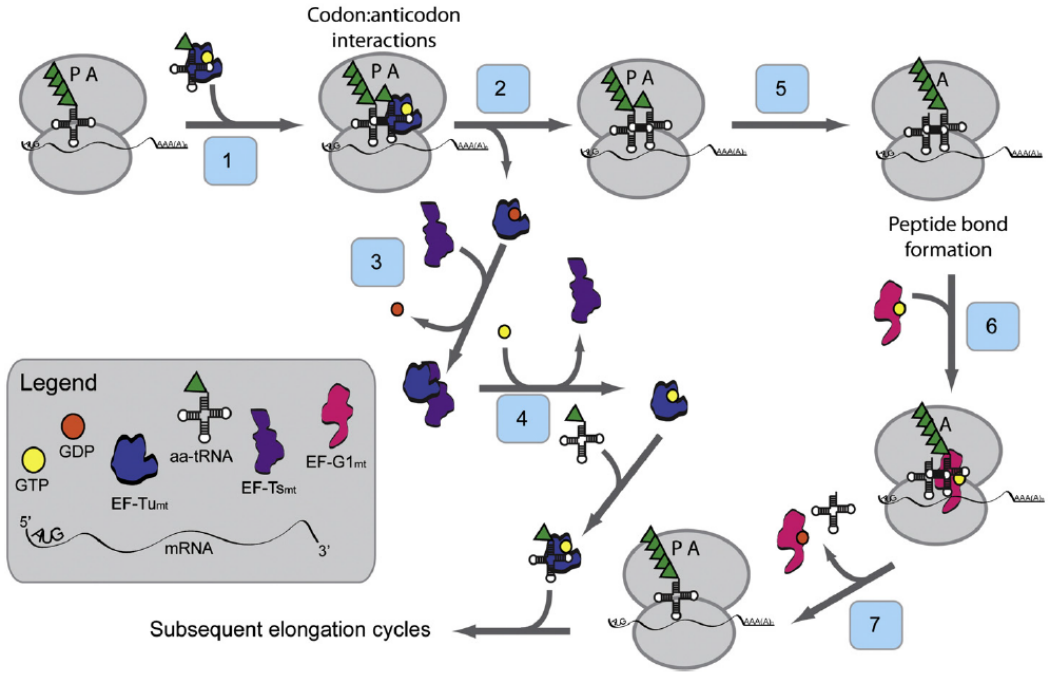

Figure 1.6 Model for the elongation phase of mitochondrial translation.

The tRNA containing the growing polypeptide chain is located in the P-site of the ribosome. EF-Tu_{mt} brings the aa-tRNA to the A-site of the ribosome (Step 1). In concert with the hydrolysis of GTP to GDP, EF-Tu_{mt} leaves the ribosome (Step 2). EF-Ts_{mt} binds to EF-Tu_{mt}, displacing the GDP molecule and forming an EF-Tu_{mt}·EF-Ts_{mt} complex (Step 3). A GTP molecule displaces EF-Ts_{mt}, and an EF-Tu_{mt}:GTP complex is formed (Step 4) which can then bind another aa-tRNA reforming the ternary complex. The large ribosomal subunit catalyzes peptide bond formation and the growing polypeptide chain is transferred to the tRNA in the A-site of the ribosome (Step 5). EF-$G1_{mt}$:GTP binds to the ribosome at the A-site (Step 6) and catalyzes translocation of the ribosome, moving the deacylated tRNA out of the P-site and the peptidyl-tRNA from the A-site to the P-site (Step 7). A new cycle of elongation can then begin [42].

.

The third step follows the binding of Elongation factor Ts (EF-Ts_{mt}) to EF-Tu_{mt} thus displacing GDP. Subsequently GTP molecule binds to EF-Tu_{mt} displacing EF-Ts_{mt} and forming EF-Tu_{mt}:GTP complex in the fourth step. This can now bind to another aa-tRNA to form a ternary complex for the next round (Figure 1.6) [42]. In Step 5, the large ribosomal subunit catalyzing the peptide bond formation and the growing polypeptide chain is transferred to the tRNA in the A-site of the mitoribosome thus leaving a deacylated tRNA in the P-site. In the next step (Step 6), another mitochondrial elongation factor G1 (EF-$G1_{mt}$) binds to GTP, forming EF-$G1_{mt}$:GTP that binds to A-site of ribosome. It has been reported that this binding catalyzes the translocation of mitoribosome in the final step (Step 7) thereby removing the deacylated tRNA from the P-site and moving the peptidyl-tRNA from A-site to P-site (Figure 1.6) [42]. Cryo-EM studies of the mitochondrial ribosome suggested that mitoribosomes lacks E-site [47].

(iii) Termination of translation and ribosome recycling of mammalian mitochondria:

It has been shown that UAA and UAG serve as stop codons but these stop codons are not recognized by any so far identified release factors. According to a recent study, it has been suggested that they promote a −1 frameshift thereby moving a classical UAG codon into the A-site for termination [49]. In the first step, when the termination codon UAA or UAG enters the A-site of mitoribsomes, it is recognized by mitochondrial release factor mtRF1a (Figure 1.7). In presence of GTP, mtRF1a binds to the A- site in the second step, thereby promoting the hydrolysis of the peptidyl-tRNA bond (by the peptidyl transferase center on the 39S subunit) and subsequent release of the completed polypeptide (Figure 1.7) [42]. However, the manner in which mtRF1a is released from the mitoribosome after the release of polypeptide is still elusive. In the next step (step 3) mitochondrial ribosome recycling factor ($RRF1_{mt}$) binds to the A-site of the ribosome, which is then accompanied by binding of $RRF2_{mt}$ (EF-$G2_{mt}$). This binding enhances the dissociation of ribosomal subunits and release of deacylated tRNA and mRNA in the fourth step (Figure 1.7). The dissociation of ribosomal subunits and its release is dependent on the combined action of $RRF1_{mt}$ and $RRF2_{mt}$ (EF-$G2_{mt}$) [29,50,51]. Following the release of $RRF1_{mt}$ and $RRF2_{mt}$ from the ribosomse in the final step the ribosome begins another round of protein synthesis (Figure1.7) [42].

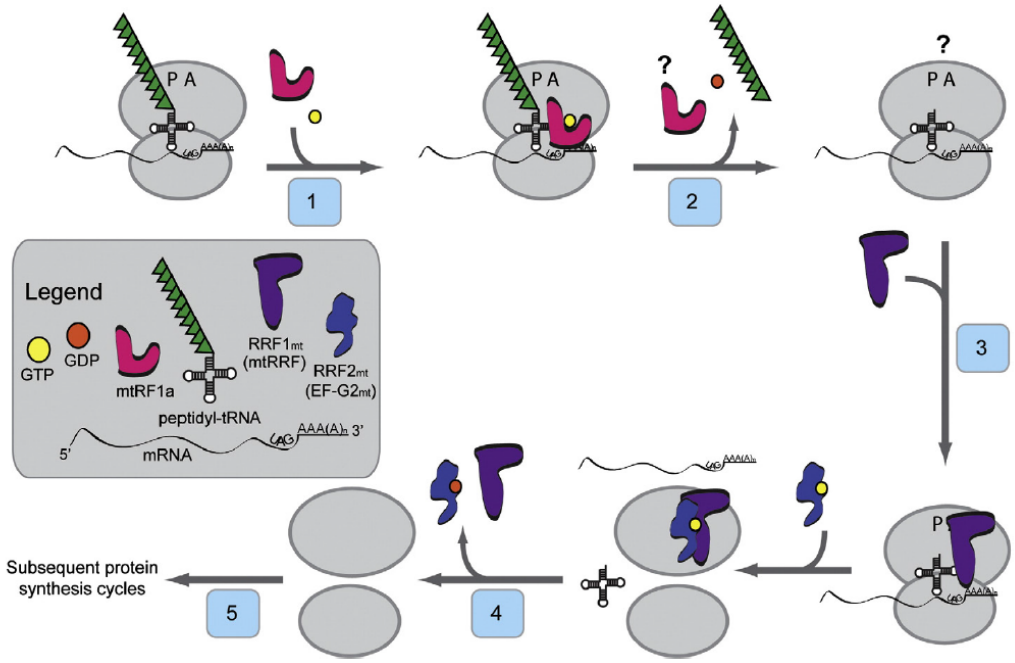

Figure 1.7 Model for the termination and ribosome recycling phases of mitochondrial protein synthesis.

As the termination codon (UAG here) enters the A-site of the ribosome, mtRF1a and GTP bind to the A-site (Step 1) and promote GTP-dependent hydrolysis and release of the polypeptide chain (Step 2). How mtRF1a is released from the ribosome is not known. RRF1mt binds to the A-site of the ribosome (Step 3) and is joined by $RRF2_{mt}$ (also termed $EF\text{-}G2_{mt}$). These factors promote the dissociation of the ribosomal subunits and release of the deacylated tRNA and the mRNA (Step 4). Following release of $RRF1_{mt}$ and $RRF2_{mt}$ (Step 5), the ribosome begins another round of protein synthesis [42].

1.7. Mitochondrial quality control (MQC)

Mitochondria are dynamic organelles possessing various essential biological roles in cellular physiology; hence to maintain a healthy mitochondrial population, several interdependent mechanisms exist, starting from the molecular, organellar to the cellular level. These conserved mechanisms known as mitochondrial quality control (MQC) maintains the mitochondrial homeostasis. There are several issues that impose significant challenges to proper mitochondrial function:

(a) The first challenge for maintaining homeostasis is the generation of reactive oxygen species (ROS), a byproduct of oxidative phosphorylation. Accumulation of ROS can cause damage to mtDNA, oxidative modification to the mitochondrial proteins, leading to misfolding and aggregation thereby disrupting their native functions (Figure 1.8A).

(b) The second problem arises from the bigenomic nature of the mitochondrial proteome (Figure 1.8B). Mitochondrial proteome comprises of almost 1500 proteins and majority

of proteins are encoded by nuclear genome, synthesized in the cytosol and imported into mitochondria through specific translocation machineries. According to recent studies, ~500 proteins reside in the matrix [52], ~60 proteins in inter membrane space (IMS) [53,54] and ~100 polypeptides located in the outer membrane (OM). But the inner membrane (IM) proteome is the most enriched consisting ~840 proteins that comprises the electron transport chain and F_1 F_O ATPase complexes (OXPHOS system) [55]. Out of the 1500 proteins, only 13 polypeptides that are subunits of the respiratory chain are encoded by the mitochondrial genome and needs to be assembled together with the nuclear encoded ones. This complex biogenesis pattern requires a coordinated expression and communication between the two genomes and proper sorting-folding and assembly of these polypeptides into right stoichiometric complexes within the IM. If there is a failure of coordination or perturbation in homeostasis especially under stress condition these newly synthesized proteins are at a risk to misfolding and aggregation. Therefore mitochondria have its own quality control team consisting of chaperones and proteolytic machineries that deal with such problems and thereby maintain integrity.

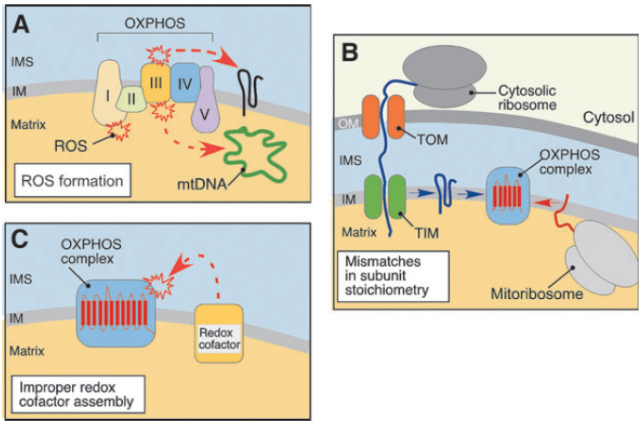

Figure 1.8 Biochemical stresses that challenge normal mitochondrial function.

(A) Stalling the high-energy electrons at respiratory complexes I and III leads to generation of superoxide anion which—either directly or via subsequent ROS radicals—can damage biological molecules like mtDNA and propel additional damage. The biogenesis of OXPHOS complexes requires tight coordination between synthesis and assembly of the mitochondrial- and nuclear-coded proteins. (B) Polypeptides derived from the nuclear genome are translated on cytosolic ribosomes and imported in an unfolded state into the mitochondrion via presequence translocases of the outer (TOM) and inner (TIM) membranes. Imported polypeptides are inserted into the IM where they are joined with mitochondria-synthesized subunits. Mismatches in subunit stoichiometry can lead to accumulation of unfolded or unassembled proteins that can affect functional integrity of mitochondria. In addition, the electron transport chain units of OXPHOS contain redox-active cofactors poised for rapid electron exchange reactions. (C) When improperly assembled, these prosthetic groups can act as pro-oxidants through their inherent ability to generate ROS via Fenton-like reactions [55].

(c) The final threat comes from the multiple redox cofactors of electron transport chain (ETC) (Figure 1.8C). If these cofactors are not assembled properly, they may act as pro oxidants through their inherent ability to generate ROS via Fenton-like reactions, thereby further adding to the challenging biochemical environment [56,57]. If these challenges are not taken care of properly, they may further distort protein homeostasis leading to progressive failure of the organelle [55].

In order to cope up with the above-mentioned challenges, cells have evolved elaborate quality control mechanisms that engage at several levels depending on the extent of damage (Figure 1.9). The molecular level of MQC is the first line of defense that comprises of highly conserved molecular chaperones and energy dependent proteases distributed across the mitochondrial compartments and also cytosolic proteolytic systems like the ubiquitin–proteasome system (UPS), which associates with the OMM [55]. The primary role of the chaperones is to ensure proper folding and assembly of mitochondrial proteins and that of proteases is to remove damaged proteins from the organelle [58]. The second line of defense is provided by the fusion and fission events that mediate organellar dynamics and regulate even redistribution of mtDNA and proteome throughout the mitochondrial network (Figure 1.9). Fusion with neighboring healthy mitochondria helps in restoring the function of damaged mitcohondria. However if the mitochondria are severely damaged, then fusion is impaired resulting in fragmentation of mitochondria that are selectively removed by mitochondria-specific type of autophagy known as mitophagy. Occurrence of mitophagy inhibits the release of pro-apoptotic proteins from damaged mitochondria thereby suppressing apoptosis, which is the final line of defense at cellular level (Figure 1.9) [58].

In last years, mitochondrial derived vesicles (MDV) carrying selected oxidized cargo and delivering to lysosomes, has been identified as a new pathway to MQC. This process has been shown to be independent of mitochondrial dynamics and mitophagy. One of the proposed roles is to remove segments of the mitochondrial membranes containing damaged, hard to dissociate protein complexes and/or reactive prosthetic groups reviewed in [55].

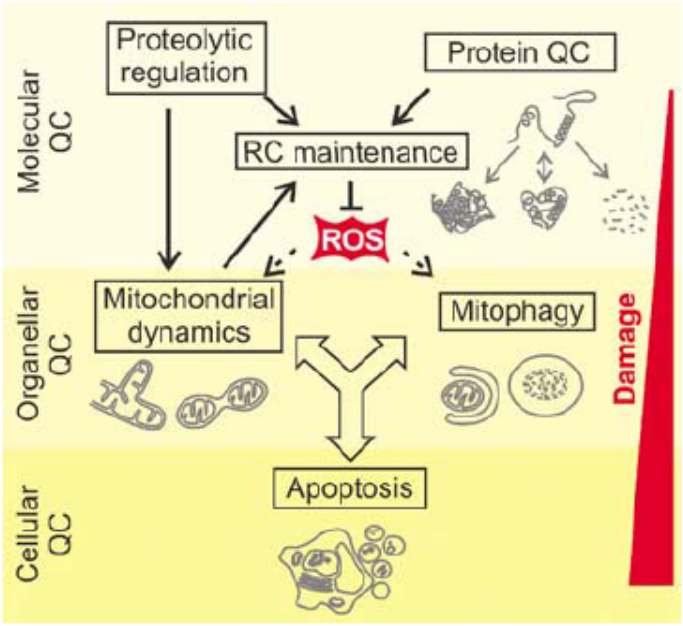

Figure 1.9 Quality control (QC) surveillance of mitochondria.

Intraorganellar proteases exert QC and regulatory functions to maintain respiratory chain (RC) activity. The functionality of damaged mitochondria can be restored by fusion and content mixing within the mitochondrial network. Severely damaged mitochondria fragment and are removed by mitophagy or induce apoptosis by the release of pro-apoptotic proteins [58].

1.7.1 MQC in the matrix:

Protein regulation and quality control is tightly regulated in the mitochondrial matrix, which is the most protein dense region since it harbors the enzymes of TCA cycle and other metabolic enzymes along with translational machinery [59]. Most of the proteins are synthesized in the cytosol and imported as unfolded polypeptides into mitochondria through the outer and inner membrane translocators (TOM and TIM23, respectively) in a membrane potential ($\Delta\Psi m$) dependent manner (Figure 1.10). A team of chaperones and proteases are involved to ensure proper translocation of these pre-proteins followed by removal of the N-terminal MTS and folding into their native state. In the first stage, mtHsp70 and J-type co-chaperones participate in import of precursor proteins that later with help of Hsp60-Hsp10 chaperone system promote folding of the imported polypeptides (Figure 1.10) [55]. mtHsp70 harbors diverse roles in mitochondrial matrix. mtHsp70 is recruited to TIM23 translocase and at the channel it functions in the multi-subunit PAM (Presequence Translocase-Associated Motor) thereby interacting with the translocating polypeptides to drive their import through the channel into the matrix [60]. At

the same time mtHsp70 transiently binds to the incoming new polypeptides and to the fully translocated polypeptides keeping them in a partially folded state thereby promoting its proper folding (the so-called holdase function) [58]. The activity of mtHsp70 is coordinated by J-type co-chaperones (in the motor complex associated with the TIM23 translocase or MDJ1 in the matrix) and the nucleotide exchange factor MGE1 [55]. In addition, mtHsp70 has also a significant role in the biogenesis of iron sulfur cluster in the matrix [60]. After import, in the second step, two subunits of MPP processing metallopeptidase complex performs the proteolytic removal of the N-terminal MTS (Figure 1.10). After the removal of MTS, some proteins undergo further processing by mitochondrial intermediate peptidase (MIP/Oct1) that removes additional residues, reviewed in [55]. Moreover, following the MTS removal, multiple matrix proteins are stabilized by additional intermediate cleaving aminopeptidase Icp55 by removing the single destabilizing N-terminal amino acid residue (Figure 1.10), reviewed in [55]. This process is proposed to be similar to the N-end rule protein stabilization pathway in cytoplasm [61] however, the proteases involved in the degradation of destabilized polypeptides are not yet identified. The free peptides generated by the action of MPP or MIP is cleared by the mitochondrial presequence peptidase, Cym1/PreP. Additionally, this conserved metallopeptidase can also clear small (up to 65 amino acid residues) unstructured oligopeptides thereby preventing accumulation that may impair mitochondrial integrity, reviewed in [55]. In addition to mtHsp70, Hsp60 chaperonin consisting of both Hsp60 and Hsp10 subunits, assists a set of small soluble proteins to reach its functional state [58]. Hsp60 assembles into large barrel/cage like structures with co chaperone Hsp10 and facilitates in the folding of partially folded polypeptides after their release from mtHsp70 (Figure 1.10). Moreover, Hsp78 (in yeast) a chaperone protein of Hsp100 family has been identified which is involved in dissolution of aggregated proteins upon heat stress [58].

There are two highly conserved major AAA+ serine proteases in matrix, Lon/Pim1 and ClpXP that are involved in degradation of proteins that fail to fold or assemble in the matrix (Figure 1.10). Lon/Pim1 protease forms a large homooligomeric complex where each subunit contains ATPase and serine protease motifs. Lon is primarily involved in removing heat damaged and oxidatively damaged proteins, particularly iron–sulfur containing proteins such as aconitase, which are susceptible to oxidative damage [55,59]. In addition, Lon has been shown to bind mtDNA that may protect the DNA from oxidative

damage [59]. Lon has an important role in regulating the stability and expression of mtDNA via proteolytic control of the abundance of mitochondrial transcription factor TFAM, reviewed in [55]. Details about ClpXP are discussed in Section 1.8.

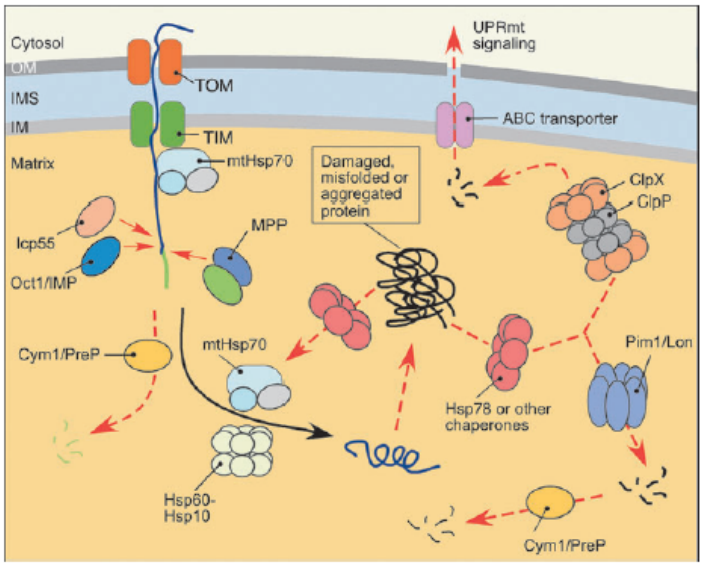

Figure 1.10 MQC in the matrix.

Multiple proteases and molecular chaperones regulate the matrix subproteome. The regulation involves control of protein maturation and accumulation and degradation of poly- and oligopeptides. Proper maturation of the precursor proteins transported via the TIM23 translocase complex requires removal of mitochondrial targeting sequence by MPP processing metallopeptidase complex and, in certain cases, additional stabilizing processing by intermediate peptidases MIP/Oct1 and Icp55. Resulting free targeting peptides, as well as other small oligopeptides, are removed by mitochondrial presequence peptidase Cym1/PreP. Subsequent protein folding is facilitated by Hsp family chaperones. Stress-damaged, misfolded, and/or aggregated proteins are recognized and cleaved by AAA+ proteases Lon/Pim1 and ClpXP. Peptides produced by these proteolytic events are either subjected to additional processing by oligopeptidases or extruded through ATP-binding cassette (ABC)-type transporters into the cytosol where they activate mitochondrial unfolded protein response (UPRmt) [55].

1.7.2 MQC in the IMM:

The mitochondrial IM is considered to be the most proteinaceous biological membrane since it houses a significant part of the mitochondrial proteome including the OXPHOS complexes and metabolite carriers [55,58]. As 13 polypeptides of RC are encoded by mitochondrial genome, a balance between the synthesis of nuclear and mitochondrial-encoded proteins is required. If the balance is disturbed it may accumulate unassembled subunits and assembly intermediates of RC. Hence one of the major challenges for mitochondrial protein homeostasis is to maintain proper assembly and function of the respiratory complexes. In addition, proteins residing in the IM are a prime target of

mitochondrial ROS. Therefore, there are various proteolytic systems in the IM that ensures proper removal of non-functional and damaged proteins [55,58]. IM-bound IMP proteolytic complex comprising of 2 subunits plays a role in processing the Mgr2 subunit of TIM23 translocase thereby stabilizing Mgr2 and promoting TIM23 assembly (Figure 1.12) [55]. Two membrane embedded ATP dependent metalloprotease complexes, termed AAA proteases are the major factors providing the quality control of the IM (Figure 1.11 & 1.12). The catalytic domain of m-AAA protease is exposed to the matrix (m-) side whereas i-AAA protease is active on the intermembrane space (i-) side of the membrane. AAA proteases are composed of subunits containing one or two transmembrane segments, an ATPase domain that is conserved throughout the AAA+ protein family of ATPases and a C-terminal Zn^{2+}-dependent metalloprotease domain. The m-AAA protease forms a large hetero-hexameric complex comprising of Yta10/AFG3L2 and Yta12/SPG7/Paraplegin subunits in yeast and human mitochondria whereas homo-oligomeric complex of m-AAA proteases comprising of AFG3L2 subunits can also be formed. Studies have shown that another subunit AFG3L1 that can substitute for AFG3L2 in rodents [62]. The i-AAA protease is similar to m-AAA except the fact that it forms homo oligomeric complex comprising of 6 subunits of Yme1/YME1L peptidase (Figure 1.11& 1.12) [59]. Unassembled and/or damaged sununits of OXPHOS complexes and nonnative membrane proteins are the known substrates of AAA proteases. Not only integral membrane proteins but also proteins peripheral to the IM like subunit 7 of ATP synthase are degraded by AAA protease. In addition to its role in quality control, m-AAA protease in involved in regulating the synthesis of respiratory chain subunits within mitochondria. Assembly of MrpL32, which is a subunit of large mitochondrial ribosome, into functional mitochondrial ribosomes, is dependent on the processing by m-AAA protease, thereby activating mitochondrial translation. Moreover, in yeast mitochondria, m-AAA protease is involved in the maturation of ROS scavenger cytochrome c peroxidase (Ccp1) in the intermembrane space thereby protecting against ROS damage [63]. Pcp1/PARL member of rhomboid family of serine proteases is part of the quality control team of IM, mediating processing of various IM polypeptides including cytochrome c peroxidase Ccp1 (processed in conjunction with m-AAA protease) (Figure 1.12) [55]. Prohibitins that form ring like structure comprising of Phb1 and Phb2 subunits has been shown to modulate the proteolysis by m-AAA proteases (Figure 1.11) [58]. The i-AAA proteases exhibit vital roles in regulating IM's integrity and dynamics via its proteolysis.

One example is the PRELI protein family members Ups1 and Ups2 that are involved in transport, synthesis, and accumulation of mitochondrial phospholipids, are regulated by the proteolytic activity of the i-AAA protease [55]. Secondly, it has been shown that the biogenesis of short isoform of the optic atrophy 1 (OPA1) dynamin-related GTPase, which is central to mitochondrial dynamics and mtDNA maintenance is regulated by the i-AAA protease [64,65]. It has been proposed that AAA proteases may cooperate with other proteases and adaptor like proteins. It has been shown that IM-associated peptidase Atp23 that is involved in maturation of the respiratory complex V [55] cooperates with the Yme1 proteolytic complex for the degradation of Ups1 (Figure 1.12) [66]. Similarly, Mgr1 and Mgr3 have been shown to possess adaptor like function facilitating the degradation of substrates by i-AAA protease in yeast mitochondria (Figure 1.11) [67,68]. Additionally, Afg1/LACE1, which is a matrix AAA+ protein has been proposed to act as an adaptor or cooperating partner of m-AAA complex thereby enhancing the degradation of its substrates (Figure 1.12) [69]. Oma1, a member of metallopeptidase family M48 is another protease in the IM that plays a role in quality control and has been shown to have overlapping function with m-AAA protease (Figure 1.11& 1.12) [69,70]. Oma1 has been proposed to process the long isoform of OPA1 thereby promoting IM fragmentation and activating the subsequent MQC system under stress conditions [64,71].

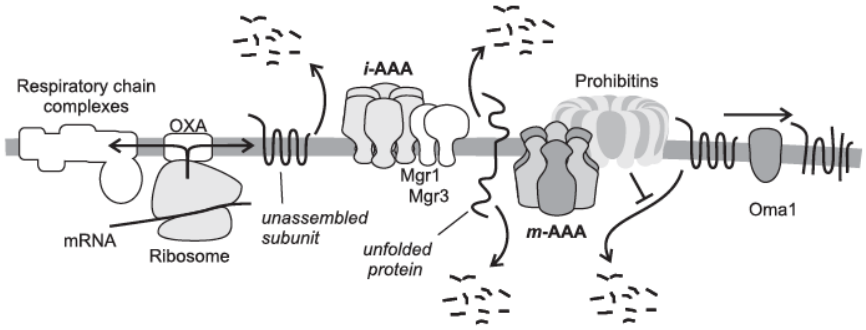

Figure 1.11 MQC in the IMM.

Newly synthesized subunits of RC are inserted into the IM by an insertion machinery (OXA). Unassembled subunits and unfolded proteins are degraded by AAA proteases. Assembly partners of AAA proteases modulate proteolytic activities. Oma1 mediates processing of membrane proteins [58].

1.7.3 MQC in the IMS:

Besides i-AAA protease, the protein quality control in the IMS is regulated by the high temperature requirement A2 serine protease (HtrA2/Omi/Ynm3). HtrA2/Omi is a homotrimer and the only protease found in the compartment that contains a PDZ-domain required for recognizing hydrophobic stretches of misfolded proteins (Figure 1.12) [55]. Htr2A that is shown to be modulated via PARL-assisted processing and by PTEN-induced putative kinase 1 (PINK1) dependent phosphorylation suggesting a possible role in regulation of mitophagy, reviewed in [55]. In addition, it has been proposed that HtrA2/Omi plays a role in apoptosis. Upon activation of apoptosis, HtrA2/Omi is released from the mitochondria into the cytosol and is responsible for cleaving the inhibitors of apoptosis, reviewed in [58]. Morever, Prd1/ Neurolysin which is an oligopeptidase localized in IMS has been shown to degrade cleaved presequences and small oligopeptides thereby preventing their accumulation in the IMS (Figure 1.12) [55].

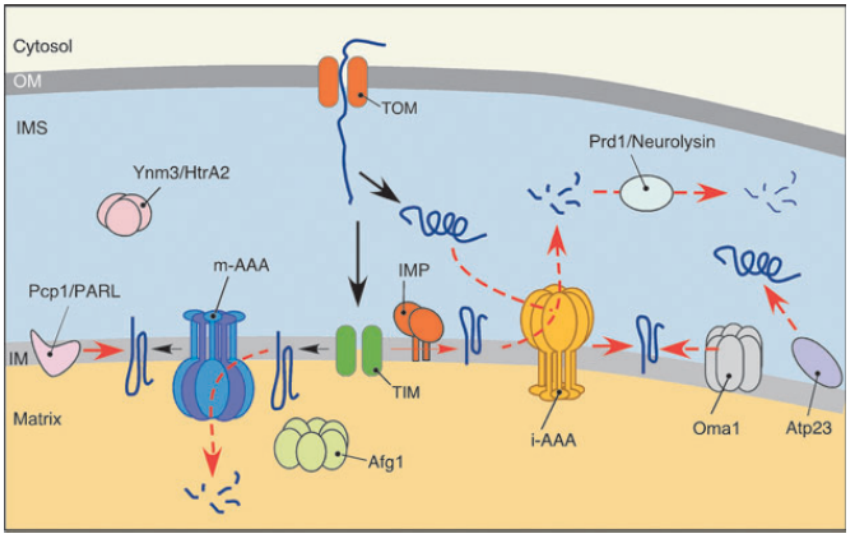

Figure 1.12 MQC in the IM and intermembrane space (IMS).

Complexity of mitochondrial IM anticipates vastly efficient systems to maintain protein homeostasis. These include two tightly coordinated proteases matrix-facing AAA metalloprotease (m-AAA) and intermembrane space-facing AAA metalloprotease (i-AAA), which along with other regulatory functions recognize excessive, misassembled, and damaged subunits of OXPHOS complexes associated with the IM. Another IM protease complex Oma1, with m-AAA-overlapping functions, is also proposed to play a major role in mitochondrial dynamics and homeostasis upon stress conditions. Rhomboid-like Pcp1/PARL protease is implicated in the intramembrane proteolysis of several IM proteins in yeast, whereas in mammalian cells, it also contributes to regulation of mitochondrial turnover. The IMS PMQC is less studied. In addition to the i-AAA, which exerts both proteolytic and chaperone functions toward IMS-localized proteins, the IMS subproteome appears to be regulated by oligopeptidase Prd1/Neurolysin and serine protease Ymn3/HtrA2 [55].

1.7.4 MQC in the OMM:

The ubiquitin protease degradation system (UPS) plays an important role in maintaining OM proteostasis where the proteins are modified by ubiquitination, extracted from the membrane and delivered to 26S proteasome for subsequent degradation in a process known as MAD (Figure 1.13) [59]. Several mitochondrial ubiquitin ligases associated with the cytosolic side of OMM such as MITOL/MARCH-V, Mdm30, MULAN/MAPL and RNF185 [55,59] have been identified so far. Similarly, another E3 ubiquitin ligase Parkin has been reported to ubiquitinate several OMM proteins thereby subjecting them to UPS mediated degradation [59]. However Parkin has been shown to possess dual roles, one in UPS mediated protein degradation and the other in clearance of damaged mitochondria via autophagy termed as mitophagy (discussed in section 1.7.6).

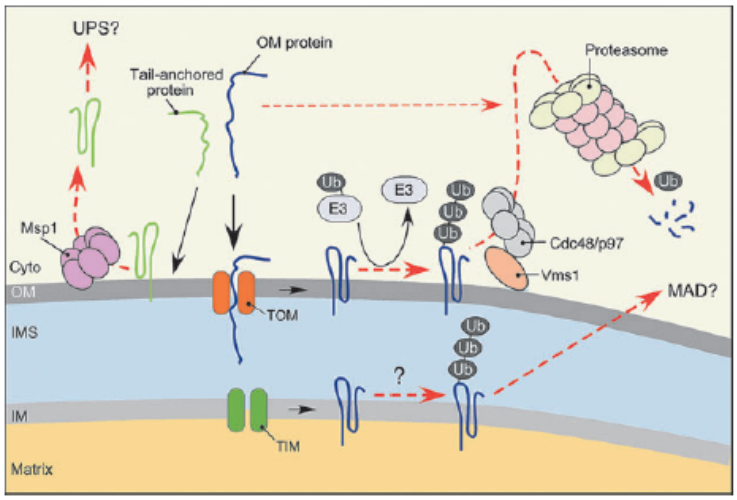

Figure 1.1.13 MQC in the OMM.
In addition to interception of mitochondria-destined proteins en route, the UPS provides an additional level of OM PMQC. It removes misfolded, damaged, or surplus proteins in the OM via the MAD process. MAD involves ubiquitylation by E3 ubiquitin ligases that tag proteins to be degraded and extraction of the peptides by the AAA+ protein VCP/Cdc48/p97 complex, which is, in turn, recruited to the OM through several mechanisms, including targeting by stressresponsive factor Vms1 or PINK1-Parkin functional tandem. Several reports suggest that some IM proteins might also be subject of MAD. Another AAA+ protein Msp1/ATAD1 targets and removes tail-anchored proteins mislocalized to the OM [55].

Recent studies have discovered VCP/p97/Cdc48-associated mitochondria stress responsive 1 (Vms1) protein that is primarily involved in extracting ubiquitinated proteins from multimeric complexes for recycling or degradation by the proteasome, in addition to its involvement in other cellular processes (Figure 1.13) [72]. In yeast mitochondria, AAA+ protein VCP/p97/Cdc48 translocates from cytosol to OMM under

stress conditions recruiting the Cdc48-Npl4 complex thereby providing an insight to the mechanistic understanding of MAD [55]. Moreover, VCP/p97/Cdc48 recruitment to damaged mitochondria has been shown to be dependent on Parkin suggesting that the mitochondrial ubiquitin ligases are involved in regulating both the mitochondrial proteome and mitophagy [73]. In addition, some recent findings have shown that proteins from all four different mitochondrial compartments were found to be ubiquitinated suggesting that the proteins may have retro translocated from their respective compartments to the OMM similar to the degradation of ER proteins via the ERAD pathway, reviewed in [59]. Recently, another OMM associated AAA+ protein Msp1/ATAD1 has been identified that is involved in preventing accumulation of mislocalized ER-destined tail-anchored proteins in the OM, thereby maintaining proper mitochondrial function (Figure 1.13) [55]. Msp1 has been proposed to be a part of the protein quality control team of mitochondria however it would be interesting to see if Msp1 is an independent part of the OMM quality control or an additional branch of MAD.

1.7.5 Mitochondrial dynamics - fusion & fission:

The fusion and fission of mitochondria is the first pathway of MQC at organellar level that comes into action when the molecular pathways get overloaded (Figure 1.9). Mitochondria undergo continuous fusion and fission events thereby mediating mitochondrial dynamics and facilitating the maintenance of mitochondrial function. Mitochondrial dynamics, by mixing or separation of contents, assists the even redistribution of mtDNA and proteome throughout the mitochondrial network, resulting in the dilution of damaged molecules and/or replenishment of depleted components in malfunctioning organelles [55]. Fusion and fission machinery is tightly regulated and respond differentially to different degree of stress: lower degree of stress favors fusion of mitochondria whereas higher stress tends to activate fission. The fusion and fission of mitochondrial membranes are mediated by four dynamin-related GTPases: Mitofusin 1 and Mitofusin 2 (MFN1 and MFN2) in the outer mitochondrial membrane and optic atrophy 1 (OPA1) in the inner mitochondrial membrane that controls the fusion event whereas the dynamin-related protein 1 (DRP1) triggers fission (Figure 1.14) [63,74]. Fusion not only promotes content mixing between intact and dysfunctional mitochondria but also protects mitochondria from mitophagy thereby protecting cells against excessive

degradation. When the level of stress is higher and protection via fusion is not sufficient, fission event kicks in by removing the damaged organelles from the network. DRP1 that mediates mitochondrial fission forms a collar around the mitochondrion's exterior and pinches it into two daughters (Figure 1.14) [44]. Out of these two daughters the one with higher membrane potential will be a preferable candidate of undergoing fusion whereas the other will be eliminated by mitophagy. Hence fission plays an important role in the quality control since it not only allows segregating irreversibly damaged mitochondria away from healthy network but also increases the number of mitochondria in the cell before mitochondrial biogenesis or cellular division [55].

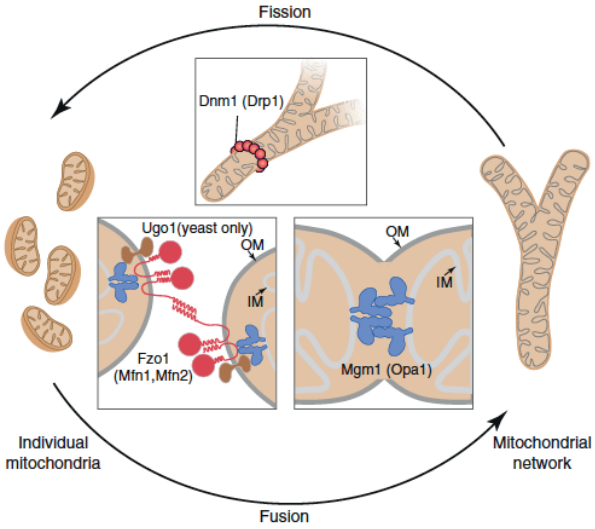

Figure 1.14 Mitochondrial dynamics in mitochondrial quality control (MQC).

Depicted is a simplified sketch showing the basic processes of mitochondrial fission and fusion (as exemplified by the yeast machinery, mammalian counterparts in parentheses) as well as their relation to mitophagy and the induction of apoptosis. The major fission factor is the small GTPase Dnm1 (Drp1), which interacts with other proteins to form a collar-like structure on the mitochondrial surface. Constriction of the Dnm1 collar severs the enclosed membranes and results in mitochondrial fission. The mitofusins Fzo1 (Mfn1, Mfn2) and Ugo1 are involved in the fusion of the outer membrane (OM). Subsequent fusion of the inner membrane is mediated by different Mgm1 (Opa1) isoforms. Mitochondrial dynamics, by the mixing and separation of contents, facilitate the maintenance of mitochondrial function [75].

1.7.6 Mitochondrial autophagy (Mitophagy):

Severely damaged and impaired mitochondria are eliminated from healthy mitochondrial network through a process called mitochondrial autophagy, or "mitophagy". Mitophagy is a form of selective autophagy ('self-eating') where the damaged mitochondria are engulfed by an autophagosome thereby delivering to lysosome for degradation and the breakdown products are made available for metabolism (Figure 1.15.A). This mitophagy

process of removing damaged mitochondria is considered as a highly specific MQC at organellar level (Figure 1.9). In mammalian system, two pathways regulating mitophagy has been characterized so far.

(a) PINK1 and the E3 ubiquitin ligase Parkin are the key players regulating mammalian mitophagy. In healthy mitochondria, PINK1 is imported in the mitochondria and cleaved by MPP and PARL. Following disruption of membrane potential, PINK1 instead of being imported into the mitochondria, accumulates in the OMM thereby recruiting the E3 ubiquitin ligase, Parkin (Figure 1.15.A), reviewed in [59]. Once Parkin is recruited its initiates ubiquitination of the OMM proteins like Hexokinase I, VDAC1, MFN1/2, and Miro [59]. Ubiquitination of MFN1/2 seems to be a prerequisite for promoting mitophagy. It is been proposed that during the degradation of these fusion proteins, Parkin may inhibit the refusion of damaged mitochondria to the healthy network thereby selecting the impaired one for mitophagy. The role of Miro has been shown to anchor mitochondria to the cytoskeleton and degradation of this protein results in the release of damaged mitochondria from the network of the healthy ones [76]. There is little disagreement in general regarding how PINK1 recruits Parkin to mitochondria. On one hand it has been proposed that Parkin directly interacts with PINK1 in the OMM [73] whereas several studies has shown cooperation of PINK1 and Parkin by sharing substrates. However, further studies are required to know the exact process. Parkin mediated ubuiquitination of mitochondrial substrates act as a signal for autophagic degradation, that is followed by the binding of the ubiquitin-binding adaptor p62 to both ubiquitinated substrates via its ubiquitin associated domain (UBA) and to LC3 on the autophagosomal membrane (Figure 1.15.A). This binding connects the ubiquitin tagged mitochondria directly to autophagosomes for engulfment. Therefore PINk1/Parkin quality control system appears to regulate at multiple levels starting from promoting fusion by degrading fusion proteins followed by releasing impaired mitochondria from the healthy network with subsequent tagging of the mitochondria via ubiquitination and finally initiating the formation of autophagosomes for final degradation [59].

(b) There is another system where proteins residing in the OMM can directly function as mitophagy receptors without the need for ubiquitination and adaptor proteins. The OMM proteins NIP3-like protein X (NIX; also known as BNIP3L) and BNIP3 can directly associate damaged mitochondria to autpohagosomes through molecular interactions with LC3 and gamma-aminobutyric acid receptor associated protein (GABARAP) on the

autophagosomes (Figure 1.15B). NIX contains WXXL-motif facing the cytosolic side that allows direct binding to LC3 and GABARAP thereby inducing mitophagy [59,77].

Thus mitophagy seems to be regulated by the above-mentioned two pathways where under stress condition the PINK1/Parkin pathway may take the front seat for the clearance of damaged mitochondria and the Nix/BNIP3 pathway may be crucial for maintaining healthy mitochondria under baseline conditions. However there might be a crosstalk between these two pathways irrespective of their distinct functions [59].

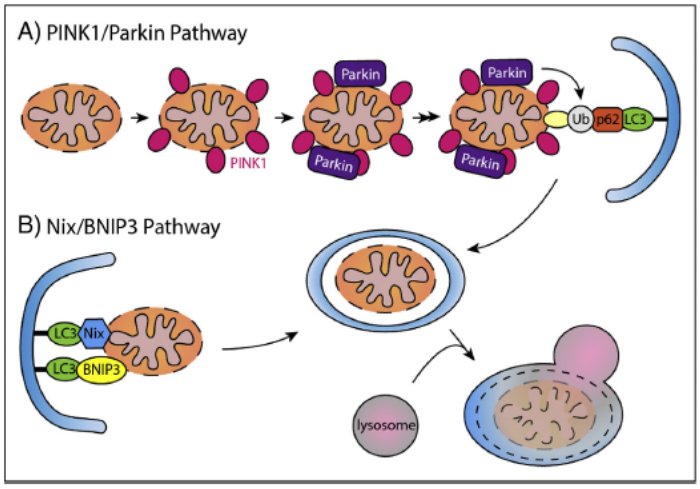

Figure 1.15 Mitochondrial Autophagy (mitophagy).

(A) Upon loss of mitochondrial membrane potential, PINK1 accumulates on the OMM surface. PINK1 recruits Parkin, which ubiquitinates OMM proteins, thus inducing engulfment of the mitochondrion by the autophagosome through p62 and LC3. (B) Nix and BNIP3 function as autophagy receptors on mitochondria by binding to LC3 on the autophagosome. Both pathways result in the autophagic sequestration of the mitochondrion, fusion with a lysosome, and degradation of the organelle [59].

1.7.7 Mitochondrial derived vesicles (MDV):

When the degree of damage to mitochondria exceeds the capacity of chaperones and proteases, portion of damaged mitochondria are pinched off for degradation (Figure 1.16). These vesicles known as mitochondria derived vesicles (MDVs) transport oxidized proteins to lysosomes for degradation [78]. The MDVs bud off functionally respiring mitochondria under normal condition and increases under oxidative stress conditions and has been shown to be independent of mitochondrial dynamics and mitophagy [78,79]. Though studies undergone have revealed that the cargo of these MDVs is highly selective depending on the type of oxidative stress, however it is still unclear why selected proteins are removed under specific oxidative stress [78]. This new mechanism of MDVs may

provide as additional strategy to remove parts of damaged mitochondrial membranes containing hard to dissociate protein complexes that cannot be catabolized within mitochondria [55]. Recently it has been reported the requirement of PINK1 and Parkin for the formation of these MDVs under oxidative stress (Figure 1.16) [80]. Though the role of PINK1 and Parkin is well established in mitophagy however this appears to represent another mechanism of MQC at organellar level.

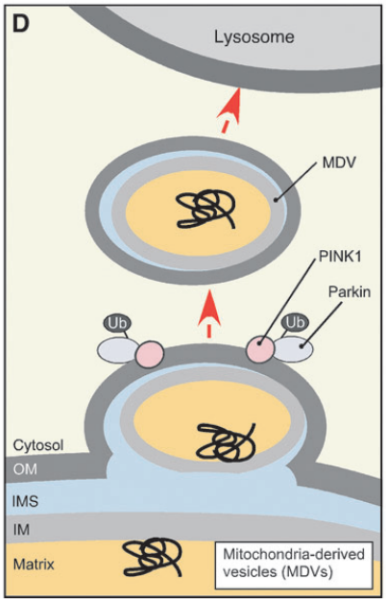

Figure 1.16 Mitochondrial derived vesicles.

Mitochondria-derived vesicles (MDVs), destined for lysosome, appear to represent yet another facet of organellar MQC. This mechanism allows selective removal of fragments of mitochondria without affecting the entire organelle. Reportedly, the MDVs contain oxidized cargo and lipids and their formation in mammalian cells depends on the function of PINK1 kinase and E3 ubiquitin ligase Parkin. When mitochondrial damage overwhelms the aforementioned mechanisms, failing organelles are segregated and targeted to autophagosomes, and subsequently to lysosomes where their content is degraded. The PINK1-Parkin functional tandem and UPS play important roles in the initiation of this process known as mitophagy [55].

1.7.8 Apoptosis:

When the load of the damage exceeds the capacity of candidates involved at molecular and organellar level, then quality control takes place at cellular level (Figure 1.9). There are two major pathways of apoptosis: extrinsic and intrinsic pathways responding to different stress induced signals or death stimuli. The intrinsic pathway of apoptosis is also known as the mitochondrial pathways due to the involvement of mitochondria that responds to different stimuli such as chemotherapeutic agents, serum starvation, irradiation and DNA damage (Figure 1.17) [81]. Mitochondria plays a key role since it is

not only the site for interaction of various anti-apoptotic and pro-apoptotic proteins determining the cell fate but also the site where the initiation of signals regarding the activation of caspases takes place.

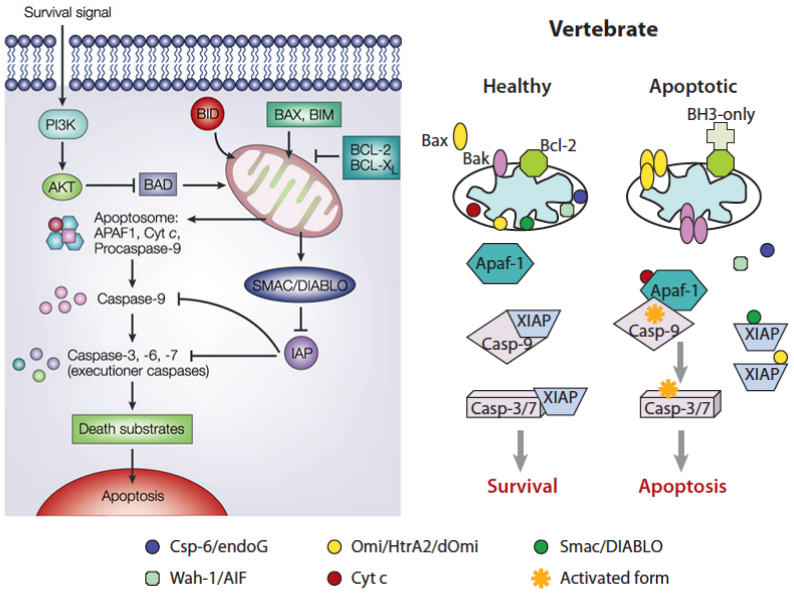

Figure 1.17 The role of mitochondria in apoptosis.

In healthy cells of vertebrates, Apaf-1 is in an auto-inhibited form and any basally processed caspase-9 and caspase-3/7 are bound by XIAP and hence, remain inactive. Upon apoptotic signaling, BH3-only proteins are either upregulated transcriptionally or activated through post-translational modification. They then bind to antiapoptotic Bcl-2 proteins to remove their inhibitory effect or activate Bax/Bak directly. Protein-lipid interaction might also be involved in Bax/Bak activation, which leads to their oligomerization and triggers release of Cyt c, Smac/DIABLO, endoG, AIF, and Omi/HtrA2. Cytosolic Cyt c then binds to Apaf-1 to induce apoptosome formation, leading to caspase-9 and caspase-3/7 activation. Smac/DIABLO and Omi/HtrA2 bind to XIAP to remove its inhibitory effect. Ortholog proteins in different species are labeled in the same color [81,82].

Whenever there is acute stress in the mitochondria the signals get transduced via one or more members of BH3-only subfamily of the pro-apoptotic Bcl-2 proteins that interacts with Bax subfamily of pro-apoptotic Bcl-2 proteins (Figure 1.17) [83]. This results in the formation of mitochondrial outer membrane permeabilization (MOMP) thereby releasing intermembrane proteins into the cytosol that will initiate apoptosis. Once cytochrome c (Cyt c) is released to the cytosol it binds to apoptotic protease activating factor 1 (APAF1) thereby initiating the formation of apoptosome. The apoptosome complex recruits and activates caspase-9, which in turn activates procaspase-3 (Figure 1.17). The activated caspase-3 along with other executioner caspases such as caspase-7 interacts with key death substrates thereby causing apoptosis. The apoptosis through mitochondria

can be inhibited at different levels by anti-apoptotic proteins such as anti-apoptotic BCL2 family members BCL2 and BCL-X_L and inhibitors of apoptosis proteins (IAPs). IAPs such as XIAP can bind to the activated caspase-9 thereby preventing its action on procaspase-3 (Figure 1.17) [83]. Therefore, second mitochondria-derived activator of caspase/ direct IAP binding protein with low pI (Smac/DIABLO) and Omi binds to XIAP thereby prohibiting their inhibitory effects on caspase activity and apoptosis can proceed (Figure 1.17) [81]. The involvement of anti-apoptotic proteins at different levels depicts a robust mechanism to prevent unnecessary activation of apoptosis in healthy cells.

1.8. CLPXP:

In order to perform mechanical work, AAA+ enzymes (ATPases associated with various cellular activities) utilizes the energy of ATP binding and hydrolysis to drive many biological processes [84,85]. CLPXP is one of the major AAA+ protease of the mitochondrial quality control located in the mitochondrial matrix that utilizes the energy of ATP binding and hydrolysis to carry out protein degradation within mitochondria. Most of the studies have been carried out extensively in prokaryotes especially in *E. coli* where we gained knowledge about ClpP structure, its specific substrates and its function. ClpXP is a build up of two proteins, hexamers of an AAA+ ATPase called ClpX and heptamers serine protease called ClpP. The ClpXP protease forms a hetero-oligomeric complex comprising of two hexameric rings of ClpX and two stacks of ClpP heptamers (Figure 1.18) [85]. EM studies have shown that the hexameric rings of ClpX may stack coaxially onto one or both ends of the ClpP tetradecameric barrel thereby forming a singly or doubly capped structures [86]. Under the circumstances when doubly capped ClpX6•ClpP14•ClpX6 complexes have formed, translocation at any given time appears to occur from only one of the two ClpX rings indicating a proper coordination of the activities of ClpX is required through ClpP [85]. ClpX possess various biochemical functions such as binding the substrates, adaptors and ClpP. ClpX component participates in recognizing short unstructured peptide sequences called degradation tags, degrons, or recognition signals in the protein substrates, unfolding the stable tertiary structure of the substrate and then translocating the unfolded polypeptide chain into the proteolytic compartment of ClpP for degradation.

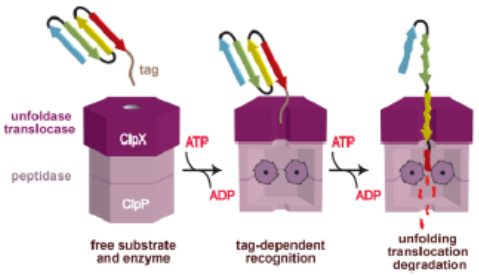

Figure 1.18 Cartoon model of substrate recognition and degradation by the ClpXP protease.

In an initial recognition step, a peptide tag in a protein substrate binds in the axial pore of the ClpX hexamer. In subsequent ATP-dependent steps, ClpX unfolds the substrate and translocates the unfolded polypeptide into the degradation chamber of ClpP for proteolysis, where it is cleaved into small peptide fragments [85].

This degradation tags or degrons in the protein targets are essential since they facilitate recognition and delivery to ClpXP for degradation. This unfolding and translocation process is entirely dependent on ATP binding and hydrolysis to power the changes in the enzyme conformation thereby driving the mechanical processes (Figure 1.18) [85]. The only function of ClpP is to serve as the proteolytic component of AAA+ proteases thereby cleaving any polypeptide chain that is being translocated into its chamber. The resulting peptides generated after cleavage are small enough to exit the chamber and be further degraded by exopeptidases to free amino acids. The proteolytic active sides of ClpP reside within a barrel shaped chamber that is formed by face-to-face stacking of two heptameric rings of ClpP [85]. Each of the 14 subunits of ClpP contains a serine active site for complete peptide hydrolysis with a classical Ser, Asp, His catalytic triad. Orthologs of ClpP are present throughout eubacteria, choloroplasts and mitochondria of many eukaryotic cells in its active form, which is a double-ring tetradecamer [87]. ClpP in its free state cannot degrade proteins longer than six amino acids [88].

Protein degradation by ClpXP is a vital cellular process that maintains protein homeostasis in various ways by removing damaged, misfolded or unassembled proteins. In addition to general protein quality control, ClpXP also contributes to stress adaptation, DNA damage repair, phage replication, and cell division. Studies have identified substrates of ClpXP in *E. coli* that were trapped in a ClpX dependent manner with a mutation of an active site in ClpP [89]. The substrates identified belong to a wide range including transcription factors, proteins involved in starvation and oxidative stress

response and metabolic enzymes. In addition to its general role in protein quality control, in *E. coli* it seems ClpXP also possess regulatory roles. One example is regulating the activity of transcription factors SigmaS and SigmaE involved in general and envelope stress responses thereby activating two-compartment specific stress response pathways [90]. In general stress response, the cellular concentration of SigmaS is regulated by ClpXP mediated degradation along with the adaptor protein regulator of SigmaS protein B (RssB) [91]. Due to its constant degradation by ClpXP, under normal conditions the cellular concentration of SigmaS is low. But under stress conditions, specific inhibitors of RssB (known as antiadaptors) prevents RssB mediated degradation thereby upregulating the transcription of SigmaS regulon [92–95]. In this case ClpXP acts as a negative regulator of the response whereas in the envelope stress response its acts as a positive regulator activating transcription of SigmaE regulon [90]. Another example is regulating the levels of RecN, which is a DNA damage repair protein that comprises an AA-COOH degron that is targeted to ClpXP for constitutive degradation [89]. When damage to DNA occurs, it induces the SOS transcriptional response thereby increasing the synthesis of recN mRNA and protein which starts to accumulate irrespective of their constant degradation by ClpXP [85]. Once the DNA damage induced SOS transcription slows down or stops, the levels of RecN in the cells become low due to degradation by ClpXP. In *E. coli*, ClpXP plays a very specific role in the quality control of protein synthesis. In case of stalled ribosomes during protein synthesis in *E.coli*, the ssrA tag is added to C-terminus of the incomplete nascent polypeptide chain by the tmRNA system. Th ssrA tags are recognized and degraded by ClpXP, reviewed in [85]. This ssrA tag consistis of 11 residues, but in order to be recognized by ClpX just two C-terminal alanines and the negatively charged α –carboxyl group (AA-COOH) are needed [96]. Other residues of the ssrA tag mediate binding of ClpXP adaptor protein stringent starvation protein B (SspB) that further accelerates the degradation of these ssrA tagged polypeptide chains [96,97].

Orthologs of ClpX and ClpP are present in most bacteria, mitochondria and chloroplasts. Hence it is involved in diverse roles in various organisms. In *E. coli*, lack of ClpP results in delayed recovery both from stationary phase and following a shift to nutrient poor media [98]. In *Bacillus subtilis*, ClpP has been shown to be involved in development of competence, motility, growth at high temperature and sporulation [99]. In *Caulobacter crescentus* ClpXP has been shown to be important for viability and cell cycle progression [100]. ClpP is essential for stress tolerance and biofilm formation in *Actinobacillus*

pleuropneumoniae [101] and virulence in many bacterial pathogens including *Staphylococcus aureus*, *Streptococcus pneumonia*, *Salmonella typhimurium*. In *Podospora anserine*, deletion of *ClpP* leads to an increase in lifespan of the fungus including a healthy phenotype [75]. In *C. elegans*, ClpXP has been shown to mediate the signals for unfolded protein response (UPR^{mt}) [102,103]. When the levels of unfolded proteins exceeds the amount of available chaperones then ClpXP mediates the degradation of these polypeptides into small peptides that are effluxed out of the mitochondria via the ABC transporter HAF-1 which then translocate activating transcription factor associated with stress-1 (ATFS-1) to the nucleus which further activates transcription of chaperones and proteases thereby restoring mitochondrial proteostasis [102–104]. This proposed model is suitable to sense any imbalance between the proteins of nuclear and mitochondrial origin especially subunits of OXPHOS complexes. Later another study showed that ATFS-1 bearing a mitochondrial targeting sequence at its N-terminus is imported into the mitochondrial matrix and degraded by Lon protease under healthy condition. However under stress condition, import of ATFS-1 ceases and it gets accumulated in the cytosol. ATFS-1 also possesses a nuclear localization sequence (NLS) close to its bZip domain, which is then trafficked to the nucleus where it initiates the transcription response to cope up with the stress [104]. In mammals, not much is known about the mechanism of UPR^{mt}. There have been few studies carried out in cultured mammalian cells that showed upregulation of chaperones mainly HSP60, CLPP protease and the transcription factor CHOP (C/EBP homology protein), gave the first indication of existence of UPR^{mt} [105,106]. Though the UPR^{mt} is conserved among worms, mice and humans it is still unclear if the stress sensing and signaling mechanisms are identical to the ones identified in worms. Recent study has identified mutations in *CLPP* causing Perrault syndrome in humans that is characterized by sensorineural hearing loss and ovarian failure [107].

1.9. Objectives:

There is relatively little knowledge regarding the biological role of CLPP and its specific substrates in mammals. Here we have generated *Clpp* conditional knockout mouse model in order to dissect the role of CLPP in mammalian mitochondria. With this model we aimed to analyze the consequences of absence of CLPP at physiological and molecular level. Moreover, since to date there are no studies regarding the specific substrates of CLPP in mammals, we aimed to identify its substrates. Substrates identification will allow us in understanding the role of CLPP in the affected molecular and biochemical processes

2. Materials and Methods

2.1 Mouse Experiments

2.1.1 Animal Care

Animal care was performed in accordance to the guidelines of the institutional animal care committee. All animal procedures were conducted in compliance with protocols, approved by local government authorities (Bezirksregierung Köln, Cologne, Germany) and were in accordance with NIH guidelines. Animals were housed in groups of 3 - 5 mice per cage at an ambient temperature of 22 – 24 ^{o}C and kept at a 12-hour light / 12-hour dark cycle. Animals were fed normal chow diet (NCD; Teklad Global Rodent 2018; Harlan) containing 53.5% carbohydrates, 18.5% protein, and 5.5% fat (12% of calories from fat) and drinking water. All animals had access to water and food, except 8 hours fasting prior to glucose tolerance test experiments. The animals were maintained in the pathogen-free animal facility of the CECAD. Mice were sacrificed by cervical dislocation.

2.1.2 Mouse handling and breeding

General mice handling and breeding was performed according to Silver (Silver, 1995).

2.1.3 Mice- Genetic ablation of Clpp gene by homologous recombination

Caseinolytic peptidase, ATP dependent proteolytic subunit (*Clpp*) gene targeting was carried out at Taconic Artemis, Germany, in Art B6/3.5 embryonic stem cell line on a genetic background of C57BL/6 NTac. LoxP sites flanked exons 3 to 5 of Clpp gene; positive selection marker (Puromycin resistance-PuroR) was inserted into intron 5 and was flanked by F3 sites. The targeted locus was transmitted through germline that resulted in heterozygous $Clpp^{+/PuroR\text{-}loxP}$ mice. These mice were bred with B6 Flp_deleter transgenic (TG) to remove the selection marker PuroR. Finally $Clpp^{+/loxP}$ mice were mated with mice expressing Cre recombinase under the promoter of *beta-actin* resulting in deletion of exons 3 to 5. This deletion finally resulted in loss of function of *Clpp* gene, by removing a part of the protease domain and generated a frameshift from exon 2 to 6. $Clpp^{+/-}$ heterozygous mice were intercrossed to obtain the $Clpp^{-/-}$ homozygous knockout mice. For all experiments, whole body *Clpp* deficient mice (homozygous knockout) and wildtype (control) littermates were used.

2.1.4 Body weight

After weaning, animals were fed on normal chow diet (NCD). The body weight of each mouse was assessed weekly or biweekly from age 4-36 weeks.

2.1.5 Analysis of body composition (NMR)

Body fat content of live animals was measured using Nuclear Magnetic Resonance (NMR) analyzer minispeq mq7.5 (Bruker Optik, Ettlingen, Germany).

2.1.6 Food intake and indirect calorimetry

Daily food intake was calculated as the average intake of NCD from custom made food racks within the desired time frame. Mice were allowed to adapt to the food intake settings for minimum five days. Food intake measurements were performed for three consecutive days and the weight of the racks were determined on a daily basis.

PhenoMaster System (TSE systems, Bad Homburg, Germany) was used for calorimetry measurements. This PhenoMaster system assessed metabolic performance and activity by an infrared light-beam frame (TSE systems). Mice were placed in metabolic chambers (7.1 litre) for an initial training period of five days thereby allowing them to adapt to the single housing. During this time proper adjustments to drinking and feeding dispensers were recorded. The calorimetric analysis was performed at 22-24°C over a period of 48-72 hours, which also recorded oxygen consumption, carbon dioxide production and locomotor activity (light barrier frame, TSE systems). Energy expenditure was measured via indirect calorimetric measurements. Food intake and indirect calorimetry experiemnets were performed with the help of Steffen Hermans and Jens Alber.

2.1.7 Determination of blood glucose and lactate levels

Tail bleeding of mice was performed as described (Silver, 1995). Glucose concentrations from venous blood, under fed and starved conditions were measured using glucose strips (Roche, Mannheim, Germany) with glucometer (ACCU-CHEK AVIVA, Roche, Mannheim, Germany). Similarly blood lactate levels under fed and starved conditions were measured using lactate strips with (Roche, Mannheim, Germany).

2.1.8 Glucose Tolerance Test

For glucose tolerance test animals were fasted for approximately 8 hours with proper access to drinking water. Blood glucose levels were measured using glucose strips with glucometer (ACCU-CHEK AVIVA, Roche, Mannheim, Germany) under fast condition (time point 0 min). Then 20% glucose solution (1-2g/kg body weight) was given via intraperitoneal (IP) injection and blood glucose was measured at 15, 30, 60, and 120

minutes. To determine glucose tolerance, the mean blood glucose values for each group of mice were plotted versus time.

2.1.9 Insulin Tolerance Test

Insulin tolerance test was performed using random fed animals. After determining the basal glucose level, insulin (0.75 U/kg body weight; Insuman Rapid 40 IU/ml) was injected intraperitoneally. Blood glucose was measured 15, 30, 45 and 60 minutes after injection. For assessing of insulin tolerance, blood glucose levels at each time point were calculated as percentage of its blood glucose levels at 0 minute (relative to basal glucose level) and then plotted versus time.

2.1.10 Measurement of rectal body temperature

Rectal body temperature was measured with the help of rectal thermometer (Bioseb Invivo Research Instrument) at two time points (time point o minute and 30 minutes) according to manufacturer's instructions.

2.2 Molecular Biology

2.2.1 Isolation of genomic DNA from mice tails

Mice tail biopsies were incubated overnight in lysis buffer (50 mM Tris-HCl pH 8.0, 2.5 mM EDTA, 0.5% (w/v) SDS, 0.1 M NaCl, 10 mg/ml Proteinase K; Applichem GmbH, Darmstadt, Germany) in a thermoshaker (Eppendorf, Hamburg, Germany) at 55^{o}C. DNA was precipitated by adding an equivalent volume of isopropanol (100%) and centrifuged at maximum speed for 20 minutes in a benchtop centrifuge (Eppendorf, Hamburg, Germany). The supernatant was removed and the pellet was washed with 70% (v/v) ice-cold ethanol and further centrifuged at maximum speed for 15 minutes. Then, the supernatant was removed and the DNA pellet was air dried for 2-5 minutes and was resuspended in 50µl dH_2O by shaking at 37 °C for 30 minutes.

2.2.2 Isolation of genomic DNA from mice tissues

A small piece of shock-frozen mice tissues (about 3 mm^3) was taken and incubated (2-12 hours) in lysis buffer (50 mM Tris-HCl pH 8.0, 2.5 mM EDTA, 0.5% (w/v) SDS, 0.1 M NaCl, 20 mg/ml Proteinase K; Applichem GmbH, Darmstadt, Germany) in a thermoshaker (Eppendorf, Hamburg, Germany) at 55^{o}C, upto a speed of 900 rpm until the tissue dissolves. DNA was then precipitated by adding 75 µl of 8 M potassium acetate

and 0.5 ml chloroform, and centrifuging at maximum speed for 15 minutes in a benchtop centrifuge at 4°C. The upper aqueous phase, without disturbing the lower chloroform phase, was transferred to a new 1.5 ml eppendorf tube. The tube was inverted several times after adding 1 ml of 95% ethanol (2 folds volume) to the samples where DNA gets visible. The samples were then centrifuged at maximum speed for 15 minutes at 4°C. The supernatant was removed and the pellet was then washed with ice-cold 70% (v/v) ethanol and centrifuged for an additional 5 minutes at 4°C. Afterwards, the samples were pulsed down and DNA pellets were resuspended in 100 µl ddH_2O depending on the size of the pellet. The pellet was left overnight at 4°C allowing for complete dissolve.

2.2.3 Isolation of total RNA from mice tissues

Total RNA was isolated from mouse tissue using TRIzol reagent (Life Technologies GmbH, Darmstadt, Germany). 50-100 mg (3 mm^3 tissue cube) tissues were dissected and transferred into Precellys (Bertin Technologies, Versailles, France) 1.5 ml tubes with beads. After adding 500µl of TRIzol reagent, the tissues were homogenized by a Precellys 24 (Bertin Technologies, Versailles, France) fast-prep machine at 5500 rpm for 2x30 seconds. Afterwards, instructions from the manufacturers were followed.

2.2.4 Quantification of nucleic acids

DNA and RNA concentrations were measured by sample absorption at 260 nm and 280 nm with a NanoDrop ND-1000 UV-Vis spectrophotometer (Peqlab, Erlangen, Germany). As an index of purity of DNA/RNA, a ratio greater than 2 of absorptions at 260 nm (DNA/RNA) divided by the absorption at 280 nm (protein) was used.

2.2.5 Polymerase chain reaction (PCR)

To detect whether the mouse genome contains wild type (+/+), floxed (loxP flanked) exons or full body knockout (-/-) and cre-recombinase gene (cre), PCR reactions were done with primers described in Table 2.1.

Reactions were performed in a Verti Thermal Cycler (Applied Biosystems, Life Technologies GmbH, Darmstadt, Germany) in a total reaction volume of 20 µl. For wild type (+/+) and knockout (-/-) PCR, the following reagents were added to 1 µl of sample DNA; 11.55 µl of dH_2O, 4 µl of 5x GoTaqBuffer (Promega), 1 µl of dNTPs (1.25 mM each), 0.8 µl of each primer (10 µM), and 0.05 µl of GoTaq (5 U/µl, Promega) For cre PCR, 10.5 µl of dH_2O, 4 µl of 5x GoTaqBuffer, 3.2 µl of dNTPs (1.25 mM each), 0.6 µl of each primer (10 µM) and 0.1 µl of GoTaq (5 U/µl) were added to 1 µl of sample DNA. Bands were determined by visualization of PCR products using 2% agarose gel with

ethidium bromide or GelRed (Biotium, Hayward, CA).

Table 2.1 Genotyping PCR primer sequences

Primer	Sequence
Forward$^{+/+}$	GTGGATGATGGTCAGTAGAATCC
Reverse$^{+/+}$	CCCAGACATGATTCCTAGCAC
Forward^{KO}	TGTGCATTCTTACCATAGTCTGC
Forward^{cre}	CACGACCAAGTGACAGCAAT
Reverse^{cre}	AGAGACGGAAATCCATCGCT

PCR programs for wild type (+/+) and knockout (-/-) began with 5 minutes of denaturation at 95^{o}C, followed by 28 cycles comprising of denaturation at 95^{o}C for 30 seconds, annealing at 60^{o}C for 30 seconds and elongation at 72^{o}C for 1 minute, and a final elongation step at 72^{o}C for 10 minutes.

PCR programs for cre PCR started with 5 minutes of denaturation at 95^{o}C, followed by 35 cycles consisting of denaturation at 95^{o}C for 30 seconds, annealing at 53^{o}C for 30 sec and elongation at 72^{o}C for 30 sec, and a final elongation step at 72^{o}C for 5 min.

2.2.6 Southern blot analysis for mitochondrial DNA (mtDNA) quantification

After DNA was isolated from mice tissues (as mentioned earlier), 5 µg DNA was digested by *SacI* restriction enzyme (New England Biolabs, Ipswich, USA) overnight at 37^{o}C. DNA was precipitated by addition of 10 µl 5M NaCl and 500 µl 95% EtOH (ice cold) to the digestions. The samples were mixed very well and then were placed at -80^{o}C for 30 minutes. Next the samples were centrifuged at 14000 rpm for 15 minutes in a benchtop centrifuge at 4^{o}C. After discarding the supernatant, the pellet was washed with 1 ml 70% EtOH by centrifuging at 14000 rpm for 15 minutes at 4^{o}C. The supernatant was removed, the pellet was air dried and dissolved in 20µl dH_2O. After measuring the concentration of DNA (as mentioned before) 6 µl 6X DNA loading dye (Fermentas, St. Leon-Rot, Germany) was added to the DNA samples and were run on a 0.8% agarose gel with 5 µl PeqGreen, at 35V overnight. Next day, an image of the gel along with the ladder was captured in BioRad Universal Hood II. Then the gel was soaked in 0.2 M HCl for 10 minutes with gentle shaking followed by rinsing twice with dH_2O. Further the gel was denatured in denaturation solution (1.5 M NaCl and 0.5 M NaOH) with gentle

shaking twice for 20 minutes. After rinsing shortly with dH_2O, the gel was then neutralized with gentle shaking twice for 20 minutes in neutralization solution (1.5 M NaCl and 1 M Tris-HCl pH 7.5). After rinsing shortly with water again, the gel was blotted overnight. The blot was assembled by preparing a sandwich with two long, bridging Whatman papers -presoaked in 20X saline-sodium citrate (SSC) (3M NaCl and 300 mM sodium citrate)-, two Whatman papers similar to the size of the gel (presoaked in 20X SSC), gel (surrounded tightly with plastic wrap to circumvent shortcuts), Hybond N+ nylon membrane (GE Healthcare, Munich, Germany), two Whatman papers similar to the size of the gel (presoaked in 20X SSC), about 10-15 cm of paper staple, glass plate and a weight of 500 g on top. After disassembling of the blot, the wells were marked with pen and the membrane was soaked for 2 minutes in 2X SSC solution (without shaking). Then the membrane was air dried for 10 minutes by placing them in between 2 Whatman papers. Finally the membrane was baked at 80^{o}C for one hour and thirty minutes. Afterwards, the membrane was placed in a glass hybridization bottle and prehybridized in 10 ml rapid-hyb buffer (GE Healthcare, Munich, Germany) for 60 minutes at 65^{o}C. In the meantime, the probe, PAM1 – for the whole mouse mitochondrial genome- was labelled with Prime-It II Random Primer Labeling Kit (Agilent Technologies, Waldbronn, Germany) and α-^{32}P-dCTP for 15 minutes. The probe was denatured at 99^{o}C for 5 minutes and was added to the glass hybridization bottle and hybridized for 2 hours at 65^{o}C. The membrane was then first washed in 2X SSC/0.1% SDS for 20 minutes at room temperature, then in 1X SSC/0.1% SDS for 20 minutes at 65°C and finally in 0.1X SSC/0.1% SDS for for 20 minutes at 65°C. The membrane was wrapped in a plastic bag and exposed to Amersham Hyperfilm (GE Healthcare, Munich, Germany) overnight.

2.2.7 Northern blot analysis for mRNA, rRNA and tRNA levels

After RNA was isolated (as mentioned earlier) and estimating the concentration of RNA, 2 µg total RNA was taken and topped up with nuclease-free H_2O to 10 µl. 10 µl RNA Loading dye (Sigma Aldrich, Seelze, Germany) was added to the samples and heated to 70^{o}C for 10 minutes. The agarose gel was prepared by adding 72 ml DEPC H_2O to 1.2 g Agarose (Agarose-LE from Ambion, Life Technologies GmbH, Darmstadt, Germany). The mixture was heated up in the microwave till it dissolves followed by addition of 10 ml of 10X MOPS Running Buffer (Ambion, Life Technologies GmbH, Darmstadt, Germany) and 18 ml farmaldehyde solution (Sigma Aldrich, Seelze, Germany). The gel solution was mixed well and poured to solidify. After loading the samples in the gel, it

was run in 1X MOPS Buffer for 2 hours at 130 V. The gel was visualized under UV and an image was taken with BioRad Universal Hood II. The gel was washed three times for 15 minutes with clean, nuclease-free H_2O and then soaked in 20X SSC solution for 20 minutes. The gel was blotted overnight following the same sandwich technique mentioned in Southern blot analysis. After disassembling the blot, the wells were marked and the membrane was UV-crosslinked with Stratalinker UV Crosslinker (Agilent Technologies, Waldbronn, Germany) twice at 200000 Joule/cm^2. The membrane was placed in a glass hybridization bottle and prehybridized in 10 ml rapid-hyb buffer (GE Healthcare, Munich, Germany) for 60 minutes at 65^oC. Similar to Southern blot analysis, the probes for mitochondrial-encoded protein coding genes and ribosomal RNA were prepared with Prime-It II Random Primer Labeling Kit (Agilent Technologies, Waldbronn, Germany) and α-^{32}P-dCTP. For preparation of tRNAs probes, 10 pmol of the probe was added to 2 µl of 10X T4 Polynucleotide Kinase Reaction Buffer (New England Biolabs, Ipswich, USA), 1 µl T4 Polynucleotide Kinase (New England Biolabs, Ipswich, USA), 12 µl dH_2O and 20 µCi γ-^{32}P-dATP. After the mixture was incubated at 37^oC for 90 minutes, the probe was added to the glass hybridization bottle and hybridized for 2 hours at 65^oC (for mRNAs) or 42^oC (for tRNAs). The membrane was washed firstly in 2X SSC/0.1% SDS for 20 minutes at room temperature, followed by washing in 2X SSC/0.1% SDS for 20 minutes at 65/42°C and finally in 0.2X SSC/0.1% SDS for 20 minutes at 65/42 °C. The membrane was wrapped in a plastic bag and exposed to Amersham Hyperfilm (GE Healthcare, Munich, Germany) overnight. The probes mentioned in [39] are used for Northern blot analysis.

2.2.8 Reverse transcriptase PCR (Gene expression analysis)

RNA from tissues was isolated (as mentioned earlier) and the concentration was measured. In case of probes that didn't span exon boundaries to quantify RNA expression of target genes, DNase digestion as performed. (DNA-free Kit, Ambion, Life Technologies GmbH, Darmstadt, Germany) 2 µg of RNA was reversely transcribed into cDNA using High capacity reverse transcription kit (Applied Biosystems, Life Technologies GmbH, Darmstadt, Germany). For quantitative real-time PCR, 50 ng of cDNA was amplified using Taqman Assay-on-Demand kits (Applied Biosystems, Life Technologies GmbH, Darmstadt, Germany; see Table 2.2). The only exceptions where Brilliant III Ultra-Fast SYBR Green QPCR Master Mix (Agilent Technologies, Waldbronn, Germany) was used are listed in Table 2.3. Real-time PCR analysis was

performed in ABIPRISM 7700 Sequence detector (Applied Biosystems, Life Technologies GmbH, Darmstadt, Germany). Relative expression of the target genes was adjusted for total RNA content by Hypoxanthine-guanine phosphoribosyltransferase (*HPRT*) or TATA-binding protein (*TBP*). Relative expression of mRNAs was determined using a comparative method ($2^{-\delta\delta CT}$) according to the ABI Relative Quantification Method.

Table 2.2 Probes used for quantitative real time PCR

Gene	Catalogue number
Clpp	Mm00489940_m1
Clpx	Mm00488586_m1
Gfm1	Mm00506853_m1
12S	AJBJWSP
16S	Mm04260181_s1
ATP6	Mm03649417-g1
ND5	AIHSNT9
COXIII	Mm04225261_g1

Table 2.3 SYBR Green probes used for quantitative real time PCR

Gene	Forward	Reverse
Eral1	GGACCGTATCCTTGGATTTTCTC	GAGGACCCGTGGATTCTCAG
p32	AGATCCAGAAACACAAGTCCCT	CCTCCTCACCATCAAATGTTGG
Pnpt1	AATCGGGCACTCAGCTATTTG	CAGGTCTACAGTCACCGCTC
Mrpp1	TGTCCTCCAAAGCACCTTCTT	TGAATGCTCGACTTCATTGTAGC
Trap1	CAGGACAGTTATACAGCACACAG	CTCATGTTTGGAGACAGAACCC
Hsp60	GCCTTAATGCTTCAAGGTGTAGA	CCCCATCTTTTGTTACTTTGGGA
Lonp1	ATGACCGTCCCGGATGTGT	CCTCCACGATCTTGATAAAGCG
Afg3l2	GTTGATGGGCAATACGTCTGG	GACCCGGTTCTCCCCTTCT

2.3 Biochemistry

2.3.1 Isolation of proteins from tissues

Proteins were isolated from mice tissues by *organ lysis buffer* (50 mM HEPES, pH 7.4, 1% Triton X-100, 100 mM NaF, 10 mM sodium orthovanadat, 10 mM EDTA, 0.2% SDS, 100 mM NaCl, dH_2O and one tablet of protease inhibitor, EDTA-free (Roche, Mannheim, Germany). A piece of tissue, (around 3 mm^3) added to Precellys (Bertin Technologies, Versailles, France) 1.5 ml tubes with beads containing 500 µl of organ lysis buffer. Homogenization was done using a Precellys 24 (Bertin Technologies, Versailles, France) fast-prep machine at 6500 rpm for 2x20 seconds with 30 seconds pause. Following disruption, the homogenate was incubated on ice for 10 minutes and centrifuged at 13000 rpm for 45 minutes at 4°C. The supernatant was transferred to a new tube and the concentration of proteins was measured using Bradford reagent (Sigma Aldrich, Seelze, Germany) following the manufacturer's instructions. Finally, the proteins were stored at -80 °C till further use.

2.3.2 Isolation of mitochondria from tissues except skeletal muscle

After sacrificing the mice, tissues were rinsed well to remove blood and then transferred into a 50 ml falcon tube containing 5 ml of mitochondria isolation buffer (MIB: 100 mM sucrose, 50 mM KCl, 1 mM EDTA, 20 mM TES, 0.2% BSA free from fatty acids, pH 7.2). For heart, 1mg/ml of Subtilisin A was added and transferred into a glass homogenizer tube. The tissue was homogenized by Sartorius at 1000 rpm with 10-12 strokes until the solution became homogeneous. The homogenate was transferred into 50 ml Falcon tube with addition of 15 ml of MIB and centrifuged at 8500 g for 5 minutes at 4°C. The supernatant comprising floating fat was discarded and the pellet was resuspended in 30 ml MIB by shaking. The samples were then centrifuged at 800 g for 5 minutes at 4°C and the supernatant comprising mitochondria were transferred into new 50 ml tube. To pellet mitochondria, the supernatant was finally centrifuged at 8500 g for 5 minutes at 4°C. After discarding the supernatant the mitochondrial pellet was resuspended in 150 µl MIB without BSA. The concentration of mitochondria was measured using Bradford reagent (Sigma Aldrich, Seelze, Germany) following the manufacturer's instructions.

2.3.3 Isolation of mitochondria from skeletal muscle

After sacrificing the mice, skeletal muscle tissue was dissected and placed in 10 ml of ice-cold PBS supplemented with 10 mM EDTA. After removing hairs/blood the tissues were transferred onto a petri dish and cut into small pieces. The pieces were resuspended in 15 ml of ice-cold PBS/10 mM EDTA with addition of 0.05% trypsin and transferred into a 50 ml Falcon tube. Following incubation on ice for 30 minutes, the samples were centrifuged at 200 g for 5 min at 4°C. The supernatant was discarded and the pellet comprising tissues was resuspended in IBM1 (67 mM Sucrose, 50 mM Tris-HCl pH 7.4, 50 mM KCl, 10 mM EDTA, 0.2% BSA free from fatty acids, pH 7.4). The pieces were transferred to a glass homogenizer tube and homogenized by Sartorius at 1600 rpm with 10 long strokes until the solution became homogeneous. The homogenate was transferred into 50 ml Falcon tube and centrifuged at 700 g for 10 minutes at 4°C. The supernatant was transferred into a new 50 ml tube and was centrifuged at 8000 g for 10 minutes at 4°C to pellet mitochondria. After discarding the supernatant the mitochondrial pellet was resuspended in 5 ml of IBM2 (250 mM sucrose, 10 mM Tris-HCl, pH 7.4, 0.3 mM EGTA-Tris,). It was further centrifuged at 8000 g at 4°C for 10 minutes. The supernatant was discarded and the mitochondrial pellet was resuspended in 150 µl of IBM2. The concentration of mitochondria was measured using Bradford reagent (Sigma Aldrich, Seelze, Germany) following the manufacturer's instructions.

2.3.4 Purification of mitochondria

Mitochondria were isolated from heart as mentioned earlier. The final mitochondrial pellet was resuspended in 500 µl of 0.6 M sucrose. A gradient of 6 ml of 1.5 M sucrose and 6 ml of 1 M sucrose was prepared using 12.5 ml of ultracentrifuge tubes (Beckman Coulter). 500 µl of mitochondria was layered on top of the gradient and spun at 22,000 rpm for 30 minutes at 4°C. After ultracentrifugation, mitochondria were collected from the interface of two different solutions of sucrose concentrations and five times the volume of solution buffer (10 mM Tris-HCl, pH 7.5; 5 mM EDTA) was added. After centrifuging it for 10 minutes at maximum speed on a benchtop centrifuge, the final purified mitochondrial pellet was stored at -80°C.

2.3.5 Blue Native polyacrylamide gel electrophoresis (BN-PAGE) and in-gel activity of respiratory chain complexes I and IV

BN-PAGE was performed according to the manufacturer’s specifications using the Novex Bis-Tris system (Life Technologies GmbH, Darmstadt, Germany). For

supercomplexes, 10% digitonin was used. After the samples were transferred to PVDF membrane using wet transfer, immunodetection of mitochondrial protein complexes was performed. *In-gel* activity for Complex I was measured by incubating BN-PAGE gel in 0.1 mg/ml NADH, 2.5 mg/ml nitrotetrazolium blue (NTB; Sigma-Aldrich, Seelze, Germany) and 5mM Tris (pH 7.4) for 1 hour. *In-gel* activity for Complex IV was measured by incubating BN-PAGE gel in 0.24 unit/ml catalase, 10% Cytochrome C and 0.1% diaminobenzidine tetrahydrochloride (DAB; Sigma-Aldrich, Seelze, Germany) in 50 mM Tris (pH 7.4) for 1 hour at 37°C.

2.3.6 Western blot analysis

Protein extracts from tissues were thawed and 40 µg of proteins was mixed in SDS-PAGE sample buffer (2X Laemmli sample buffer: 4% SDS, 20% glycerol, 120 mM Tris-HCl pH 6.8, 0.02% bromophenol blue and 200 mM DTT). The protein samples were boiled and separated by SDS PAGE (either using Tris-Glycine gels or Tris-HCl gels from Criterion from BioRad, California, USA). The protein samples were blotted to nitrocellulose membranes (GE Healthcare, Munich, Germany) using wet transfer method. Membranes were blocked in 5% Milk-PBST for 1 hour at room temperature and incubated overnight at 4°C in primary antibodies (Table 2.4) diluted in 5% Milk-PBST. After washing the membrane with PBST, 3 x 5 minutes, it was incubated for 1 hour at room temperature in secondary antibody after diluting in 5% Milk-PBST or 1X PBST (all secondary antibodies were from Sigma Aldrich, Seelze, Germany and the dilution used was 1:2000). The membrane was washed again 3 x 5 minutes with PBST and ECL solution (GE Healthcare, Munich, Germany) was added to the membrane to visualize the signals after exposing to Amersham Hyperfilm chemiluminescent film (GE Healthcare, Little Chalfont, UK). Films were developed in an automatic developer (Kodak, Stuttgart, Germany). ImageJ software was used for western blot quantification as intensity per mm^2.

Table 2.4 Primary antibodies used for Western blot

Antigen	Distributor	Dilution
AFG3L2	Polyclonal antisera made by Prof. Elena I. Rugarli	1:1000
CLPP	Sigma Aldrich, Seelze, Germany	1:1000
CLPX	Sigma Aldrich, Seelze, Germany	1:1000
EF-TU_{mt}	Polyclonal made by Assistant Prof. Nono Tomita-Takeuchi	1:1000
EF-$G1_{mt}$	Abcam (Cambridge, UK)	1:500
ERAL1	Proteintech (Chicago, USA)	1:1000
IF2-mt	Polyclonal made by Prof. Aleksandra Filipovska	1:1000
IF3-mt	Polyclonal made by Prof. Aleksandra Filipovska	1:1000
HSP60	StressMarq Biosciences (British Colombia, Canada)	1:1000
LON	Abcam (Cambridge, UK)	1:1000
LRPPRC	Agrisera (Sweden)	1:1000
mtHSP70	Abcam (Cambridge, UK)	1:1000
MRPL-12	Abcam (Cambridge, UK)	1:500
MPRL-37	Sigma Aldrich, Seelze, Germany	1:1000
MRPS-35	Proteintech (Chicago, USA)	1:1000
MRPS-15	Polyclonal made by Prof. Dr. Nils-Göran Larsson	1:1000
PNPT1	Proteintech (Chicago, USA)	1:1000
P32	Millipore (Massachusetts, USA)	1:1000
TRAP1	BD Bioscience (New Jersey, USA)	1:1000
TOM20	Santa Cruz (Dallas, USA)	1:1000
VDAC	Abcam (Cambridge, UK)	1:1000
ATP5a1	Mitosciences (Abcam, Cambridge, UK)	1:1000
COXIV	Invitrogen (Karlsruhe, Germany)	1:1000
UQCRC2	Invitrogen (Karlsruhe, Germany)	1:1000
SDHA	Invitrogen (Karlsruhe, Germany)	1:10000
NDUFA9	Invitrogen (Karlsruhe, Germany)	1:1000
COX5B	Invitrogen (Karlsruhe, Germany)	1:1000
COXIII	Invitrogen (Karlsruhe, Germany)	1:1000
ACTIN	Santa Cruz (Dallas, USA)	1:5000
TUBULIN	Sigma Aldrich, Seelze, Germany	1:1000

2.3.7 Measurement of the respiratory chain complex activity

The measurements of respiratory chain enzyme complex activities were performed according to [108].

2.3.8 Measurement of the rate of oxygen consumption

Measurement of oxygen consumption rates was performed with OROBOROS Oxygraph-2k for high-resolution respirometry (Oroboros Instruments, Vienna, Austria) following substrate-uncoupler-inhibitor-titration (SUIT) protocol. First oxidative phosphorylation (OXPHOS) state for Complex I was measured with addition of substrates of Complex I (5 µl of 2 M pyruvate, 5 µl of 0.8 M malate and 10 µl of 2 M glutamate and 8 µl of 0.5 M

ADP) to 25 µg of mitochondria. Then substrate for Complex II (20 µl of 1 M succinate) was added to measure OXPHOS state for Complex I and II. Next, to evaluate mitochondrial coupling or state L respiration (oligomycin-inhibited LEAK respiration-state L), 1 µl of 4 mg/ml oligomycin was added that inhibited ATP synthase. This state L respiration is mainly caused by compensation for proton leak after inhibition of ATP synthase. Maximum respiration was achieved by a multiple-step FCCP titration (ETS-electron transfer system capacity state). Addition of FCCP reflected ETS capacity at un-coupled respiration. Then Complex I was inhibited by 0.5 µl of 2 mM rotenone, to estimate the contribution of Complex II to the maximal ETS capacity. Finally 1 µl of 5 mM antimycin A was added to analyze the residual oxygen consumption (ROX-state).

2.3.9 Analysis of de novo transcription and translation in isolated mitochondria

In organello transcription assay was performed as described earlier [39]. Mitochondria were isolated (as mentioned before) and 1 mg of mitochondria was resuspended in incubation buffer (25 mM sucrose, 75 mM sorbitol, 100 mM KCl, 10 mM K_2HPO_4, 50 µM EDTA, 5 mM $MgCl_2$, 10 mM Tris-HCl pH 7.4, 1 mg/ml BSA, 1 mM ADP, 10 mM glutamate and 2.5 mM malate,). 40 µCi of α-^{32}P-UTP was added to the mitochondria and incubated for 1 hour at 37 °C on rotary shaker for pulse. After incubation, samples were centrifuged at 13,000 g for 2 minutes to remove unincorporated nucleotides. The pellet was washed twice with 1 ml of washing buffer (10% glycerol, 10 mM Tris-HCl pH 6.8 and 0.15 mM $MgCl_2$) and resuspended in 1 ml of TRIzol reagent (Life Technologies GmbH, Darmstadt, Germany) for RNA isolation (as mentioned earlier). The RNA was further analyzed by Northern blotting (as mentioned earlier) and radiolabeled transcripts were visualized by autoradiography.

In organello translation in mitochondria from heart and liver was performed as previously described [109]. Skeletal muscle mitochondria were incubated in translation buffer containing 25 mM sucrose, 75 mM sorbitol, 100 mM KCl, 1 mM $MgCl_2$, 0.05 mM EDTA, 10 mM Tris–HCl, 10 mM K_2HPO_4 pH 7.4, 1 mg/ml fatty acid-free bovine serum albumin (BSA) with addition of 10 mM glutamate, 2.5 mM malate, 1 mM ADP. *In organello* translation was performed for 1 hour with addition of ^{35}S-met (0.25 mCi/ml) at 37°C. After this period, 100 mM of non-radioactive methionine was added to the translation buffer to stop the protein synthesis reaction. The mitochondrial was washed twice with washing buffercontaining 5 mM of non-radioactive methionine. Finally the mitochondrial pellet was resuspended in translation buffer containing all amino acids,

including 60 µg/ml of methionine and cysteine that was divided into equal halves. First half of mitochondria were isolated by incubation in the SDS-PAGE loading buffer, while the other half was incubated for additional 3 hours for the "cold-chase" experiment. After 3 hours the samples were processed similar to Pulse. All the translation products from Pulse and Chase were separated by SDS-PAGE. The gels were stained with Coomassie Brilliant Blue R-250 (MERCK), then incubated in 5% glycerol and amplify solution (GE Healthcare, Munich, Germany) respectively. Finally the gel was dried and the newly synthesized polypeptides were detected by autoradiography.

2.3.10 In cello translation in mouse embryonic fibroblasts (MEFs)

In cello translation in MEFS was performed. In brief, cells were grown in a 100 mm plate and when the plate was 75-90% confluent, medium was removed and cells were washed twice with 5 ml of labeling medium (- Dulbecco's modified Eagle's medium, high glucose; cysteine and methionine free, 10 % dialyzed FBS, glutamine, sodium pyruvate). Meanwhile the labeling medium and normal growth medium (DMEM, high glucose; 10% FBS, glutamine and sodium pyruvate; Gibco Life Science, USA) were equilibrated to 37 °C and 5% CO2. Next, 25 µl of emetine (Sigma), irreversible inhibitor of cytoplasmic translation was added to 5 ml of labelling medium and incubated for 5 minutes in the incubator. 70 µl of ^{35}S methionine and cysteine mixture was added and incubated at 37°C and 5% CO2 for 60 minutes (Pulse). After pulse labeling, the medium was removed and cells were incubated for 10 minutes in 5 ml of normal growth medium. After washing with PBS, cells were scarped with 1 ml of 1 mM EDTA/PBS and collected as pellet by centrifugation. The cells were further washed with PBS twice and then the final pellet was resuspended in 50 µl of solution containing PBS+ 1 mM PMSF. Protein concentration was measured with Bradford reagent (as mentioned earlier) and 50 µg of protein was finally resuspended in SDS PAGE sample loading buffer. 1 µl of benozonase (to remove nucleic acids from samples) was added and incubated at 37°C for 15 minutes. Finally the translation products from Pulse were separated by SDS-PAGE. Rest was followed similar to *in organello* translation.

2.3.11 tRNA aminoacylation analysis

For analysis of aminoacylation of tRNAs, total RNA was isolated with TRIzol reagent as mentioned before. RNA was resuspended in resuspension buffer consisting of 0.3 M NaOAc (pH 5.0) and 1 mM EDTA as described earlier[110]. To determine the levels of aminoacylation, 2 µg of acidic RNA was separated by acid-urea PAGE, consisting 6.5%

(19:1) polyacrylamide, 8 M urea gel in 0.1 M NaOAc (pH 5.0) buffer. Gels were run with 30 mA for 48 hours at 4°C with frequent change of running buffer (0.1 M NaOAc, pH 5.0). To measure the levels of deacylation, 2 µg of acidic RNA was incubated with 1M Tris pH 9.0 at 70°C for 10 minutes. tRNAs were finally detected using specific γ-^{32}P-dATP labeled oligonucleotide probes as mentioned before [39].

2.3.12 Analysis of mitoribosomes and RNA using sucrose density ultracentrifugation

Sucrose density ultracentrifugation of mitochondrial ribosome was performed as described earlier [34]. 0.9-1.0 mg of mitochondria were lysed in lysis buffer (260 mM sucrose, 100 mM KCl, 20 mM $MgCl_2$, 10 mM Tris-HCl pH 7.5, 1% Triton X100, 0.08 U/µl RNaseOUT™ Recombinant Ribonuclease Inhibitor (Invitrogen), supplemented with EDTA-free complete protease inhibitor cocktail (Roche). Next mitochondrial lysates were loaded on top of 10%-30% linear sucrose gradient comprising of 100 mM KCl, 20 mM $MgCl_2$, 10 mM Tris-HCl, pH 7.5 and EDTA-free complete protease inhibitor cocktail (Roche). rRNA and mRNA sedimentation profile was performed as described previously [111]. RNA was isolated from one third of fraction collected, using Trizol®LS (Life Technologies GmbH, Darmstadt, Germany) according to manufacturer's instructions. The samples were further subjected to DNase treatment (Ambion) and then reverse transcribed to cDNA using High-Capacity cDNA Archive kit (Applied Biosystems). To detect each mitochondrial transcripts, TaqMan gene expression assays were used (Applied Biosystems) as mentioned earlier.

2.4 Cell culture

2.4.1 Preparation of primary mouse embryonic fibroblasts and immortalization

Primary MEFs were isolated from E13.5 days resulted from an intercross of *Clpp* heterozygous (+/-) mice as described earlier [112]. Labeling was done accordingly: B1, B5, C2, C3, C6, C7, D5, D6, E5, F5, F8 for wild type; A5, A8, B8, C1, C9, D1, D7, E2, E4 for knockouts. Cells were grown in Dulbecco's modified Eagle's medium (DMEM) (4.5g/L glucose, with GlutaMAX/Glutamin and sodium pyruvate; Gibco Life Science, USA) supplemented with 10% FBS and 100 units/ml penicillin and 100 µg of Streptomycin. Cells were maintained at 37°C with 5% CO_2. Immortalization of the

following primary MEFs B1, B5, C2 WT and A5, A8, B8 KO were carried out using plasmid encoding SV40 T antigen.

2.4.2 Immunostaining

Cells grown on cover slips over night were stained for mitochondria by incubation with MitoTrackerRed CMXRos (Invitrogen, Karlsruhe, Germany), (dilution 1:10,000 in cultivation medium - DMEM with Glutamax, 4.5 % (w/v) Glucose; Gibco Life Science, USA; 10 % (v/v) FCS, 50 µl/ ml Penicillin, 50 µg/ ml (w/v) Streptomycin) for 15 minutes at 37 °C, 5% CO_2. After exchanging the staining medium with fresh cultivation medium, cells were incubated for additional 15 minutes in the incubator. For immunolabeling of DNA, cells were washed shortly with PBS and fixed with 4% formaldehyde solution in PBS for 20 minutes at room temperature (300 µl/cover slip). Cover slips were then washed twice for 5 minutes in PBS and cells were permeabilized by incubation with 0.5 % (v/v) Triton X-100 in PBS for 5 minutes (300 µl/cover slip). After washing again the cover slips twice for 5 minutes in PBS, blocking of unspecific binding was done by incubation with 5 % (w/v) bovine serum albumin in PBS for 5 minutes (200 µl/cover slip). Finally, immunodetection was carried with the primary monoclonal mouse antibody against DNA (dilution 1:100 in blocking solution) for 1hour at room temperature (150 µl antibody solution/cover slip). Cover slips were washed twice with PBS for 5 minutes. The primary antibody was detected after incubation with secondary antibody IgM 488 (150 µl/cover slip, dilution 1: 400 in blocking solution) for 30 minutes. Cover slips were washed once with 0.5% Triton-X100 in PBS for 5 minutes (300 µl/cover slip) and PBS for 10 minutes at room temperature. The samples were finally mounted with one drop MOWIOL with 2.5 µg/ ml DAPI (AppliChem, Darmstadt, Germany). Samples were further analysed using the confocal microscope Leica TCS SP5.

2.5 Computational analysis

2.5.1 Software

All graphical representations and figures were created using Microsoft Excel (Microsoft Corp., Redmond WA, USA), Adobe Illustrator CS4 (Adobe Systems, San Jose CA, USA) and Inkscape for Mac. This thesis was written using Micorosoft® Word 2011 for Mac.

2.5.2 Statistical analysis

Statistical calculations were done using Microsoft Excel (Microsoft Corp., Redmond WA, USA). To determine statistical significance, a two-tailed unpaired student's t-test was used. The p values below 0.05 were considered significant. Error bars represent standard error of the mean (S.E.M.) *p<0.05; **p<0.01; ***p<0.001 compared to control (+/+).

2.6 Chemicals and biological material

Size markers for agarose gel electrophoresis (Gene Ruler DNA Ladder Mix) and for SDS-PAGE (Page Ruler Prestained Protein Ladder Mix) were from Fermentas, St. Leon-Rot, Germany. GoTaq® Green Master Mix and DNA Polymerase were obtained from Promega, Mannheim, Germany. Chemicals used in this work are listed in table 2.5. Solutions were prepared with double distilled water.

Table 2.5 Chemicals used and suppliers

Chemical	Supplier
β-mercaptoethanol	Applichem, Darmstadt, Germany
2,2,2-Tribromoethanol (Avertin)	Sigma-Aldrich, Seelze, Germany
2-Methyl-2-Butanol	Sigma-Aldrich, Seelze, Germany
Acetic Acid	Merck, Darmstadt, Germany
Acetone	KMF Laborchemie, Lohmar, Germany
Acrylamide	Roth, Karlsruhe, Germany
Adenosine 5'-diphosphate monopotassium	Sigma-Aldrich, Seelze, Germany
Agarose	Sigma-Aldrich, Seelze, Germany
Agarose (Ultra Pure)	Life Technologies, Darmstadt, Germany
Ammonium Acetate	Merck, Darmstadt, Germany
Ammoniumpersulfat (APS)	Sigma-Aldrich, Seelze, Germany
Antimycin A	Sigma-Aldrich, Seelze, Germany
Bovine serum albumin (BSA)	Sigma-Aldrich, Seelze, Germany
Bromophenol	Merck, Darmstadt, Germany
Calcium Chloride	Merck, Darmstadt, Germany

Chloroform	Merck, Darmstadt, Germany
DMEM	Gibco Life Science, USA
D-Sorbitol	Applichem, Darmstadt, Germany
Deoxynucleotides (dNTPs)	Sigma-Aldrich, Seelze, Germany
Dimethylsulfoxide (DMSO)	Merck, Darmstadt, Germany
di-Natriumhydrogenphosphate	Merck, Darmstadt, Germany
Dipotassium phosphate	Sigma-Aldrich, Seelze, Germany
Dithiothreitol	Sigma-Aldrich, Seelze, Germany
Enhanced chemiluminescence (ECL)	GE Healthcare, Munich, Germany
Ethanol, absolute	Applichem, Darmstadt, Germany
Ethidium bromide	Sigma-Aldrich, Seelze, Germany
Ethylendiamine tetraacetate (EDTA)	Applichem, Darmstadt, Germany
EGTA-Tris	Applichem, Darmstadt, Germany
FBS	Gibco Life Science, USA
FCCP	Sigma-Aldrich, Seelze, Germany
Formaldehyde solution	Sigma-Aldrich, Seelze, Germany
Formamide	Applichem, Darmstadt, Germany
Galactose	Merck, Darmstadt, Germany
Glucose	Merck, Darmstadt, Germany
Glycine	Applichem, Darmstadt, Germany
Glycerol	Sigma-Aldrich, Seelze, Germany
HEPES	Applichem, Darmstadt, Germany
Hydrochloric acid (37%)	Applichem, Darmstadt, Germany
Hydrogen peroxide	Sigma-Aldrich, Seelze, Germany
Isopropanol (2-propanol)	Roth, Karlsruhe, Germany
L-cysteine hydrochloride monohydrate	Sigma-Aldrich, Seelze, Germany
L-methionine	Sigma-Aldrich, Seelze, Germany
L-Glutamine	Sigma-Aldrich, Seelze, Germany
Oligomycin	Sigma-Aldrich, Seelze, Germany
MOPS	Applichem, Darmstadt, Germany
Magnesium chloride	Merck, Darmstadt, Germany
Methanol	Roth, Karlsruhe, Germany
Nitrogen (liquid)	Linde, Pullach, Germany
Non fat dried milk	Applichem, Darmstadt, Germany
Penicillin	Gibco BRL, Eggenstein, Germany
PonceauS	Sigma-Aldrich, Seelze, Germany
Potassium acetate	Sigma-Aldrich, Seelze, Germany
Paraformaldehyde (PFA)	Sigma-Aldrich, Seelze, Germany
Phenylmethylsulfonylfluoride (PMSF)	Sigma-Aldrich, Seelze, Germany
Phosphate buffered saline (PBS)	Gibco BRL, Eggenstein, Germany
Potassium chloride	Merck, Darmstadt, Germany
Potassium hydroxide	Merck, Darmstadt, Germany
Protease Inhibitor Cocktail Tablets	Roche, Basel, Switzerland
Rotenone	Sigma-Aldrich, Seelze, Germany
Sodium acetate	Applichem, Darmstadt, Germany
Sodium azide	Sigma-Aldrich, Seelze, Germany
Sodium chloride	Applichem, Darmstadt, Germany

Sodium citrate	Merck, Darmstadt, Germany
Sodium dodecyl sulfate	Applichem, Darmstadt, Germany
Sodium fluoride	Merck, Darmstadt, Germany
Sodium hydroxide	Applichem, Darmstadt, Germany
Sodium pyruvate	Sigma-Aldrich, Seelze, Germany
Sodium orthovanadate	Sigma-Aldrich, Seelze, Germany
Streptomycin	Gibco BRL, Eggenstein, Germany
Sucrose	Applichem, Darmstadt, Germany
Tetramethylethylenediamine (TEMED)	Sigma-Aldrich, Seelze, Germany
TES	Applichem, Darmstadt, Germany
Trishydroxymethylaminomethane(Tris)	Applichem, Darmstadt, Germany
Triton X-100	Applichem, Darmstadt, Germany
Tween 20	Applichem, Darmstadt, Germany
Trypsin	Gibco BRL, Eggenstein, Germany
Urea	Fluka Analytical, Seelze, Germany

3. Results

3.1. *Clpp* (caseinolytic peptidase, ATP dependent proteolytic subunit) knockout mice are smaller than littermates and not born in Mendelian proportion

To decipher the *in vivo* role of caseinolytic peptidase, ATP dependent proteolytic subunit (CLPP) in mammals and to elucidate the effects of CLPP deficiency at physiological and molecular levels, we have developed a conditional knockout allele for *Clpp* by homologous recombination in ES cells. Exons 3 to 5 of *Clpp* gene were flanked by loxP sites, allowing Cre-mediated recombination arising in deletion of Exons 3 to 5 that resulted in loss of function of *Clpp* gene, by removing a part of the protease domain and generated a frameshift from Exon 2 to 6 (Figure 3.1).

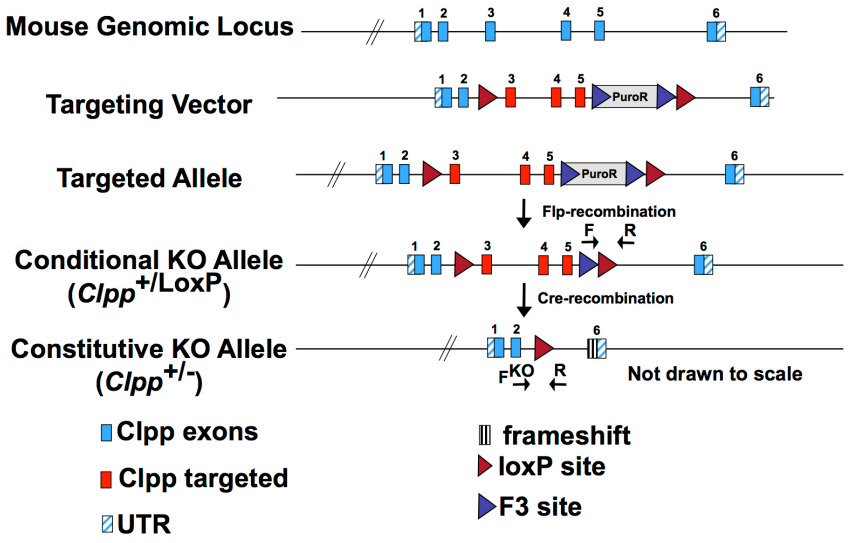

Figure 3.1 Disruption of *Clpp* in the germline

Targeting strategy for the generation of conditional and constitutive knockout *Clpp* alleles. PuroR-Puromycin resistance, positive selection marker; Arrows depicts PCR primers used for genotyping of the alleles. The position of the forward and reverse primers has been marked with arrows detecting the presence of wild type (+/+, control) and loxP allele. The forward knockout (F^{KO}) will detect the knockout ($Clpp^{-/-}$) allele.

The targeting strategy was accomplished at Taconic Artemis. The targeted locus was transmitted through germline that resulted in heterozygous $Clpp^{+/PuroR\text{-}loxP}$ mice. These mice were crossed with mice expressing Flp recombinase to remove the selection marker

PuroR. The *Clpp*$^{+/loxP}$ mice were obtained from Taconic Artemis, which were finally mated with mice expressing Cre recombinase under the promoter of beta-actin that resulted the *Clpp*$^{+/-}$ heterozygous mice. *Clpp*$^{+/-}$ heterozygous mice were intercrossed to obtain the *Clpp*$^{-/-}$ homozygous knockout mice (Figure 3.1).

The homozygous knockout mice (*Clpp*$^{-/-}$) were confirmed by genotyping PCR of tail DNA from mice at 2-3 weeks of age. (Figure 3.2 B). Southern blot analysis performed by Taconic Artemis detecting the correct homologous recombination at 5'side and cointegration of proximal loxP sites in the ES clones (Figure 3.2 C). We also observed almost no presence of CLPP transcripts thereby confirming *Clpp* homozygous knockout mice (Figure 3.2 D; from Dr. Alexandra Kukat).

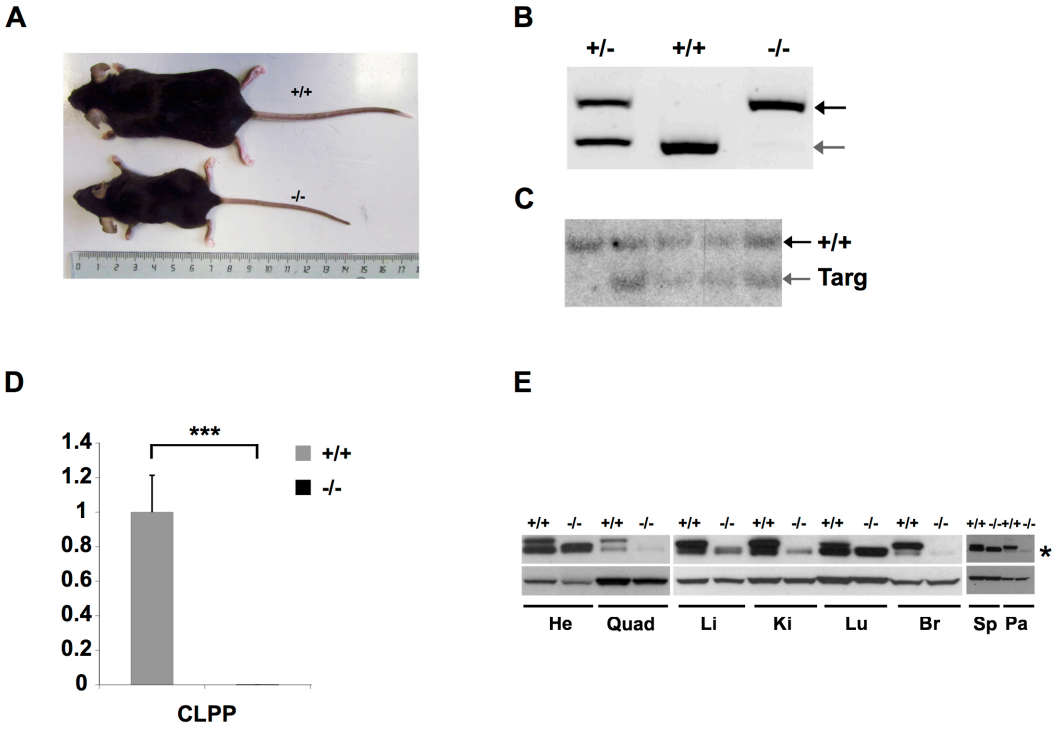

Figure 3.2 Confirmation of disruption of *Clpp* in mice

(A) Comparison of body sizes of one wild type (+/+) and one homozygous knockout (-/-) CLPP animals (Males). **(B)** Genotyping PCR indicating one heterozygous (+/-), one wild-type (+/+), and one homozygous knockout (-/-) CLPP animals. Grey arrow illustrating DNA fragments corresponding to the wild type (WT–199 bp), and black arrow indicates knockout (KO–273 bp) CLPP loci. **(C)** Southern Blot analysis of genomic DNA digested with *BspHI* in control (W) and Targeted (targ) ES cells. Black and grey arrow pinpoints (+/+) 14.7kb and targeted (Targ) 12.8kb respectively. **(D)** qPCR analysis of CLPP RNA levels in heart of control (+/+) and *Clpp* knockout (-/-) mice (n=4). Error bar represents ± S.E.M. Asterisks denotes statistical significance (Student's t-test, * $p<0.05$, ** $p<0.01$, *** $p<0.001$). **(E)** Western blot analysis detecting CLPP protein levels in Heart (He), Quadriceps (Quad), Liver (Li), Kidney (Ki), Lung (Lu), Brain (Br) of control (+/+) and *Clpp* knockout (-/-) mice. * indicates cross-reacting band.

Western blot analysis also confirmed complete loss of CLPP in heart (He), quadriceps (Quad), liver (Li), kidney (Ki), lung (Lu), brain (Br), spleen (Sp) and pancreas (Pa) at 12 weeks (Figure 3.2 E).

We observed that *Clpp* knockouts were not born according to Mendelian proportion (Figure 3.3 A). Only 15% of the *Clpp* knockouts and 43% of heterozygous mice were born instead of 25% and 50% respectively. The *Clpp*$^{-/-}$ homozygous knockout mice were smaller than littermates (wild type +/+ as Control) (Figure 3.2 A). However question still remains open if the knockout mice were born smaller or not since we observed the difference at the time of weaning.

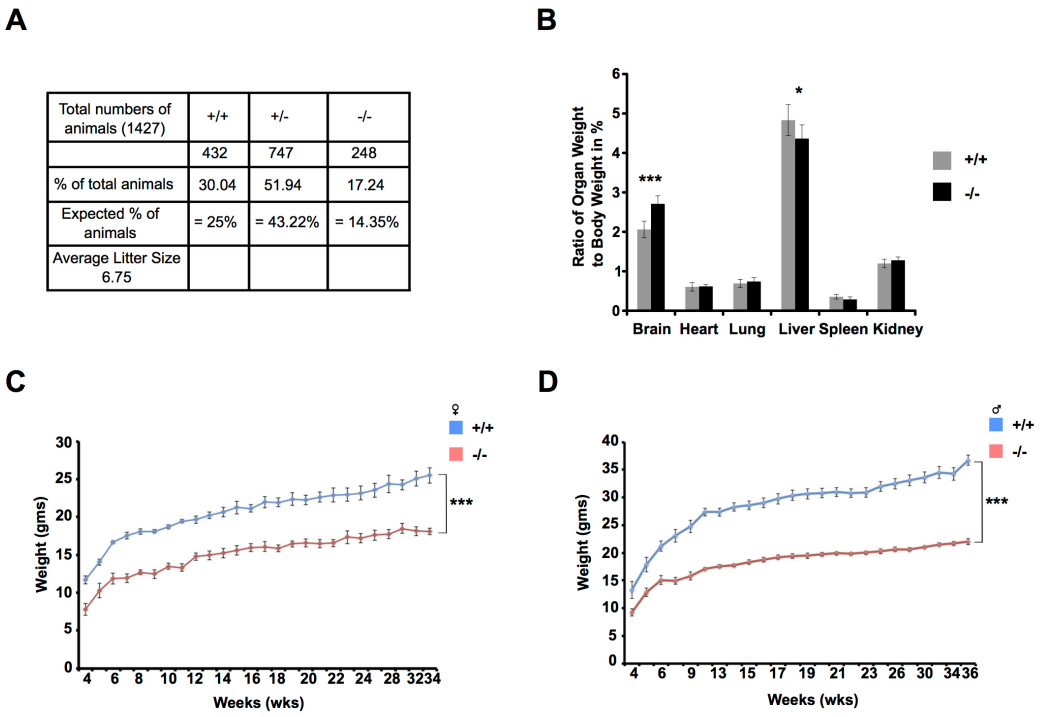

Figure 3.3 Phenotypic characterization of CLPP deficiency mouse

(A) Tabular representation of Mendelian statistics of newborn littermates of control (+/+) and *Clpp* knockout (-/-) mice. **(B)** Ratio of organ to body weight in mice at 11-15 weeks of age (n=6-7). Error bar represents ± S.E.M. Asterisks denotes level of statistical significance (Student's t-test, *p<0.05, ** p<0.01, *** p<0.001). **(C)** Graphical representation of change in body weight over time in control (+/+) and *Clpp* knockout (-/-) mice, Females. **(D)** Graphical representation of change in body weight over time in control (+/+) and *Clpp* knockout (-/-) mice, Males.

We calculated different organ to whole body weight ratio at 11-15 weeks of age and found little difference for most organs in *Clpp* knockout mice. We did observe a higher brain weight to body weight ratio in the *Clpp* knockouts (Figure 3.3 B). This is likely to

be a consequence of little change on brain weight during development and smaller body size. We also measured the body weight of control (+/+) and *Clpp* knockout (-/-) mice for both females and males from 4-36 weeks of age and found a significant difference in weight (Figure 3.3 C&D). These data suggest that *Clpp* knockouts are born not following Mendelian proportion, smaller and weigh less than their littermates and implying that CLPP might play an important role in the developmental stages of the organism.

Part 1: Role of CLPP in mammalian metabolism

3.2. *Clpp* knockout mice have reduced body fat content, enhanced energy expenditure and less ambulatory activity.

We observed a significant reduction of body weight in *Clpp* knockout (-/-) animals (Figure 3.3 C-D); this compelled us to further analyze the role of CLPP on whole-body physiology and metabolism. This part of the work has been done with the help of Dr. Alexandra Kukat. Nuclear magnetic resonance analysis of the body composition of the animals revealed a prominent decrease in body fat content of *Clpp* knockout mice (-/-) (Figure 3.4 A). We also performed micro computed tomography (microCT) analysis that showed a significant decrease in the fat ratio (ratio of average fat to total volume) (Figure 3.4 B). The observed reduction in body weight might be due to the reduced fat content.

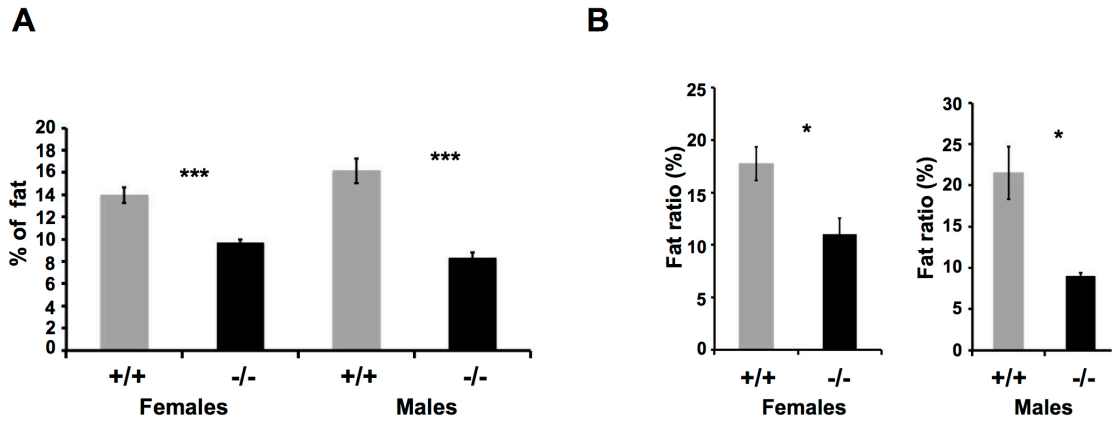

Figure 3.4 Decreased fat mass in *Clpp* knockout (-/-) mice.

(A) Average total body fat content measured by NMR in 32-35 weeks old of control (+/+) and *Clpp* knockout (-/-) mice (n= 7 for females; n= 9-11 for males). **(B)** Fat ratio measured by micro computed tomography (microCT) in 32-35 weeks old of control (+/+) and *Clpp* knockout (-/-) mice (n= 7 for females; n= 3 for males). Error bar represents ± S.E.M. Asterisks denotes statistical significance (Student's t-test, * $p<0.05$, ** $p<0.01$, *** $p<0.001$).

To further elucidate the reason behind reduced body fat in *Clpp* knockout mice (-/-), we performed indirect calorimetry on mice fed with normal chow diet. We didn't find any major difference in the food intake between *Clpp* knockout mice (-/-) and controls (+/+) (Figure 3.5 A-B). We also detected an increase in energy expenditure in *Clpp* knockout females (-/-) as compared to controls (+/+) (Figure 3.5 C). However we found no major difference in energy expenditure in *Clpp* knockout males (-/-) as compared to controls (+/+) (Figure 3.5 D). It remains to be determined if the observed changes reflect gender specific differences or are result of low number of animals used in the current

experiments. Thus, the enhanced energy expenditure is likely to be a cause for reduced body at content in *Clpp* knockout mice.

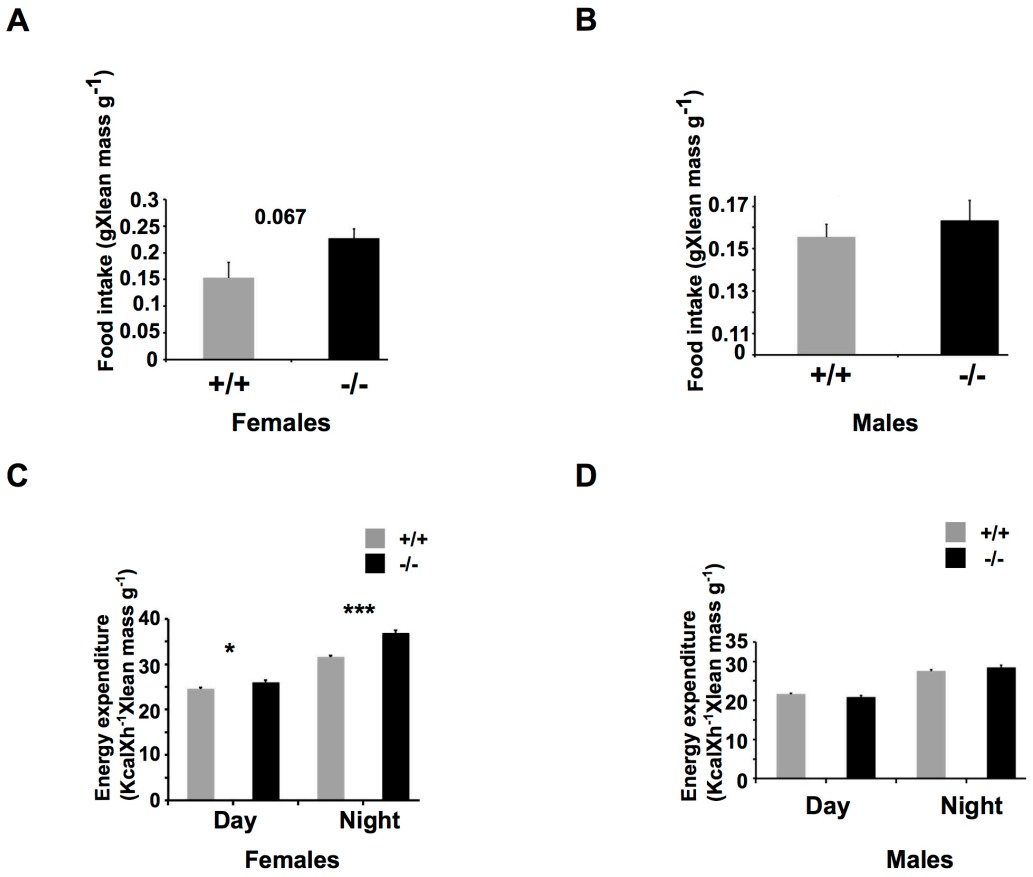

Figure 3.5 Increased energy expenditure in *Clpp* knockout (-/-) mice.

(A-B) Average food intake per day per body weight and per lean mass of control (+/+) and *Clpp* knockout (-/-) females and males respectively, 32-35 weeks old (n= 6-7 for females; n= 4-5 for males). **(C-D)** Energy expenditure normalized to body weight and lean mass for control (+/+) and *Clpp* knockout (-/-) females and males respectively, 32-35 weeks old (n= 7 for females; n= 6-8 for males). Error bar represents ± S.E.M. Asterisks denotes statistical significance (Student's t-test, * $p<0.05$, ** $p<0.01$, *** $p<0.001$).

To investigate the source of energy expenditure we analyzed locomotor activity in these *Clpp* knockout animals (-/-) and found a decrease in activity especially during night for both females and males as compared to controls (+/+) (Figure 3.6 A). We also measured the rectal body temperature hypothesizing that the energy spend might be dissipated as heat. We found no difference in rectal body temperature in *Clpp* knockout mice (-/-) as compared to controls (+/+) (Figure 3.6 B). However the question still remains regarding the source of energy expenditure. Hence we need to perform further analysis in

measuring the adsorption rate and accessing the calorie content of feaces and urine. In addition, it might also be possible that *Clpp* knockout mice (-/-) are spending more energy to maintain optimum body temperature similar to controls (+/+).

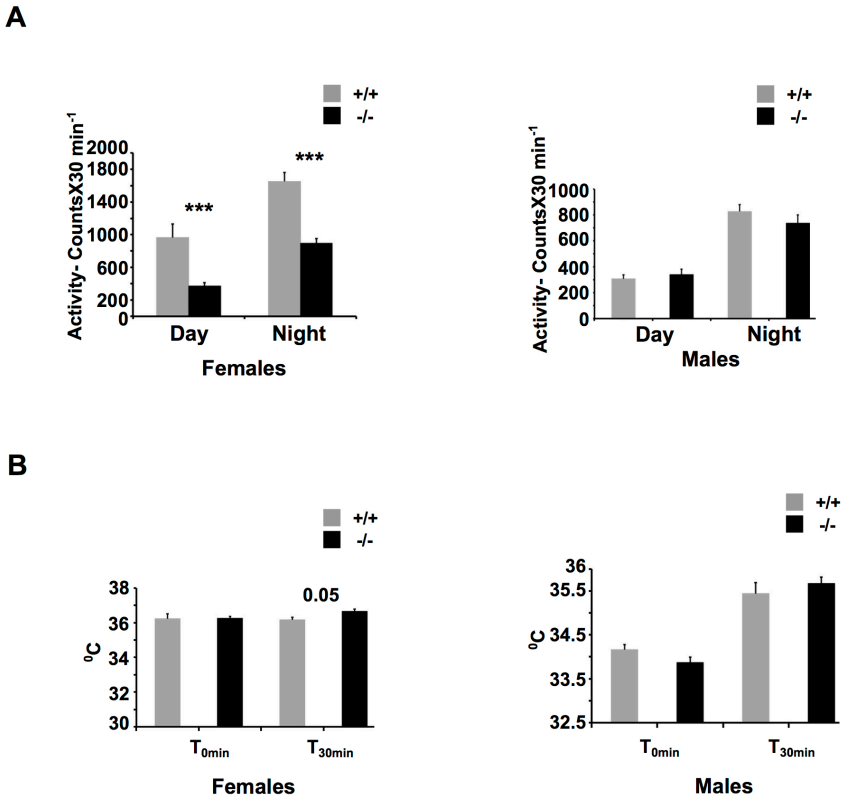

Figure 3.6 Less activity in *Clpp* knockout (-/-) mice.

(A) Average ambulatory activity counts per 30 minutes of control (+/+) and *Clpp* knockout (-/-) females and males respectively, 32-35 weeks old (n= 7 for females; n= 6-8 for males). **(B)** Average rectal body temperature at time point 0 and 30 minutes of control (+/+) and *Clpp* knockout (-/-) females and males respectively, 32-35 weeks old (n= 7 for females; n= 6-8 for males). Error bar represents ± S.E.M. Asterisks denotes statistical significance (Student's t-test, * $p<0.05$, ** $p<0.01$, *** $p<0.001$).

3.3. *Clpp* knockout mice have an increase in respiratory quotient (RQ) during night, improved glucose tolerance and higher insulin sensitivity.

Indirect calorimetry also provided respiratory quotient (RQ), which is determined as a ratio of $CO_{2\ eliminated}/O_{2\ consumed}$. RQ values for *Clpp* knockout (-/-) animals were around

0.8 during day and above 1 during night indicating a shift towards fat metabolism and carbohydrate metabolism respectively (Figure 3.7 A-B).

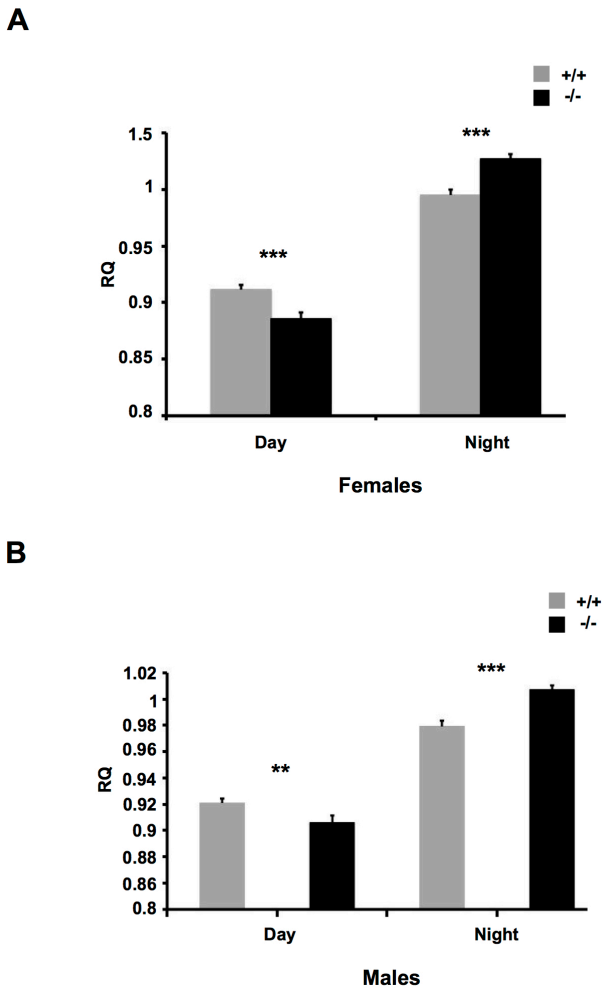

Figure 3.7 Increase in respiratory quotient (RQ) in *Clpp* knockout (-/-) mice.

(A-B) Respiratory quotient (RQ) (determined by the ratio of $CO_{2\ eliminated}/O_{2\ consumed}$) of control (+/+) and *Clpp* knockout (-/-) females and males respectively (during day and night), 32-35 weeks old (n= 7 for females; n= 6-8 for males). Error bar represents ± S.E.M. Asterisks denotes statistical significance (Student's t-test, * $p<0.05$, ** $p<0.01$, *** $p<0.001$).

Next we wanted to understand if CLPP deficiency affects glucose homeostasis in addition to changes in body weight. We measured glucose concentrations under starved (fasting) and random fed (non fasting) conditions. We observed no change in glucose levels between *Clpp* knockout (-/-) and control (+/+) animals under random fed (non fasting) conditions (Figure 3.8 A-B). However, we found a significant decrease in glucose concentration between *Clpp* knockout (-/-) and control (+/+) animals under starved (fasting) conditions (Figure 3.8 A-B).

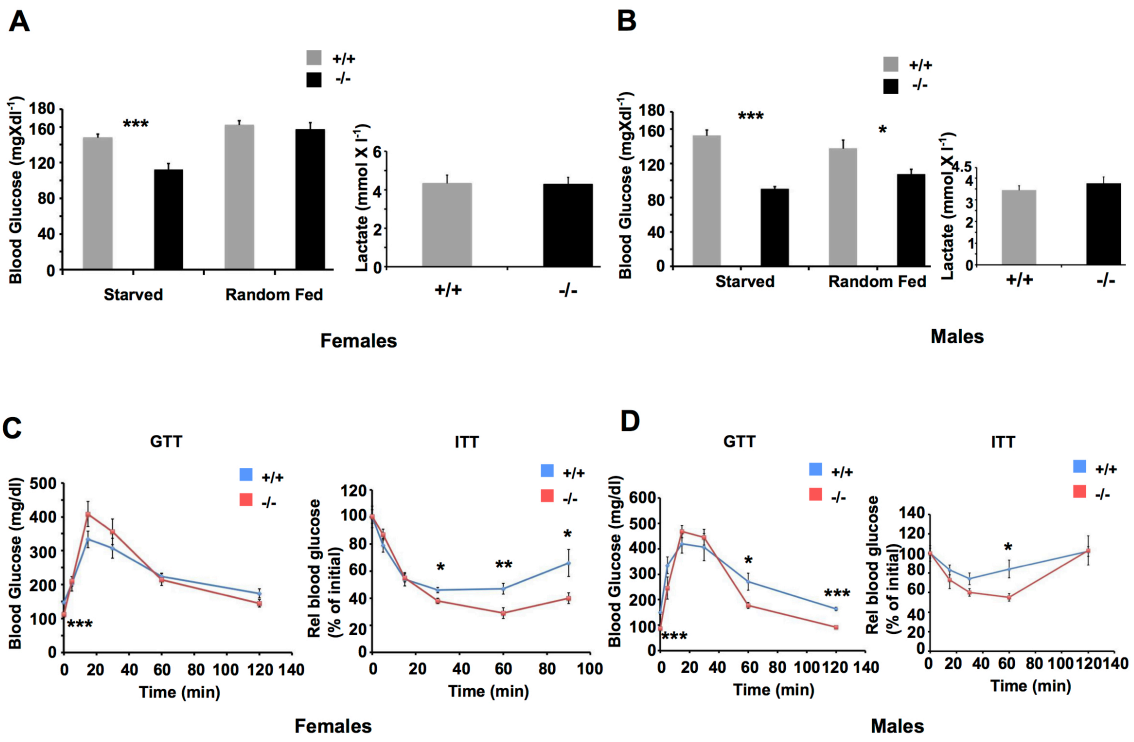

Figure 3.8 Increase in respiratory quotient (RQ), improved glucose tolerance and enhanced insulin sensitivity in *Clpp* knockout (-/-) mice.

(A-B) Blood glucose and lactate concentrations in starved and random fed conditions of control (+/+) and *Clpp* knockout (-/-) females and males respectively (n= 7 for females; n= 6-8 for males). **(C-D)** Intraperitoneal glucose tolerance test and intraperitoneal insulin tolerance test performed in 32-35 weeks old of control (+/+) and *Clpp* knockout (-/-) females and males respectively (n= 7 for females; n= 6-8 for males). Error bar represents ± S.E.M. Asterisks denotes statistical significance (Student's t-test, * $p<0.05$, ** $p<0.01$, *** $p<0.001$).

In addition, glucose tolerance test performed in *Clpp* knockout (-/-) females revealed no major change in glucose tolerance as compared to control (+/+), but showed a delayed response in insulin secretion and faster rate of glucose uptake (Figure 3.8 C). We observed an enhanced/improved glucose tolerance for *Clpp* knockout (-/-) males (Figure 3.8 D). Moreover, insulin tolerance test revealed higher insulin sensitivity in *Clpp* knockout (-/-) animals with respect to control (+/+) (Figure 3.8 C-D).

3.4. *Clpp* knockout mice age 12-15 weeks have reduced body fat content, enhanced energy expenditure and less ambulatory activity.

We performed similar analysis for younger mice age 12-15 weeks and obtained results

consistent with the previous ones in older mice (32-35 weeks). We found a significant decrease in body fat content of *Clpp* knockout (-/-) animals as compared to controls (+/+) (Figure 3.9 A).

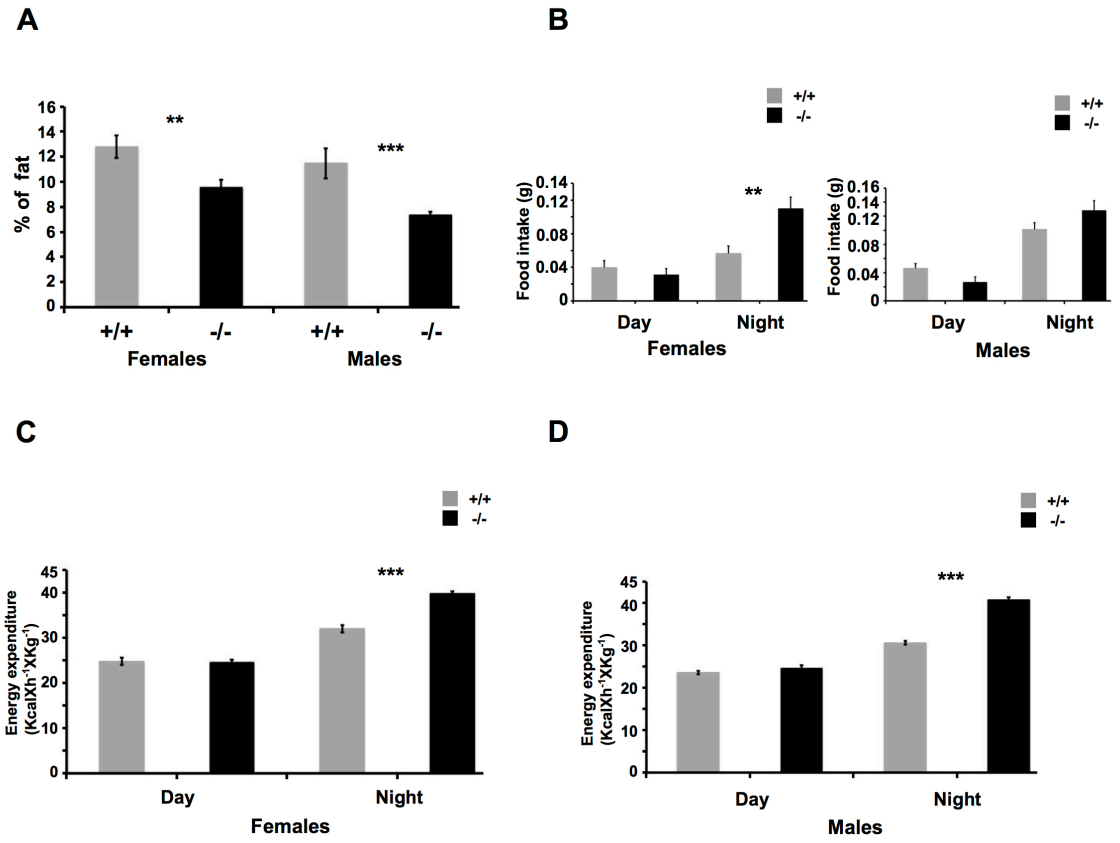

Figure 3.9 Decreased fat mass, increased energy expenditure in *Clpp* knockout (-/-) mice.

(A) Average total body fat content measured by NMR in 12-15 weeks old of control (+/+) and *Clpp* knockout (-/-) mice (n= 20 for females; n= 7-12 for males). **(B)** Average food intake per day of control (+/+) and *Clpp* knockout (-/-) females and males respectively, 12-15 weeks old (n= 3-6 for females; n= 4-6 for males). **(C-D)** Energy expenditure normalized to body weight and lean mass for control (+/+) and *Clpp* knockout (-/-) females and males respectively, 12-15 weeks old (n= 3-6 for females; n= 4-6 for males) Error bar represents ± S.E.M. Asterisks denotes statistical significance (Student's t-test, * $p<0.05$, ** $p<0.01$, *** $p<0.001$).

After performing indirect calorimetry on a normal chow diet we did not find any major difference in food intake between *Clpp* knockout males (-/-) and controls (+/+), but on the other hand found an increase in food intake for knockout females (-/-) (Figure 3.9 B). This discrepancy might be gender specific at earlier age or might be due to the fact that we could only use 3 controls for females as compared to 6 controls for males at this age. Also, we have performed the data analysis based on absolute values and not adjusted to body weight like before. In accordance to our previous result we also found an increase in

energy expenditure adjusted to body weight in *Clpp* knockout mice as compared to controls during night (Figure 3.9 C-D).

Analysis of locomotor activity correlated with our previous results. We found a decrease in activity especially during night for *Clpp* knockout females (Figure 3.10 A). On the contrary we observed an increase in activity for knockout males during night (Figure 3.10 B). This increase in activity might likely explain the enhanced energy expenditure in *Clpp* knockout males (-/-), however we need to repeat the experiment since we have undergone the analysis at this age with much lesser number of animals. RQ values obtained from indirect calorimetry for *Clpp* knockout (-/-) animals were around 0.8 during day and above 1 during night indicating a shift towards fat metabolism and carbohydrate metabolism respectively (Figure 3.10 C-D).

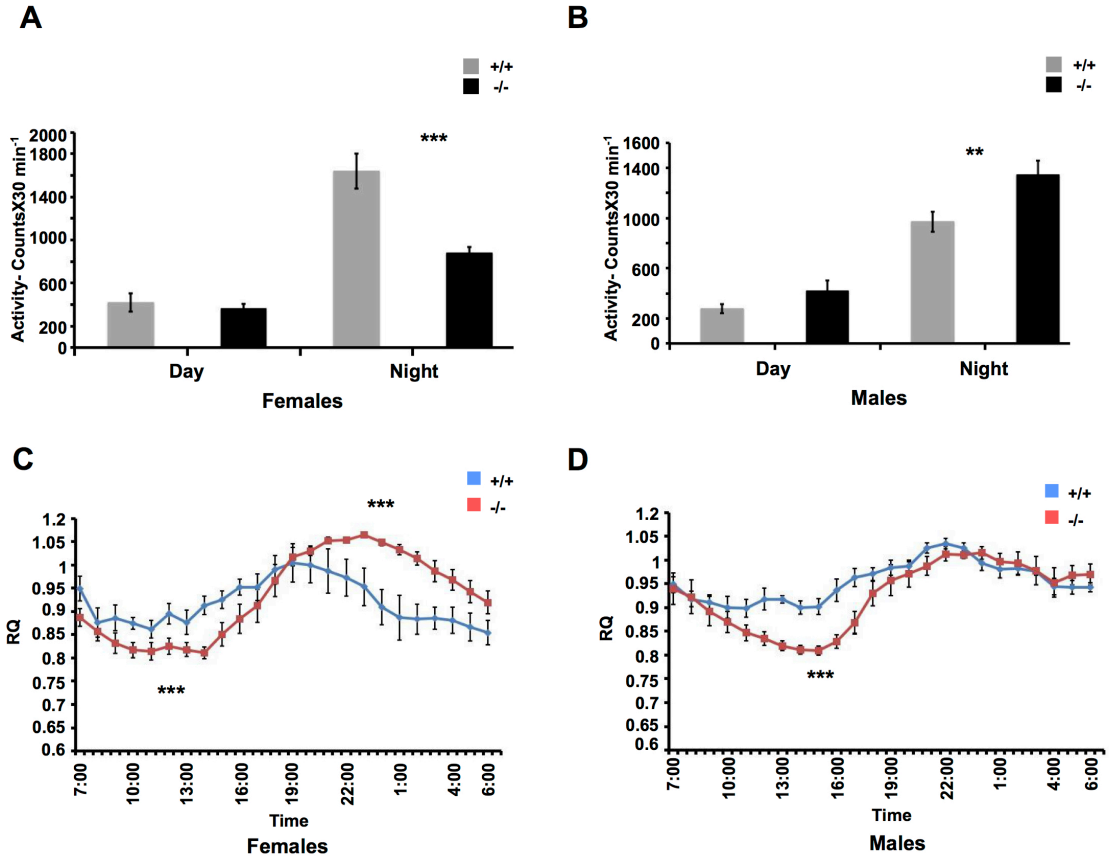

Figure 3.10 Less activity in *Clpp* knockout (-/-) mice.

(A-B) Average ambulatory activity counts per 30 minutes of control (+/+) and *Clpp* knockout (-/-) females and males respectively, 12-15 weeks old (n= 3-6 for females; n= 4-6 for males). **(C-D)** Respiratory quotient (RQ) of control (+/+) and *Clpp* knockout (-/-) females and males respectively (during day and night), 12-15 weeks old (n= 3-6 for females; n= 4-6 for males). Error bar represents ± S.E.M. Asterisks denotes statistical significance (Student's t-test, * $p<0.05$, ** $p<0.01$, *** $p<0.001$).

These are some preliminary interesting observations obtained during the course of on-going work on elucidating the role of CLPP at molecular level. Hence we need to perform more analysis to understand the role of CLPP in regulating metabolism in mammals. The initial studies should include measurement of insulin concentrations, circulating free fatty acids, triglycerides, cholesterol, glucose uptake, measuring mass of muscle, glycogen content in muscle, activity in brown adipose tissue (BAT) and feeding these animals on high fat diet.

Part 2: Role of CLPP in regulating ribosomal biogenesis in mammals

3.5. Characterization of mitochondrial proteome revealed oxidative phosphorylation (OXPHOS)-respiratory chain, energy metabolism, mitochondrial transcription and translation processes to be primarily affected in *Clpp* knockout mice.

Since CLPP is a mitochondrial matrix protease suggested to play a primary role in quality control, thereby maintaining homeostasis in the organelle, we initially wanted to observe the global profile changes in relation to protein abundance in the absence of CLPP. This analysis also provided us with a global impression of the processes affected and the candidates playing roles in those affected process. Thereby, we purified mitochondria from heart of *Clpp* knockout (-/-) and control (+/+) mice using sucrose gradient and subjected them to a liquid chromatographic-electrospray ionization-tandem mass spectrometric (LC-ESI-MS/MS) analysis**.** LC-ESI-MS/MS based label free quantitative proteomics was carried out in our CECAD proteomic facility. Out of all proteins identified 527 were eligible for quantification and have been plotted (Figure 3.11A). Value of log2 {ratio of *Clpp* knockout (-/-) vs control (+/+)} above zero represents upregulation of the proteins and below zero represents down regulation of the proteins. An increasing value of –Log {p value *Clpp* knockout (-/-) vs control (+/+)} along X-axis indicates higher significance in the change of expression. We found a number of key biochemical and molecular processes along with metabolic processes to be affected in absence of CLPP. Out of them, transcription and translation, mitochondrial respiration and oxidative phosphorylation (OXPHOS) and metabolism were the key affected processes. Proteins that showed higher difference in abundance/expression in the above mentioned affected processes were plotted accordingly (Figure 3.11 B-D).

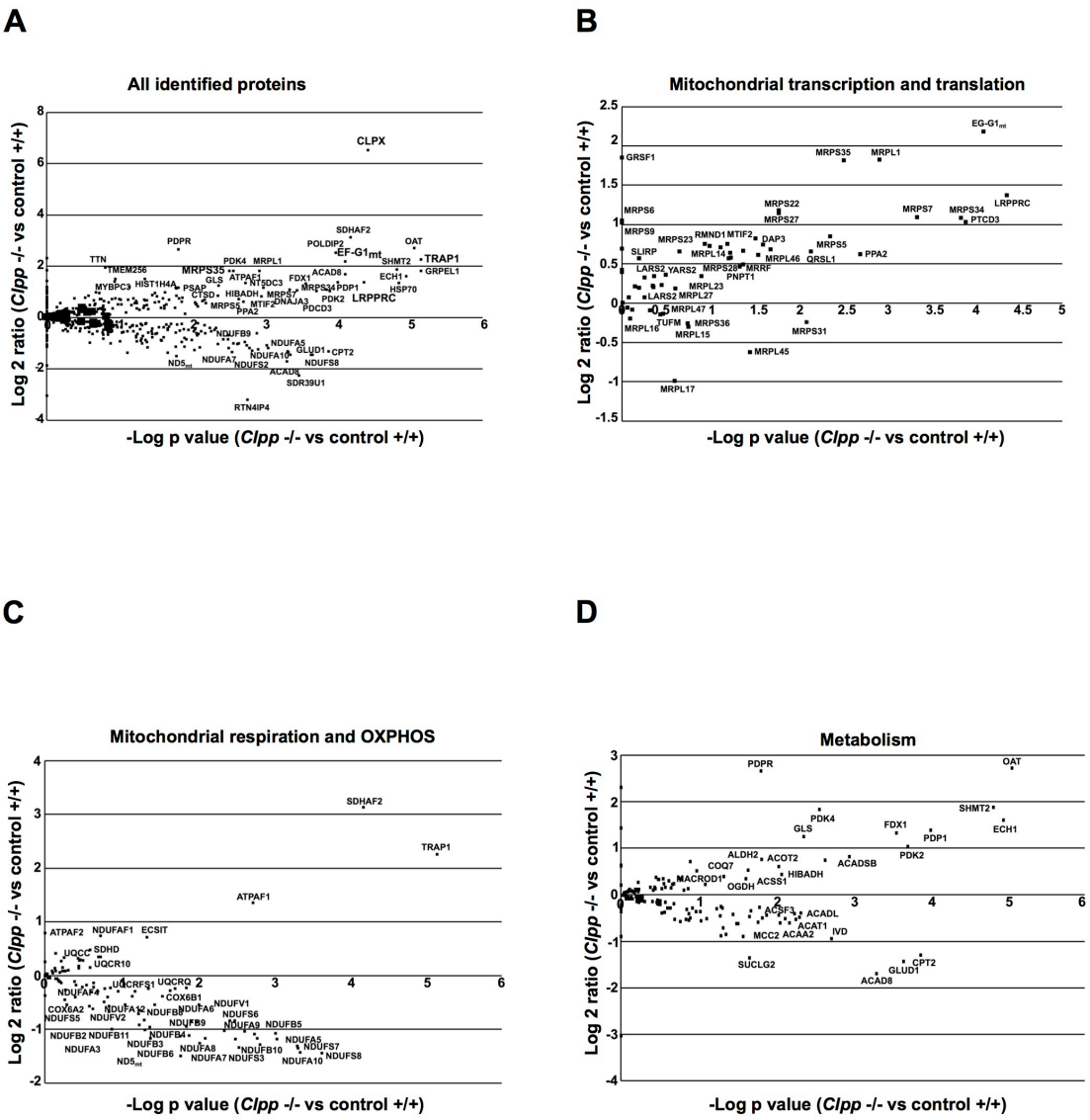

Figure 3.11 Quantitative mitochondrial proteome profiling using LC-ESI-MS/MS

(A) A liquid chromatographic-electrospray ionization-tandem mass spectrometric (LC-ESI-MS/MS 4 hr. gradient) analysis for the quantification of proteins from purified heart mitochondria of control (+/+) and *Clpp* knockout (-/-) mice (n=4). **(B-D)** Representation of the differentially expressed proteins involved in the affected biochemical and molecular pathways in absence of CLPP.

3.6. CLPP deficiency leads to a specific decrease in Complex I activity, followed by a decrease in Complex IV activity later in life.

Label free quantification analysis of mitochondrial proteome showed that mostly respiratory chain & oxidative phosphorylation (OXPHOS), mitochondrial translation and metabolic processes were affected. Hence, we wanted to first investigate the biochemical

effects of CLPP deficiency in heart by measuring the levels of mitochondrial respiratory chain (MRC) activities (Figure 3.12 A) in collaboration with Dr. Rolf Wibom (Karolinska Institute, Sweden). We observed an isolated Complex I deficiency at 15 weeks, which was followed by combined decrease in Complex I and Complex IV activity later in life (35 weeks). Complex II, which is encoded by nuclear DNA, remained unaffected. This indicates that mitochondrial gene expression is specifically affected in *Clpp* deficient mice. Decrease in Complex I (Figure 3.12 B) and Complex IV activity (Figure 3.12 C) was also reflected in *in-gel* activity in heart and achieved similar results for Complex I and Complex IV in skeletal muscle (Skm) (Figure 3.12 B-C).

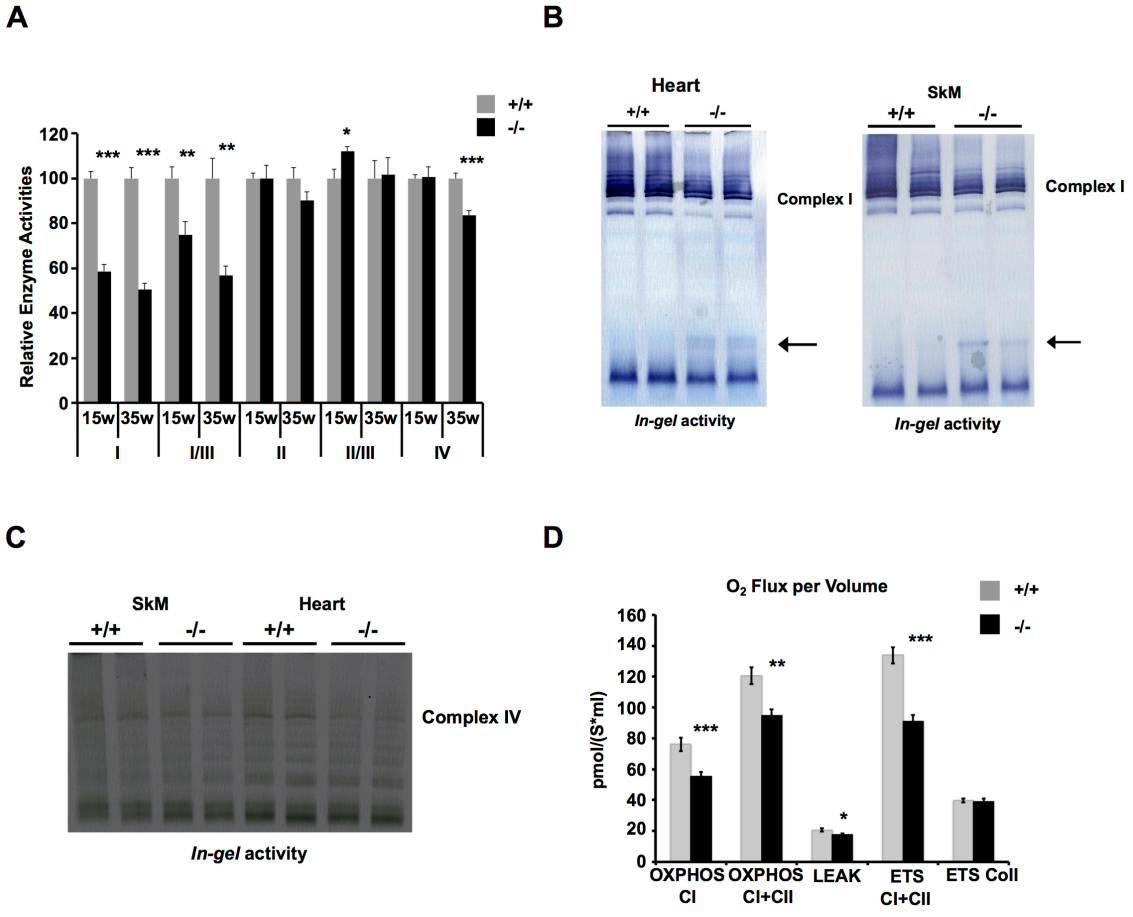

Figure 3.12 Loss of CLPP causes mitochondrial dysfunction in *Clpp* knockout mice

(A) Relative MRC activities in isolated heart mitochondria of control (+/+) and *Clpp* knockout (-/-) mice (n=4) of 15 weeks and 35 weeks of age. **(B-C)** *In gel* activity of Complex I and Complex IV in heart and skeletal muscle (SkM) after running BN-PAGE. **(D)** Measurement of oxygen consumption of isolated heart mitochondria of control (+/+) and *Clpp* knockout (-/-) mice (n=7). Error bar represents ± S.E.M. Asterisks denotes statistical significance (Student's t-test, * $p<0.05$, ** $p<0.01$, *** $p<0.001$).

Furthermore, we measured oxygen consumption in isolated heart mitochondria when supplied with substrates of Complex I (pyruvate-glutamate-malate) and ADP, OXPHOS state CI; followed by addition of substrates of Complex II (succinate), OXPHOS state CI+CII. LEAK respiration (state L) is the LEAK oxygen flux, compensating for proton leak. LEAK respiration determines the mitochondrial respiration in the LEAK state after adding oligomycin that is an inhibitor of ATP synthase (inhibits state 3- phosphorylating respiration). The capacity of the electron transfer system (ETS) was evaluated by complete uncoupling by addition of uncoupler carbonyl cyanide p-[rifluoromethoxyl]-phenyl-hydrozone (FCCP) thereby stimulating maximum flux. Finally addition of rotenone that inhibits Complex I show the contribution of Complex II to the maximal ETS capacity. We obtained a reduction in oxygen consumption rate for both OXPHOS state CI and OXPHOS state CI+CII in *Clpp* knockout mice (Figure 3.12 D). We also found a decrease in LEAK respiration and lower capacity of the ETS in *Clpp* knockout mice supporting the results of the complex activities.

We next proceeded to assess the levels of assembled respiratory chain complexes by using Blue Native Polyacrylamide Gel Electrophoresis (BN-PAGE) and detected lower levels of Complex I and mild reduction of Complex IV in *Clpp* knockout heart and skeletal muscle mitochondria of 15-19 weeks age (Figure 3.13 A). In addition to the fully assembled complexes, we also detected a smaller band (marked by arrow, Figure 3.13 A) that likely corresponds to F1 of Complex V in *Clpp* knockout heart. Similar observations have been previously reported in other knockout mouse models with impaired mtDNA expression [34,39,41,111,113]. We also procured lower levels of Complex I and Complex IV for assembled respiratory supercomplexes (Figure 3.13 B). Since Complex I seemed to be primarily affected we then examined the assembly status for Complex I by performing two-dimensional blue native/ SDS gel electrophoresis in collaboration with Prof. Leo Nijtmans (NCLMS, Netherlands) (Figure 3.13 C). After separating the intact OXPHOS complexes by first dimension blue native PAGE, the second dimension denaturing electrophoresis resolves the individual subunits of respective complexes. The distribution of these subunits thereby determines possible subcomplexes. Western blot analysis using Complex I subunit specific antibodies NDUFS3 and NDUFA9 showed no accumulation of subcomplexes of either partially assembled or breakdown products thereby indicating no assembly defect for Complex I. This indicates that Complex I deficiency likely stems from the increased turnover of Complex I.

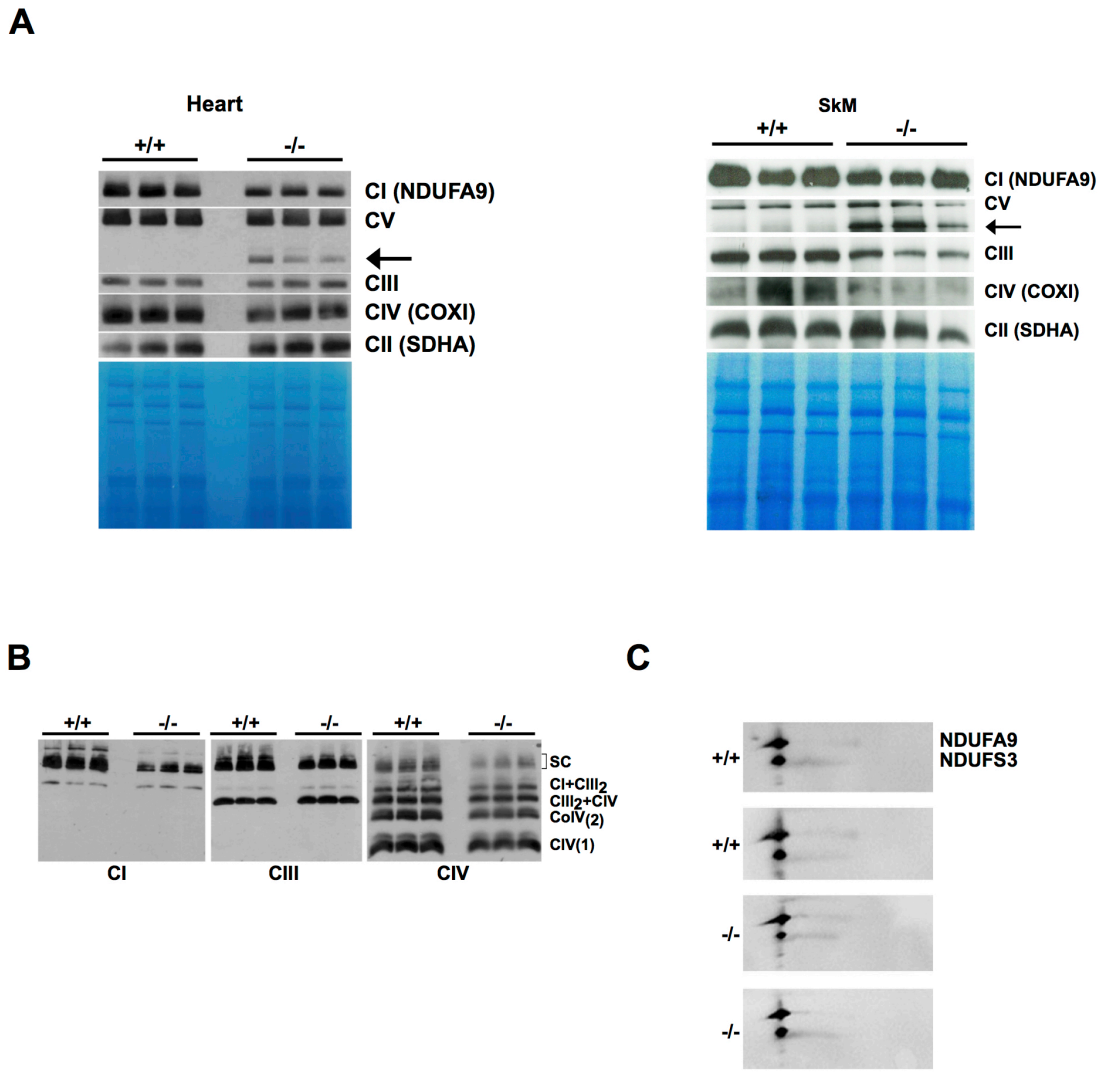

Figure 3.13 Lower levels of Complex I and Complex IV in *Clpp* knockout mice.

(A) BN Page analysis of the assembled respiratory chain complexes in heart and SkM mitochondria of control (+/+) and *Clpp* knockout (-/-) mice of 12-15 weeks respectively. **(B)** BN Page analysis of the assembled respiratory chain super complexes in heart mitochondria of control (+/+) and *Clpp* knockout (-/-) mice of 12-15 weeks respectively. Immunoblotting was performed to detect nuclear-encoded subunits of complex I (NDUFA9), complex II (SDHA), complex III (UQCRC2), complex IV (COXI) and complex V (ATP5A1). **(C)** 2D BN Page analysis in heart mitochondria of control (+/+) and *Clpp* knockout (-/-) mice. Immunoblotting was done to detect NDUFA9 and NDUFS3 subunits of complex I.

3.7. Loss of CLPP leads to increase in transcription followed by increased steady state levels of mtDNA transcripts

The respiratory chain dysfunction driven by loss of CLPP prompted us to inspect mtDNA levels and mtDNA expression. Southern blot analysis showed mild increase in levels of

mtDNA in the heart of *Clpp* knockout (-/-) mice as compared to control (+/+) (Figure 3.14 A). This finding of ours disputes with previous study [114] where it has been reported a significant increase of mtDNA levels in heart of *Clpp* knockout (-/-) mice as compared to control (+/+). This difference may be due to the methods used in both studies. Quantitative real time PCR was used in the previous study whereas we performed Southern blot.

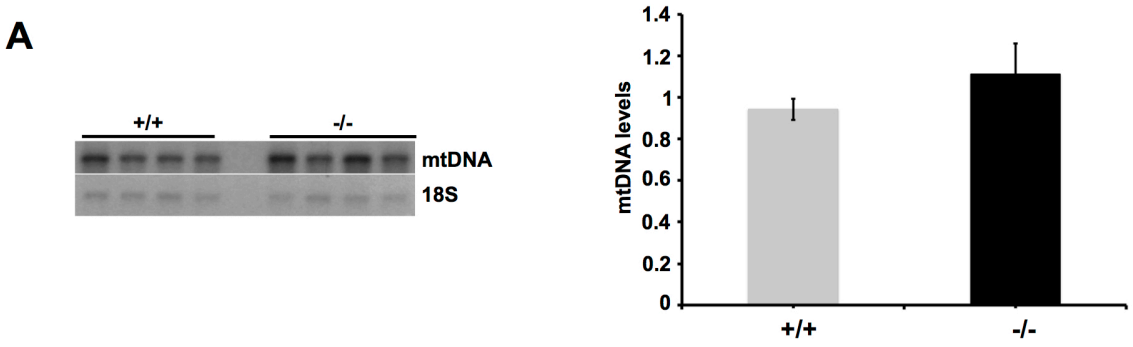

Figure 3.14 Steady state levels of mtDNA in heart of *Clpp* knockout mice

(A) Southern blot analysis of mtDNA levels in heart of control (+/+) and *Clpp* knockout (-/-) mice. Quantification of mtDNA levels (n=4) of control (+/+) and *Clpp* knockout (-/-) mice of 15 weeks of age. Error bar represents ± S.E.M. Asterisks denotes level of statistical significance (Student's t-test, *p<0.05, ** p<0.01, *** p<0.001).

We next examined the steady state levels of mRNAs, tRNAs and rRNAs generated from the heavy strand promoter (HSP) and light stand promoter (LSP) of mtDNA in the heart of *Clpp* knockout (-/-) mice (Figure 3.15 A-B). We found a significant increase in mRNAs and tRNAs transcribed from HSP & LSP of mtDNA in heart of *Clpp* knockout (-/-) mice. The levels of 16S rRNA were mildly decreased, whereas we found elevated levels of RNA19; that circumscribe 16S rRNA and ND1 (Figure 3.23 A). This might imply towards impairment in processing of transcripts (Figure 3.23 A), here more specifically the processing of RNA19.

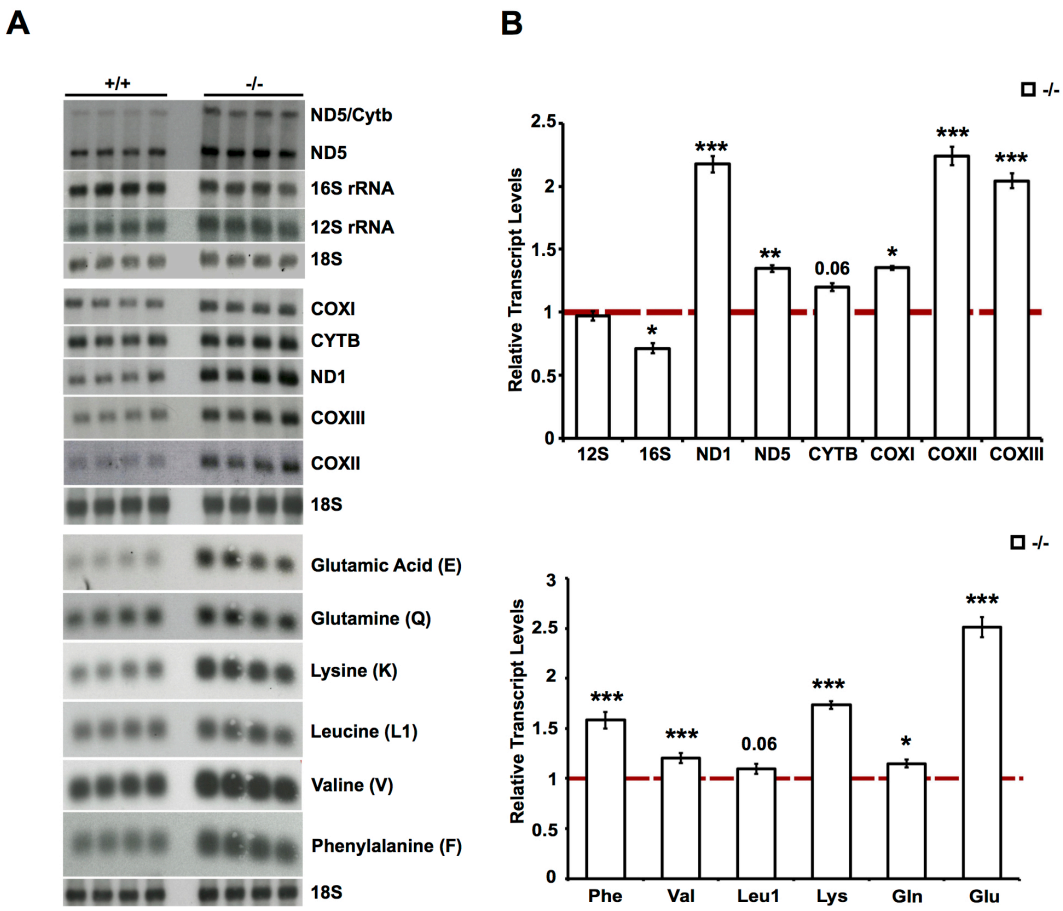

Figure 3.15 Steady state levels of mitochondrial transcripts in heart of *Clpp* knockout mice

(A) Northern blot analysis of mitochondrial rRNA, mRNA and tRNA of control (+/+) and *Clpp* knockout (-/-) mice. 18S rRNA is used as loading control. **(B)** Quantification of mitochondrial rRNA, mRNA and tRNA levels in heart which is presented as percentage of control (+/+) (n=4). Error bar represents ± S.E.M. Asterisks denotes level of statistical significance (Student's t-test, *p<0.05, ** p<0.01, *** p<0.001).

In addition, increase in steady state levels of LRPPRC that is known to regulate mitochondrial mRNA stability [111] corresponds to the increase in steady state levels of most mRNAs (Figure 3.16 A). Later we also performed *in organello* transcription (with Dr. Alexandra Kukat) that resulted in an increase of *de novo* transcription of mtDNA in heart and SkM of *Clpp* knockout (-/-) mitochondria (Figure 3.16 B). This upregulation of transcription is likely to be a secondary response or a compensatory mechanism to respiratory chain deficiency. Interestingly we found a decrease in *de novo* transcription of mtDNA in liver (Figure 3.16 B).

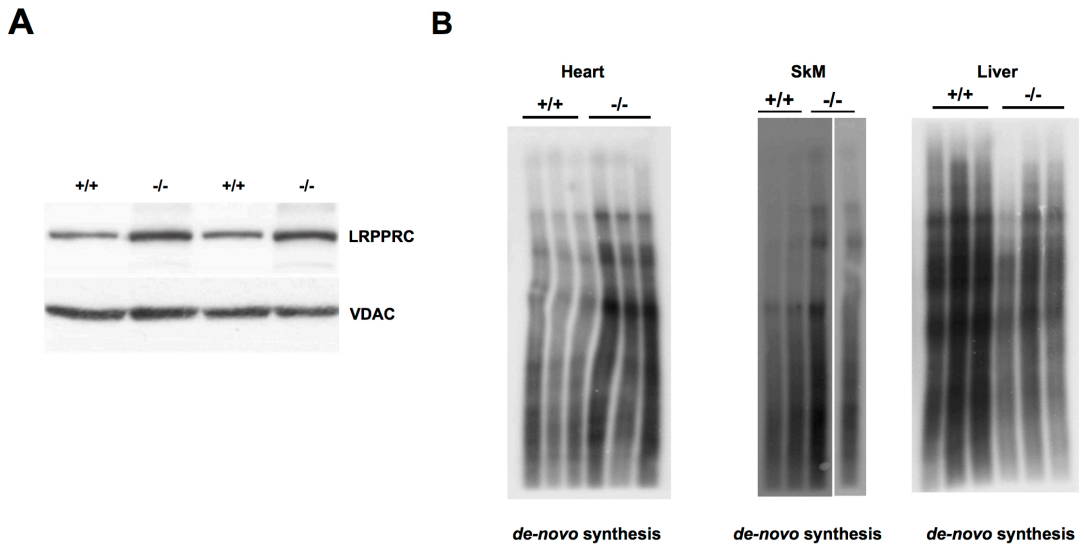

Figure 3.16 *In organello* transcription in heart of *Clpp* knockout mice

(A) Western blot analysis of steady state levels of LRPPRC protein that regulates mitochondrial mRNA stability. **(B)** *In organello* transcription of control (+/+) and *Clpp* knockout (-/-) heart, SkM and liver mitochondria.

3.8. Loss of CLPP leads to impaired mitochondrial protein synthesis accompanied by increased levels of small ribosomal subunits, thereby affecting the stoichiometry of proper functioning ribosomes

The upregulation of transcription induced by loss of CLPP compelled us to also inspect *de novo* protein synthesis in isolated mitochondria from heart, SkM and liver of *Clpp* knockout (-/-) mice. We found moderate decrease in mitochondrial translation as depicted in 1 hour radioactive S^{35} labeling (Pulse-Figure 3.17 A) of newly synthesized mitochondrial proteins. To analyze the stability of the newly synthesized polypeptides, 3 hours Chase was performed in the presence of cold methionine. Moderate aberrations in mitochondrial translation lead us to analyze the assembly status of mitochondrial ribosomes. We analyzed the integrity of mitochondrial ribosomes by gradient sedimentation analysis of mitochondrial extracts (Figure 3.18 A). We detected an increase in steady state levels of small ribosomal subunits (28S) while large ribosomal subunits (39S) and monosomes (55S) appeared to be present in almost normal levels. This is in contrast with the previous observation where 16S rRNA levels are decreased. This suggests that the stoichiometry of mitochondrial ribosomes might be affected leading to dysfunction of monosomes.

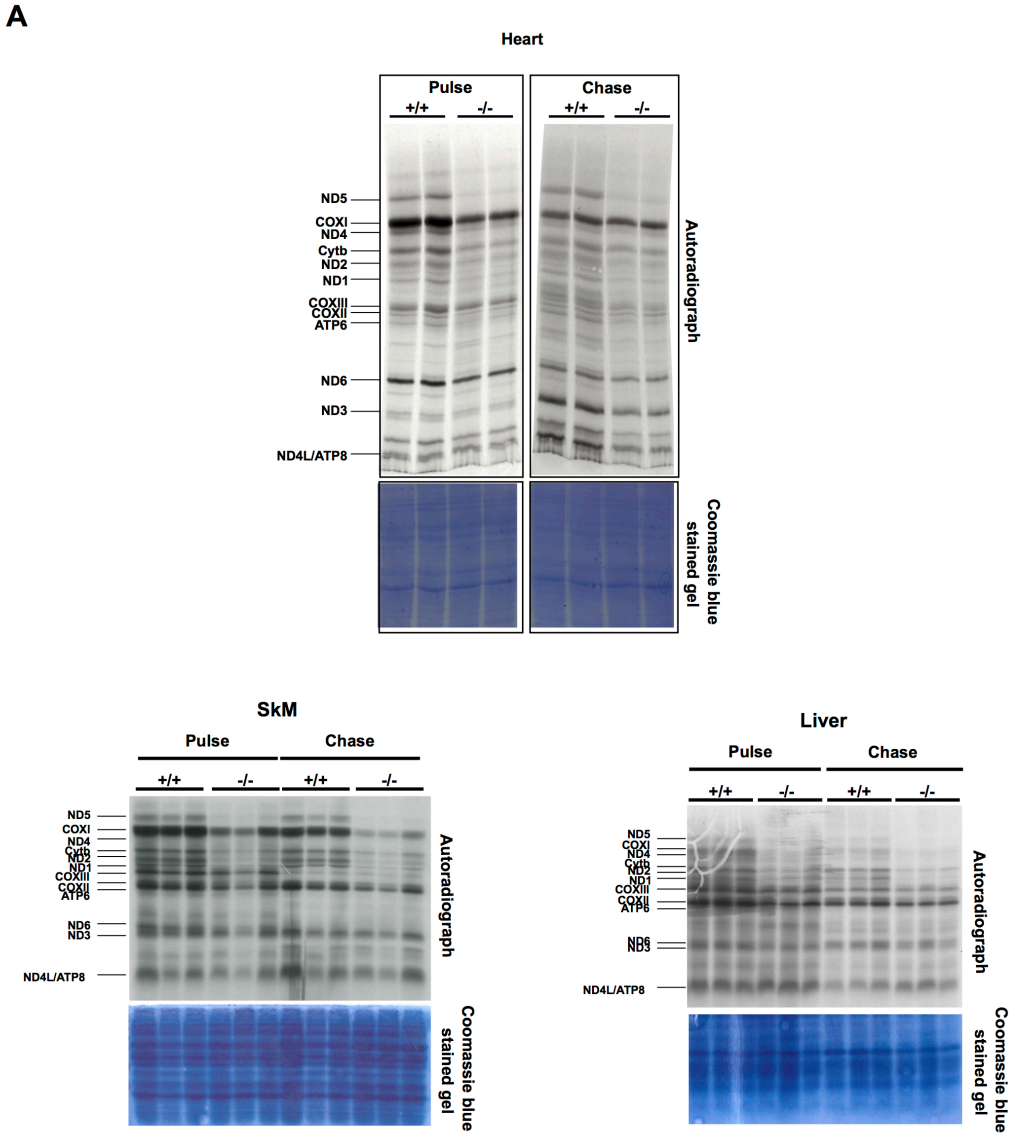

Figure 3.17 Deregulated protein synthesis in *Clpp* knockout heart, SkM and liver.

(A) *In organello* translation of isolated heart, SkM and liver mitochondria from control (+/+) and *Clpp* knockout (-/-) mice. *De novo* synthesized mitochondrial encoded proteins were isolated after labeling with ^{35}S-methionine for 1 hour (Pulse). Positions of individual mitochondrial encoded proteins are indicated. Coomassie blue stained gel is used to indicate equal loading of all lanes.

Moreover, we also detected an increase in small ribosomal subunits MRPS15 and MRPS35, with mild increase in large ribosomal subunits MRPL37 (Figure 3.18 B). This is in agreement with the biogenesis of mitochondrial ribosomes and also supports the observation from sedimentation analysis. This increased mitochondrial ribosomal biogenesis might be a response to respiratory chain deficiency caused by a possible problem in translation in the absence of CLPP.

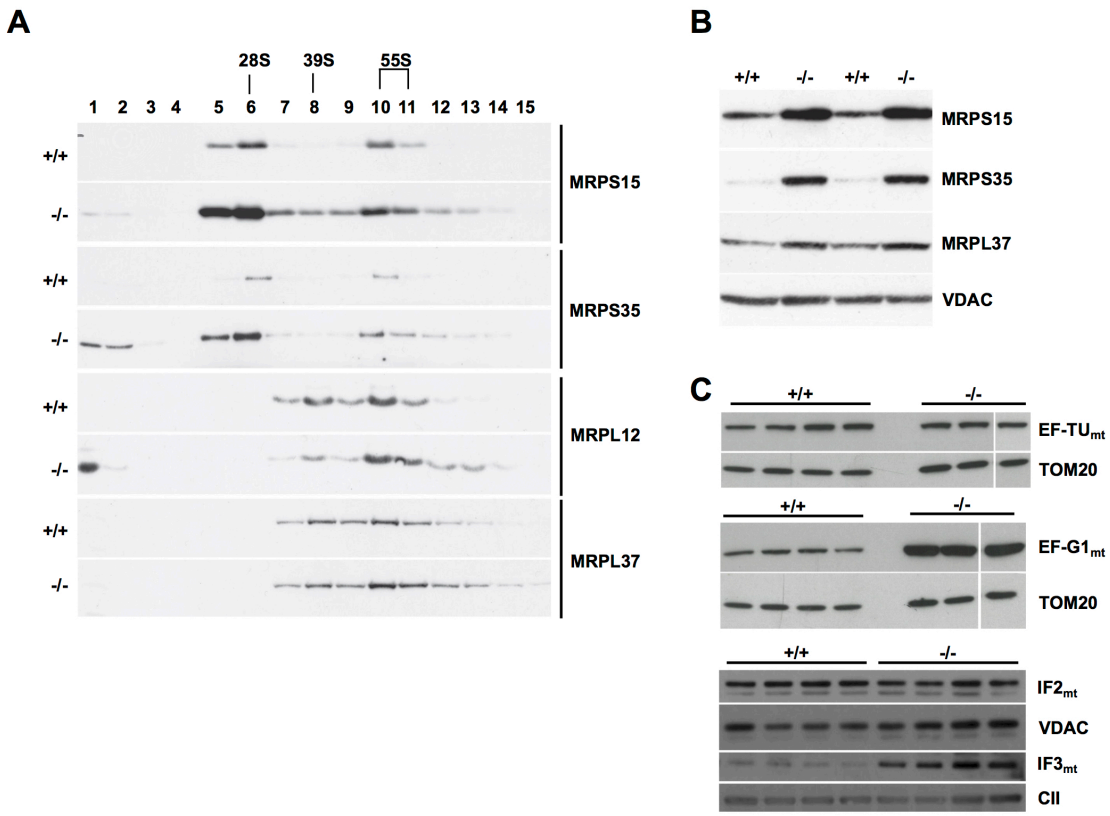

Figure 3.18 Biogenesis of small ribosomal subunits in *Clpp* knockout heart

(A) Sedimentation analysis of small (28S), large (39S) ribosomal subunits and assembled (55S) ribosome in heart mitochondria from of control (+/+) and *Clpp* knockout (-/-) heart mitochondria by centrifugation through linear 10%–30% sucrose density gradient. The migration of ribosomal subunits and assembled (55S) ribosome was detected by immunobloting with MRPS15, MRPS35, MRPL12 and MRPL37 specific antibodies. **(B)** Steady state levels analyzed by Western blot of MRPS15, MRPS35 of the small (28S) ribosomal subunit and MRPL37 protein of the large (39S) ribosomal subunit from of control (+/+) and *Clpp* knockout (-/-) heart mitochondria. VDAC is used as a loading control. **(C)** Western blot analysis of mitochondrial translation proteins EF-TU_{mt}, EF-$G1_{mt}$, $IF2_{mt}$, $IF3_{mt}$ of control (+/+) and *Clpp* knockout (-/-) heart mitochondria. TOM20, VDAC are used as loading controls.

To further address the observed defect of mitochondrial translation, we performed Western blot analysis of the mitochondrial translational factors. We observed no change in steady state levels of EF-TU_{mt} and increase in steady state levels of EF-$G1_{mt}$ (translational factors involved in elongation) (Figure 3.18 C). We didn't detect any change in the levels of initiation factor $IF2_{mt}$ of mitochondrial translation which goes well with its primarily role in binding of GTP and then to the small ribosomal subunit (28S) [39]. We found an increase in steady state levels of $IF3_{mt}$ that is involved in interacting with the 55S mitoribosome thereby loosening the interaction of 28S and 39S in the first step of initiation of mitochondrial translation. This leads to the release of 39S and formation of

28S:IF3$_{mt}$ complex in the second step of initiation [42]. All the above results implied to impairment in the assembly of small ribosomal subunit that also might affect the function of fully assembled ribosomes.

3.9. tRNA acetylation is not affected in absence of CLPP in heart

Impaired mitochondrial translation and accumulation of small ribosomal subunits might lead to the possibility of stalled ribosomes, since in bacteria it has been shown that CLPP plays a role in rescuing stalled ribosomes[115]. This led us to the following hypothesis:

a. Absence of ClpXP protease in the mice might inhibit the proteolysis process in mitochondria thereby preventing generation of peptides, which in turn will lead to fewer amounts of amino acids. This scarcity of amino acids will result in less amount of acylated tRNAs (charging of tRNAs) thereby impeding the mitochondrial translation process.

b. Aberration of mitochondrial translation might also be due to the any premature stalling of ribosomes on mRNA that has been cleaved due to the lack of a stop codon. In such scenario, recruitment of release factors takes place that cleaves the peptidyl-tRNA releasing the nascent polypeptide chain. CLPP being one of the primary mitochondrial matrix protease involved in the quality control process might be responsible for degradation of this nascent polypeptide chains into small peptides. But in absence of CLPP, these polypeptides might not be degraded into peptides which will result in less amount of amino acids thereby affecting the charging of tRNAs necessary for mitochondrial translation.

c. Stalling of ribosomes in *Clpp* knockout (-/-) heart might also inhibit the ribosomal subunit dissociation and preventing the release of deacylated tRNA and mRNA. This will also result in lesser amount of uncharged (deacylated) tRNAs.

Therefore we estimated the levels of aminoacylated tRNAs by separating the charged and uncharged forms of tRNA under acidic conditions (Figure 3.19 A). We found an increase amount of both charged (acylated) and uncharged (deacylated) tRNAs in *Clpp* knockout (-/-) heart and liver. Elevated levels of charged tRNAs might be due to higher steady state levels of tRNAs (Figure 3.15 A-B). This observation also implies that there is no problem regarding the availability of the amino acids hence ruling out our hypothesis in a&b. Moreover, increased amount of uncharged tRNAs also rules out the hypothesis in c since

deacylated tRNA are getting released at the end of elongation phase and available for successive rounds of translation. This indicates that the translation process till elongation phase is likely proceeding without major inhibition.

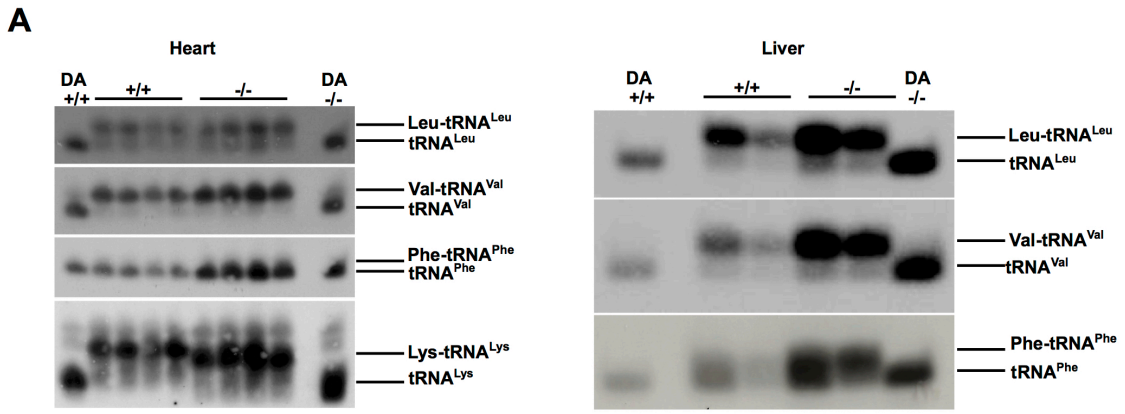

Figure 3.19 Increase in levels of charged and uncharged forms of tRNAs in absence of CLPP in heart and liver.

(A) Aminoacylation assay for mitochondrial $tRNA^{Leu}$, $tRNA^{Val}$, $tRNA^{Phe}$ and $tRNA^{Lys}$ in heart and liver of control (+/+) and *Clpp* knockout (-/-) mice. Positions of charged (AA-$tRNA^{AA}$) and uncharged ($tRNA^{AA}$) tRNAs are indicated. Deacylated (DA) or uncharged ($tRNA^{AA}$) tRNAs from control (+/+) and *Clpp* knockout (-/-) mice are used as Control for the experiment.

3.10. Identification of CLPP candidates with a possible role in mitochondrial translation

To identify the substrates of CLPP and its possible role in mitochondrial translation we developed a catalytically inactive version of CLPP by mutating Serine 149 to Alanine. This mutational disruption of active site inactivated the catalytic activity of CLPP, thereby leading to trapping of the substrates inside the channel of CLPP barrel when produced by its partner CLPX. We did the trapping of substrates of CLPP in mouse embryonic fibroblasts cells (MEFs). For trapping of CLPP substrates the above mentioned immortalized cells were used. Trapping of CLPP and identification of substrates and interactors has been performed by Dr. Karolina Szczepanowska. Transient expression (48 hours) was obtained after transfection of *Clpp* knockout MEFs with the constructs driven under CMV promoter as depicted in (Figure 3.20 A). Mitochondria was isolated followed by co immunoprecipitation with Anti-FLAG antibody and subsequently send for Mass Spectrometry analysis. Of the total number of proteins identified 286 (approximately 50%) were mitochondrial proteins, 134 proteins were shared between WT

($CLPP^{+/+}$), KO ($CLPP^{-/-}$) and TRAP ($CLPP^{TRAP}$). From this analysis, the most promising candidates in relation to post-transcriptional and translation processes are represented in the table (Figure 3.20 B) which are ERAL1, P32, EF-$G1_{mt}$, PNPT1 and MRPP1.

- ERAL1 has been previously shown to be associated with small mitoribosomal proteins including 12S rRNA, act as a chaperone protecting 12S rRNA, involved in assembly of the 28S small ribosomal subunits of and formation of functional small ribosomal subunits [116,117].
- P32 has been shown to be multifunctional, possessing important role in mitochondrial translation, apopotosis and formation of functional ribosomes [118,119]
- EF-$G1_{mt}$ is the elongation factor and is known to be involved in mitochondrial translation [50].
- PNPT1 has been shown to be a RNA binding protein and engaged in numerous RNA metabolic processes. PNPT1 is involved in mRNA processing and polyadenylation and hydrolyzes single-stranded polyribonucleotides in the 3'-5' direction. It also plays a role in RNA import into matrix [120–123].
- MRPP1 is ribonuclease P Protein 1 has been shown to be involved in 5'processing of mitochondrial tRNAs, is essential for RNA modification and translation [124].

A

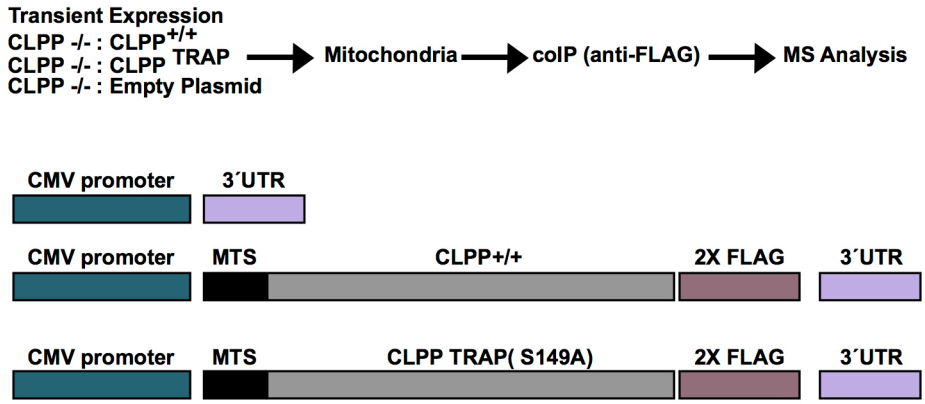

B

Promising Candidates	Empty Plasmid (No. of peptides)	+/+ (No. of peptides)	TRAP (No. of peptides)
ERAL1	0	0	6
P32 (C1QBP)	0	0	8
EF-G1$_{mt}$	0	0	7
MRPP1	0	0	2
PNPT1	0	2	10

Figure 3.20 Selected substrates and partners of CLPP involved in mitochondrial translation and RNA processing identified in *Clpp* knockout (-/-) MEFs.

(A) Strategy of identification of CLPP substrates and partners in mammalian *Clpp* knockout (-/-) MEFs. **(B)** Tabular representation of selected substrates and partners of CLPP.

In order to determine if the above mentioned promising candidates are substrates of CLPP, they need to fulfill the following criteria:

a. No change in their expression at transcript levels.

b. They are stabilized in *Clpp* deficient cells and are increased in their steady state levels.

c. Direct interaction between the candidates and CLPP.

d. *In vitro* degradation of the candidates by CLPP.

To validate ERAL1, EF-G1$_{mt}$, MRPP1 and CLPX as the substrates of CLPP, we performed real time PCR analysis and found non-significant changes of the transcripts in heart of *Clpp* knockout (-/-) mice. (Figure 3.21 A, from Dr. Alexandra Kukat) thereby

fulfilling the first criteria. Moreover, we detected an increase in the steady state levels of ERAL1, EF-G1$_{mt}$, MRPP1, CLPX, PNPT1 whereas no change in levels of P32 (Figure 3.21 B) fulfilling one of the requirements of being substrates. We got similar results from label free analysis of purified heart mitochondria from control (+/+) and *Clpp* knockout (-/-) mice supporting that the elevated levels of the substrates is due to its accumulation in the mitochondria in absence of CLPP and not due to upregulation of transcription.

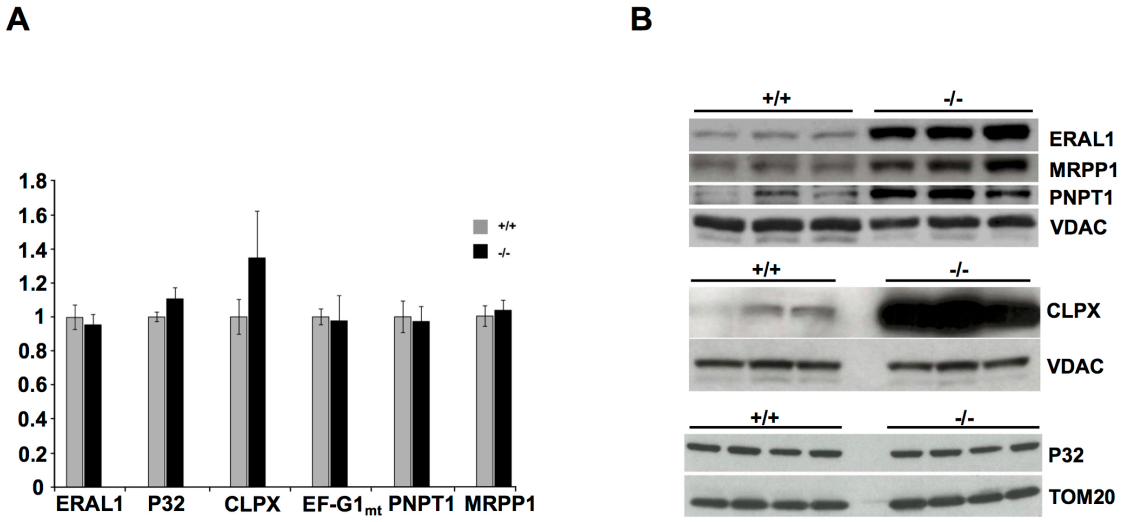

Figure 3.21 Steady state levels of potential candidates at RNA and protein levels

(A) Relative expression levels of ERAL1, P32, CLPX, EF-G1$_{mt}$, PNPT1 and MRPP1 from control (+/+) and *Clpp* knockout (-/-) heart (n=4). Error bar represents ± S.E.M. Asterisks denotes level of statistical significance (Student's t-test, *p<0.05, ** p<0.01, *** p<0.001). **(B)** Western blot analysis of promising candidates ERAL1, MRPP1, PNPT1, CLPX and P32 of control (+/+) and *Clpp* knockout (-/-) heart mitochondria. VDAC and TOM20 are used as loading controls**.**

After performing cyclohexamide (CHX) chase of cytoplasmic protein synthesis, the stability (turnover, half-life) of ERAL1, EF-G1$_{mt}$, MRPP1 were enhanced, supporting strongly that ERAL1, EF-G1$_{mt}$ and MRPP1 are substrates of CLPP (Figure 3.22 A, from Dr. Karolina Szczepanowska). We observed no change in the stability of P32 and PNPT1 thereby leaving a possibility of being interactors. It has been shown previously that CLPP interacts with CLPX [125]. From the co-immunoprecipitation analysis of CLPP (FLAG) and CLPX with P32 (Figure 3.22 B, from Dr. Karolina Szczepanowska), we observed that P32 interacts with CLPP. Currently we are performing experiments showing interaction between other candidates and CLPP.

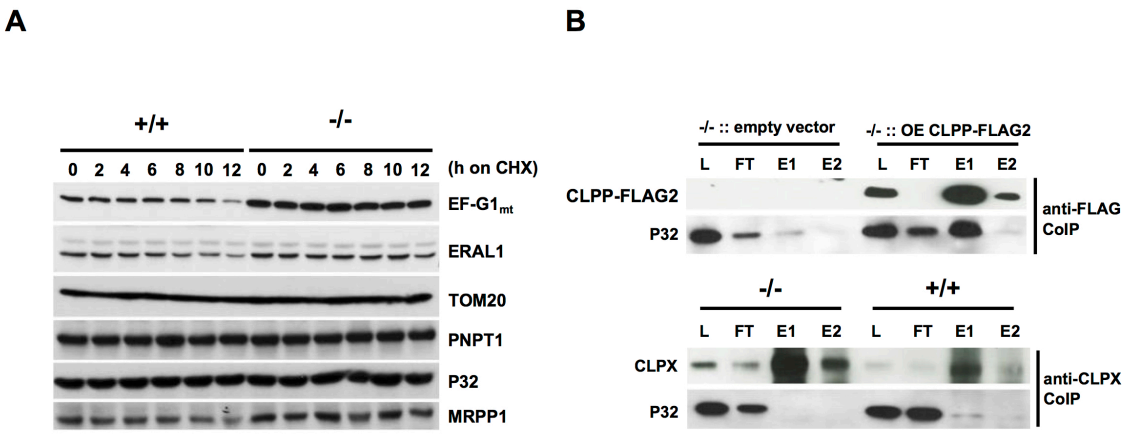

Figure 3.22 Stabilization of potential candidates

(A) Determination of the stability (turnover, half-life) of selected candidates using the cycloheximide (CHX) chase of cytoplasmic protein synthesis. **(B)** Co-immunoprecipitation of CLPP (FLAG) and CLPX with P32 in mitochondria from MEFs expressing CLPP-FLAG2. Western blot analysis of loading, flow through, eluate fractions shows that P32 antibody specifically immunoprecipitate CLPP (detected with anti-Flag antibody) and CLPX.

3.11. A possible role of CLPP in processing of RNA transcripts

Interestingly we found a significant accumulation of precursors of mRNAs and tRNAs in absence of CLPP indicating towards a problem in the processing of transcripts involving MRPP1 which has been shown to be a substrate (Figure 3.23 A). Previously accumulation of precursor for mRNA transcripts has been reported in knockout mouse models of MTERF3 known as a negative regulator of mtDNA transcription initiation [39], MTERF4 that has been shown to control mitochondrial ribosomal biogenesis and translation [41]. In addition, loss of function of GRSF1, an RNA binding protein interacting with RNase P lead to accumulation of tRNA precursors due to aberrant mitochondrial RNA processing [126]. However to address the question if CLPP has any specific role in maturation of the transcripts in general involving MRPP1 and PNPT1 we are currently performing further experiments.

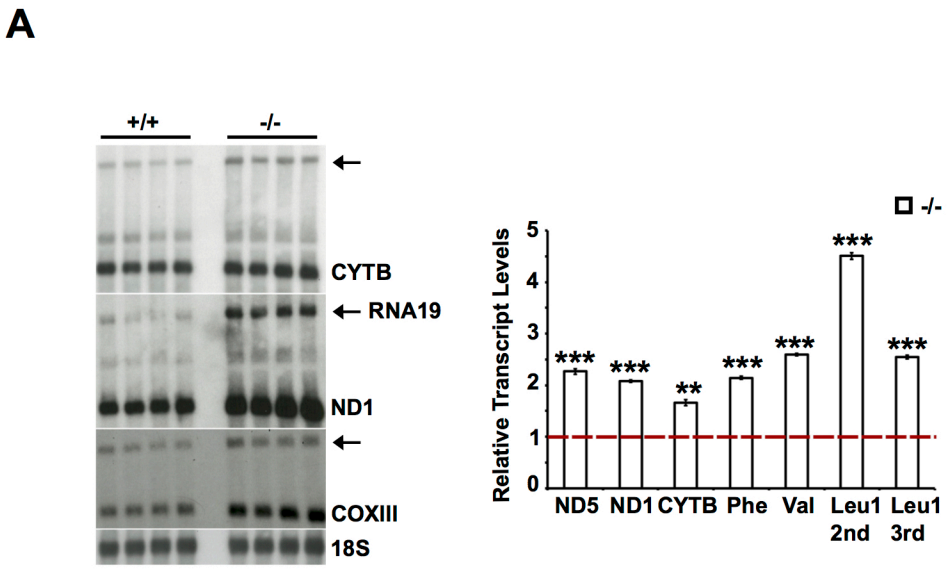

Figure 3.23 Accumulation of precursors of mRNAs and tRNAs in absence of CLPP

(A) Northern blot analysis of mitochondrial mRNA and accumulation of precursors (indicated by arrows) of control (+/+) and *Clpp* knockout (-/-) mice. Quantification of mitochondrial mRNA and tRNA precursor levels in heart, which is presented as percentage of control (+/+) (n=4). Error bar represents ± S.E.M. Asterisks denotes level of statistical significance (Student's t-test, *p<0.05, ** p<0.01, *** p<0.001).

3.12. ERAL1 and P32 interacts with the mitoribosomes

To investigate the migration of the substrates and interactors of CLPP with small, large subunits and monosomes, we performed gradient sedimentation analysis of mitochondrial extracts from heart of *Clpp* knockout (-/-) mice. Co migration of MRPS35 and MRPL12 has been used as markers for 28S (small) and 39S (large) ribosomal subunits respectively (Figure 3.24 A). Co migration of MRPS35 and MRPL12 were used as markers for fully assembled monosomes (55S). We observed an abnormal migration pattern of all the candidates in *Clpp* knockout (-/-) where it is present in much higher abundance through out the small, large and monosomes in differential amount. Migration of ERAL1 implied mostly with the small (28S) ribosomal subunit and P32 largely with large (39S) ribosomal subunit along with monosomes (55S). CLPX and EFG1 showed similar migration pattern predominantly with small (28S) and large (39S) ribosomal subunits

(Figure 3.24 B). However we also observe migration of CLPX and EF-G1$_{mt}$ with monosome (55S) but in lower amount. This might be due to sample loss during the processing of experiment.

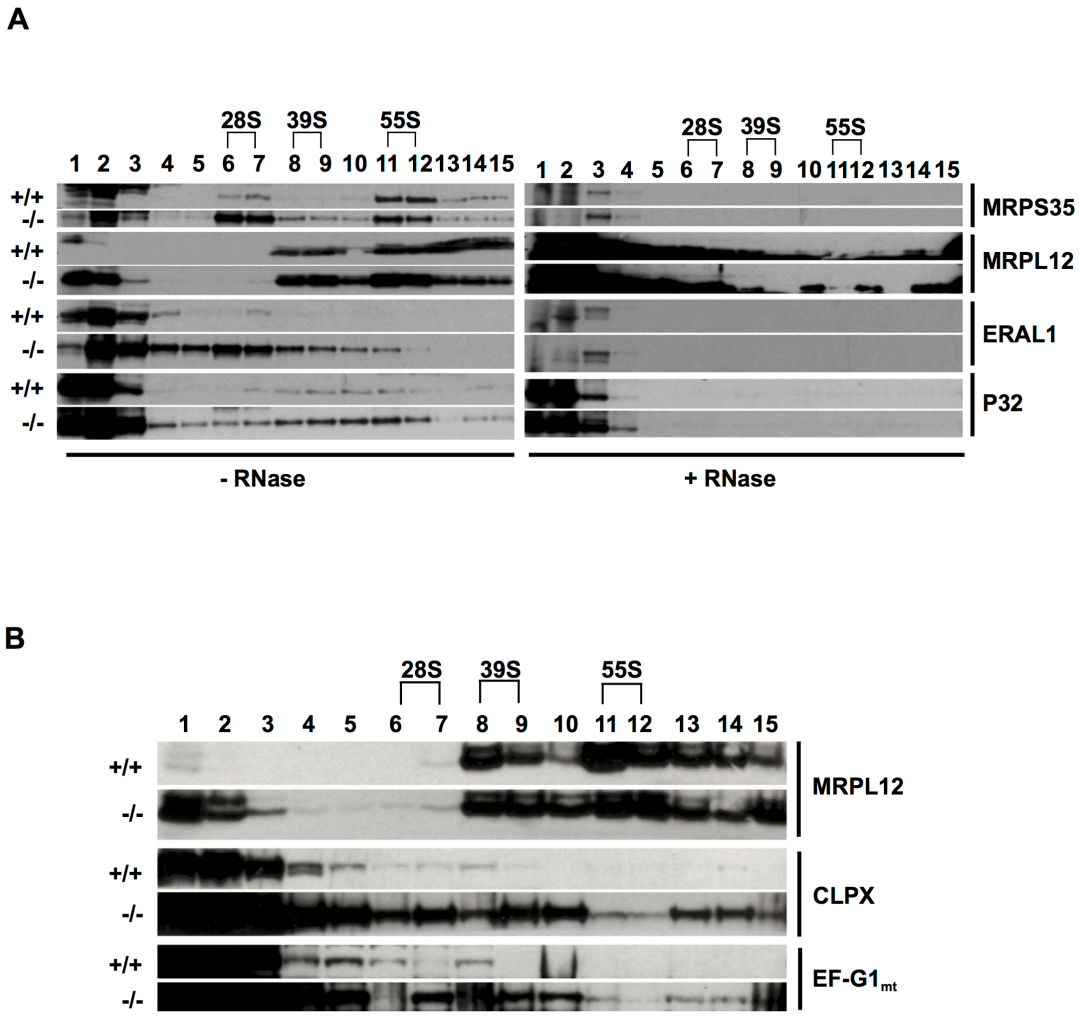

Figure 3.24 Substrates and interactors of CLPP are associated with mitochondrial ribosomes.

(A) Sedimentation analysis of ERAL1, P32 along with small (28S), large (39S) ribosomal subunits and assembled (55S) ribosome in heart mitochondria from of control (+/+) and *Clpp* knockout (-/-) heart mitochondria by centrifugation through linear 10%–30% sucrose density gradient. The migration of the potential candidates was detected by immunoblotting with MRPS35, MRPL12 ERAL1 and P32 antibodies. Furthermore in a parallel experiment Mitochondria were lysed and then treated with RNase A for 30 min at 37C to disintegrate mitochondrial ribosomes and analyze the association of the potential candidates with mitochondrial ribosomes **(B)** Similar to (A) the migration of migration of the potential candidates was detected by immunoblotting with CLPX and EFG1 antibodies.

3.13. *Clpp* deficiency leads to impairment of 12S rRNA assembly into monosomes leading to lower loading of mitochondrial mRNAs.

ERAL1 has been shown to be a substrate of CLPP and found to be mostly bound to the small (28S) ribosomal subunit (Figure 3.24 A). This implied primarily towards a problem with the assembly of small (28S) ribosomal subunit since ERAL1 is known as a chaperon for 12rRNA. This assembly defect in turn might perturb the stoichiometry of fully assembled monosome (55S) thereby affecting its proper function. To validate this we next performed similarly sucrose gradient sedimentation analyses of mitochondrial extracts from heart of *Clpp* knockout (-/-) mice (with Dr. Alexandra Kukat). MRPS35 and MRPL12 have been used as markers for migration of small (28S), large (39S) ribosomal subunits and monosomes (55S) (Figure 3.25 A). We then used TaqMan specific probes to measure levels of 12S rRNA and 16S rRNA in the different fractions and found that 12S rRNA co migrated with MRPS35 protein and 16S rRNA with MRPL12 in Control (+/+) mitochondria (Figure 3.25 B). We observed an abnormal distribution of 12S rRNA to a greater extent in small subunit fraction (28S) and to a much lesser extent in monosome fraction (55S). Later we analyzed migration of three different mRNAs and observed two different prominent pools of these mRNAs in Control (+/+) mitochondria. The first pool was towards the top of the gradient pertaining to low molecular weight region (fractions 2-3) followed by the second pool migrated towards the bottom of the gradient resembling to high molecular weight region with the assembled monosomes (55S) (fractions 11-12). The abundance of mRNAs in these two pools differed in *Clpp* knockout (-/-) mitochondria, with much higher levels in the first pool (fractions 2-3) than in second pool (fractions 11-12) as compared to Control (+/+). This suggested that only a fraction of mRNAs is getting translated in a particular time indicating a possible hindrance in translation process. This might be due to highest levels of ERAL1 that caused an impairment of 12S rRNA assembly into small subunit finally leading to lower loading of mitochondrial mRNAs on monosomes.

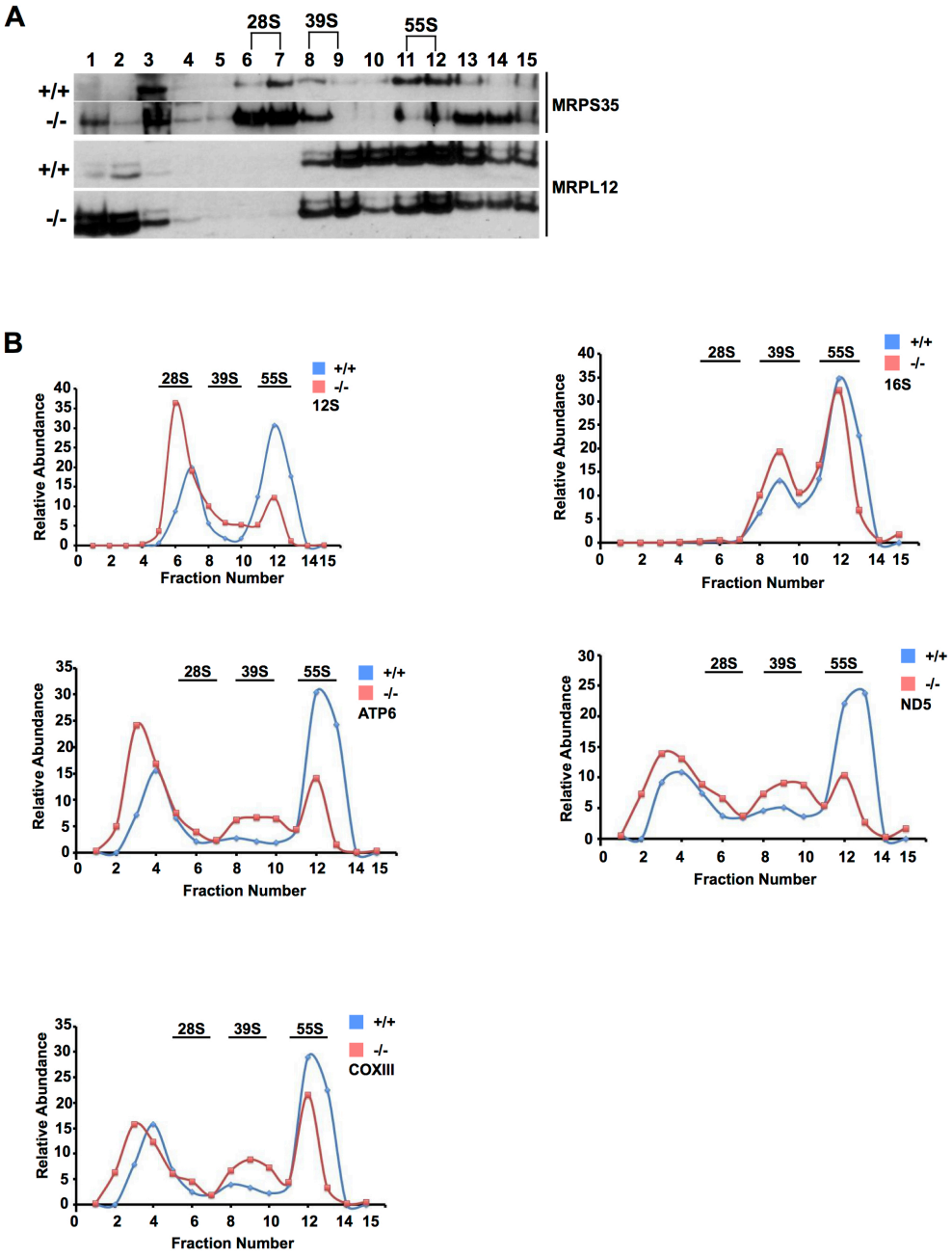

Figure 3.25 Substrates and interactors of CLPP likely to be involved in the assembly of 12S RNA into the small ribosomal subunit thereby affecting the function of monosomes

(A) Sedimentation analysis of small (28S), large (39S) ribosomal subunits and assembled (55S) ribosome from control (+/+) and *Clpp* knockout (-/-) heart mitochondria by centrifugation through linear 10%–30% sucrose density gradient. The migration of the small and large ribosomal subunits was detected by immunobloting with MRPS35 and MRPL12 antibodies and was used as reference. **(B)** Sedimentation profiles of mitochondrial transcripts in heart mitochondrial of control (+/+) and *Clpp* knockout (-/-) mice. Individual mitochondrial transcripts were detected using TaqMan-specific probes. The abundance of mRNA in each fraction is represented as percentage of the sum of the total abundance in all fractions.

3.14. Investigation of phenotype in *Clpp* knockout MEFs revealed lower levels of assembled respiratory chain supercomplexes.

To further elucidate the course of action through which CLPP along with its substrates and interactors are regulating the translation process, we are currently performing siRNA knockdown of the possible substrates thereby hoping to rescue the defect. Initially, in order to search for a phenotype in *Clpp* knockout (-/-) MEFs resembling the observed effect in *Clpp* knockout (-/-) mice, we focused on the physiological aspect in terms of growth rate (population doublings) (Figure 3.26 A, from Dr. Alexandra Kukat). We didn't find any significant changes in the growth rate of control (+/+) and *Clpp* knockout (-/-) MEFs grown both in glucose and galactose supplemented medium. We then carried out *in cello* translation in control (+/+) and *Clpp* knockout (-/-) MEFs grown on both glucose and galactose medium but didn't see any translational aberration after labeling with ^{35}S-methionine for 1 hour (Pulse) (Figure 3.26 B, from Dr. Alexandra Kukat). Furthermore, fluorescence microscopy images exhibited no deformation of the mitochondrial network in *Clpp* knockout (-/-) MEFs (Figure 3.26 C, from Dr. Alexandra Kukat). Next we performed gradient sedimentation analysis of mitochondrial extracts from MEFs grown on glucose and then switching then to galactose for 13 hours shifting cellular energy dependency using OXPHOS (Figure 3.26 D). Here we found lower amounts of small ribosomal subunits (28S) and large ribosomal subunits (39S). Though the migration pattern of ERAL1 and P32 in *Clpp* knockout (-/-) MEFs was similar to that observed in mice, but both of them migrated primarily with small ribosomal subunits (28S). We also did the similar sedimentation analysis for MEFs grown in galactose medium (Figure 3.26 E). Here we found lower amounts of small ribosomal subunits (28S) and no change in large ribosomal subunits (39S) along with monosome (55S). The migration pattern of both ERAL1 and P32 was primarily with small ribosomal subunits (28S) alike the previous sedimentation analysis. However interestingly, we found a shift in the distribution of monosomes in *Clpp* knockout (-/-) MEFs (fractions 9-11) as compared to control (+/+) (fractions 10-12). This implies that the formation of functional monosomes (55S) is affected thereby altering the stability. We used TaqMan probes to measure levels of 12S rRNA, 16S rRNA in different fractions and surprisingly found that 12S rRNA didn't co migrated with MRPS35 protein in Control (+/+) MEFs (Figure 3.26 E, with Dr. Alexandra Kukat), whereas 16S rRNA did co migrated with MRPL12. In

addition, for *Clpp* knockout (-/-) MEFs, 12S rRNA and 16S rRNA both comigrated with MRPS35 and MRPL12 respectively. We also analyzed the migration of three different mRNAs and observed a major pool towards the top of the gradient pertaining to low molecular weight (fractions 2-4). This suggested that a major fraction of mRNAs is not getting translated in a particular time due to unstable monosomes (55S). Nonetheless, we need to repeat this experiment since there is discrepancy of the migration of 12S rRNA with MRPS35. We have identified lower levels of Complex I for assembled respiratory supercomplexes in *Clpp* knockout (-/-) MEFs grown in galactose (data not shown). Currently we are performing siRNA knockdown experiments of the substrates of CLPP and observing the rescue at the level of assembled respiratory supercomplexes.

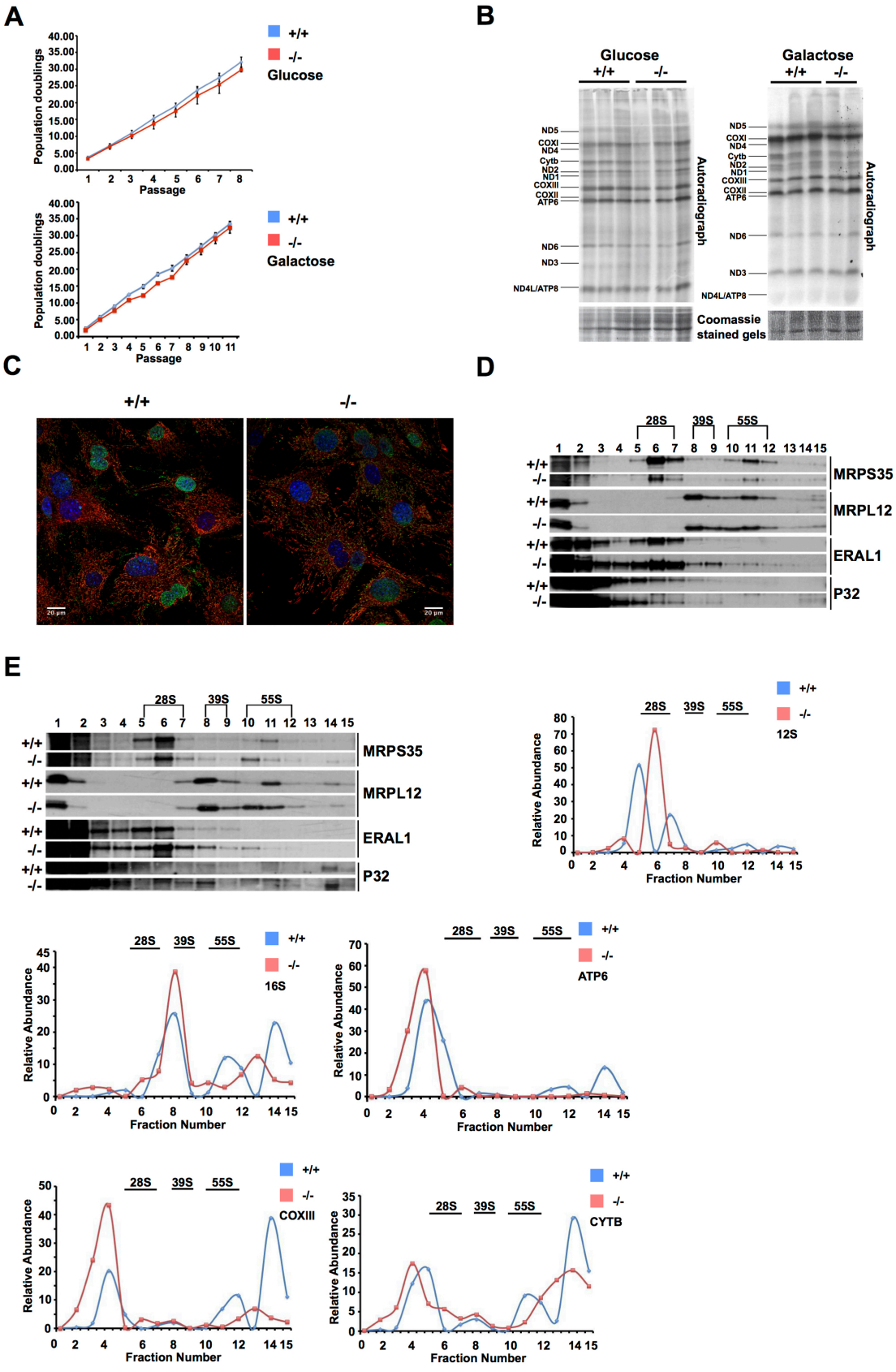
A
Population doublings
Passage
+/+
-/-
Glucose
Galactose
B
Glucose
Galactose
+/+
-/-
ND5
COXI
ND4
Cytb
ND2
ND1
COXIII
COXII
ATP6
ND6
ND3
ND4L/ATP8
Autoradiograph
Coomassie stained gels
C
+/+
-/-
20 µm
D
28S
39S
55S
MRPS35
MRPL12
ERAL1
P32
E
Relative Abundance
Fraction Number
12S
16S
ATP6
COXIII
CYTB

Figure 3.26 Phenotypic characterization of *Clpp* knockout MEFs

(A) Population doublings of control (+/+) and *Clpp* knockout (-/-) immortalized MEFs over passages. **(B)** *In cellular* translation of control (+/+) and *Clpp* knockout (-/-) immortalized MEFs. *De novo* synthesized proteins were isolated after labeling with ^{35}S-methionine for 1 hour (Pulse). Positions of individual mitochondrial encoded proteins are indicated. Coomassie blue stained gel is used to indicate equal loading of all lanes. **(C)** Fluorescence microscopy images depicting the mitochondrial network of control (+/+) and *Clpp* knockout (-/-) immortalized MEFs. Mitochondrial network is detected by membrane potential dependent MitoTracker Red CMXRos red fluorescent dye and nucleus is stained by DAPI blue fluorescent stain. **(D)** Sedimentation analysis of ERAL1, P32 along with small (28S), large (39S) ribosomal subunits and assembled (55S) ribosome from control (+/+) and *Clpp* knockout (-/-) immortalized MEFs grown in glucose medium and switched to galactose medium for 13 hours. The migration of the potential candidates was detected by immunobloting with MRPS35, MRPL12 ERAL1 and P32 antibodies. **(E)** Similar to (D) the migration of 28S, 39S and 55S from control (+/+) and *Clpp* knockout (-/-) immortalized MEFs grown in galactose medium is depicted for reference. Sedimentation profiles of mitochondrial transcripts in control (+/+) and *Clpp* knockout (-/-) immortalized MEFs grown in galactose medium. Individual mitochondrial transcripts were detected using TaqMan-specific probes. The abundance of mRNA in each fraction is represented as percentage of the sum of the total abundance in all fractions.

4. Discussion

The role of CLPP in various organisms has been studied in recent years; however, the biological role of CLPP protease in mammals is poorly understood. In the current study, we investigated the role of mitochondrial matrix protease CLPP at physiological and molecular levels by assessing the *Clpp* knockout mouse. Only around 60% of *Clpp* deficient mice are born indicating an important role of CLPP in the developmental stages of the organism. It is unclear at which developmental stage of the organism the remaining embryos are getting destroyed. This is in agreement with a study performed in eubacterium *C. crescentus*, where it has been shown that ClpXP protease is essential for cell-cycle-dependent turnover of CtrA, which is an inhibitor of G_1-to-S phase transition. Therefore, cells lacking ClpXP are arrested in the G_1 phase and blocked the cell division process, indicating importance of ClpXP specific degradation of CtrA [100]. Although this study in bacteria indicated an important role of ClpXP for maintaining normal cell division and growth of the organism, we need to perform further analysis to support the important role of CLPP in mammalian development.

We observed specific phenotypes in *Clpp* knockout mice that pointed out a potential role of CLPP in regulating specific candidates involved in various molecular, biochemical and metabolic pathways. We noticed some striking phenotypes or features of the *Clpp* knockout mice, (a) they are smaller than their wild type littermates indicating growth retardation; (b) they are infertile; (c) diminished activity that can be linked to mitochondrial pathology. These features represent classical symptoms and a faithful model of human Perrault syndrome that occurs due to missense mutations in *Clpp* and is primarily characterized by sensorineural hearing loss (SNHL), premature ovarian failure and short stature [107]. Surprisingly, loss of CLPP seems not to affect the longevity, since in our hands they live for at least two years, unlike other mouse models lacking genes essential for mtDNA expression [34,39,41,111,127]. In contrast to our results, another study showed that *Clpp* knockout mice lived for around one year [114]. This contradiction in results might be due to difference in the total number of animals used for lifespan experiments although both studies obtained similar phenotypes for the *Clpp* knockout mice. This discrepancy could also be a result of different technique used to obtain the *Clpp* deficient model. The previous study used gene-trapping method to generate

knockout mice whereas we used gene targeting. Gene trapping is a random process and is not as efficient or specific as gene targeting since not every successful insertion of artificial DNA into a gene will lead to a loss of function. Since gene trapping is a random process certain genes may never get hit due to statistics or because the gene is not active in ES cells thereby not producing the marker indicating that the gene has been knocked out. In addition, various studies have shown biasness of trapping vectors and some ''cold'' genomic spots on the chromosomes that remained untrapped[143, 144,145]. However our results are supported by another study in the filamentous fungus *P. anserine*, where deletion of ClpP results in an extension of healthy lifespan under normal growth conditions [128]. It has been proposed that under normal growth conditions, lack of PaClpP might cause a mild but tolerable stress leading to mitochondrial hormesis thereby leading to beneficial activation of maintenance and repair pathways that results in this lifespan extension [129]. Currently we are performing a new study with increased number of animals to determine the maximum lifespan in our *Clpp* deficient mice.

We have observed that *Clpp* knockout mice are smaller than their littermates and have a significant reduction in body weight. It is unclear if they are born small or it is a gradual decrease in body weight with age. In the previously described *Clpp* deficient mice study, it has been reported that the *Clpp* knockout mice weigh normal until weaning followed by reduced weight gain throughout adulthood [114]. Our initial studies showed lower body fat content, enhanced energy expenditure, less ambulatory activity, increase in respiratory quotient (RQ) during night indicating towards a shift to fatty acid metabolism, improved glucose tolerance and higher insulin sensitivity in the *Clpp* knockout animals. At the same time label free quantification analysis suggested different metabolic pathways to be one of the key affected processes. Similar observations were reported in a previous study where mitochondrial transcription factor A (TFAM) in adipose tissue was disrupted [146]. These mice exhibited altered levels of proteins of electron transport chain, mitochondrial dysfunction with decreased complex I activity and increased uncoupling that resulted in increasing mitochondrial oxidation capacity. These mice also had greater food intake but were protected from age- and diet-induced obesity, glucose intolerance, and hepatosteatosis through increased energy expenditure. Another study showed autophagy deficiency protects the mice from diet induced obesity and insulin resistance by inducing fibroblast growth factor 21 (Fgf21) [147]. Due to induction of Fgf21, fatty acid oxidation and browning of white adipose tissue (WAT) was increased. Similar to *Clpp* knockout

mice, these animals have reduced muscle and fat mass, lower body weight and enhanced energy expenditure. All these evidences gave us an indication towards a similar role CLPP in regulating the metabolism of the organism. These preliminary exciting results prompted us to perform further experiments to know if CLPP plays a role in protecting the mice against age and diet induced obesity and insulin resistance.

We report here that CLPP, one of the key members of the mitochondrial quality control team, has some new and unexpected roles in regulation of ribosomal biogenesis and mitochondrial translation. Label free quantification analysis of mitochondrial proteome gave the initial hint that CLPP might be regulating various substrates or candidates involved in processes such as respiratory chain & oxidative phosphorylation (OXPHOS), translation processes and metabolic processes. While investigating the role of CLPP in biochemical and molecular pathways, we observed an early specific decrease in Complex I activity, followed by a decrease in Complex IV activity later in life in *Clpp* knockout mice. We did not observe major changes in mtDNA levels although the previous study study in *Clpp* knockout mice reported increased levels of mtDNA levels [114]. This discrepancy might be due to the difference in techniques used in both analyses. We have quantified through Southern blot analysis while the other study used a semi-quantitative RT-PCR method. In addition, this study also showed no significant changes in the steady state levels of TFAM [114]. Since it has been shown that TFAM is necessary for mtDNA maintenance [127], increase in mtDNA levels is usually correlated with the increase in steady state levels of TFAM. Hence increase in mtDNA levels with unchanged levels of TFAM is less likely. We also did not observe any major change in the levels of TFAM (data not shown). Mitochondrial dysfunction usually triggers a compensatory activation of mitochondrial biogenesis, which is often accompanied by an increase in steady state levels of mtDNA along with increase in mitochondrial transcription. This is evident from studies in various mouse models with mitochondrial dysfunction lacking genes essential for mtDNA expression, posttranscriptional modifications and other mitochondrial factors such as TFB1M [34], MTERF4 [41], MTERF3 [40] and NSUN4[142]. Interestingly in *Clpp* knockout mice we do not see any compensatory activation of mitochondrial biogenesis, however, we do observe an increase in mitochondrial transcription. This upregulation in transcription is most likely to be a compensatory response to the observed decrease in mitochondrial translation in *Clpp* deficient mice. This upregulation of mitochondrial transcription might be one of the early responses to either a mild hindrance in translation

or defect in ribosome function, also suggesting that transcription and translation are oppositely coordinated. These results obtained from *Clpp* deficient mice are in accordance to other mouse models with mitochondrial dysfunction lacking genes essential for mtDNA expression, posttranscriptional modifications and other mitochondrial factors. All these mouse models; TFB1M [34], MTERF4 [41], MTERF3 [39,40] and NSUN4 [142], caused defective translation and increase in *de novo* transcription with increased steady state levels of most of mitochondrial transcripts. Hence decrease in mitochondrial translation in absence of CLPP suggested a direct or indirect role of CLPP in the process of mitochondrial protein synthesis. Moreover, similar to *Mterf3* [39, 40] knockout mice, we observed a decrease in steady state levels of 16S rRNA although the levels of 12S rRNA were mildly decreased. But the levels of RNA19 that encompasses 16S rRNA and ND1 were increased suggesting impairment in the processing of RNA 19 that might result in lower levels of 16S rRNA. We also found a significant accumulation of precursors for other mRNAs and tRNAs in *Clpp* deficient mice. Though, accumulation of precursors has been reported in other studies [41,126], its accumulation in *Clpp* deficient mice seems to be very interesting. MRPP1 that essential for RNA modification and translation [124] is likely to be a substrate of CLPP, indicating a role of CLPP in the processing of transcripts.

The mild decrease in steady state levels of 12S rRNA might suggest towards an impairment of the stability of small ribosomal subunit. In *Tfb1m* knockout mice steady state levels of 12S rRNA were significantly reduced[34]. In this study it was shown that lack of TFB1M resulted in the loss of dimethylation of 12S rRNA followed by decrease in steady state levels of 12S rRNA, instability of the small subunit of the ribosome thereby disrupting formation of mitochondrial monosomes. Even though in our study we did not obtain a strong phenotype similar to TFB1M, lower steady state levels of 12S rRNA might indicate towards a mild impairment of stability of small ribosomal subunit. This might have resulted in the increase in the steady state levels of small ribosomal subunit and likely be the initiation point of mild impairment in translation in *Clpp* deficient mice.

Surprisingly, we found, via gradient sedimentation analysis that the mitochondrial ribosomes appears to be assembled properly and present in almost normal levels. This result was quiet perplexing since earlier studies demonstrated impaired mitoriobosome assembly as the cause behind the observed translational defect [34,40,41,142]. In *Tfb1m*

knockout mice, there was a deficiency of assembled small ribosomal subunit (SSU) and an increase in large ribosomal subunit (LSU) thereby affecting the formation or stability of the monosomes [34]. In *Mterf4* knockout, there was a drastic increase in levels of both SSU and LSU but no corresponding increase in levels of monosomes. This could be either lack of interaction between SSU and LSU to form monosomes or the stability of fully assembled monosomes could be affected [41]. In *Mterf3* deficient mice there was an increase in levels of SSU but decrease in levels of LSU and low amount of monosomes at younger stage. In addition, at later stages the levels of LSU significantly decreased that resulted in complete disruption of assembled monosomes. In *Nsun4* knockout mice it was shown an accumulation of assembled SSU and LSU without a corresponding increase in assembled ribosomes suggesting inhibition of association between the SSU and LSU to form functional ribosomes. However, in *Clpp* deficient mice we observe an increase in the levels of SSU and minor increase in levels of LSU whereas monosomes are present in almost normal levels and likely to be assembled properly.

Another striking feature was the massive increase in the steady state levels of small ribosomal subunits, while large ribosomal subunits were present in almost normal levels. This suggests either a problem with the assembly small ribosomal subunit as mentioned before or a complexity with the large ribosomal subunit where the increase in steady state levels of small ribosomal subunits is a compensatory response to it. It might also be possible that the stability of small ribosomal subunit is affected due to absence of any single small subunit. However, these possibilities lead to some open questions, if the stability of mitoribosomes is mildly affected or not and/or if these mitoribosomes are functional or not.

Further investigation revealed an impairment of 12S rRNA assembly into mitoribosomes leading to lower loading of mt-mRNAs. We noticed that in a particular time, only a fraction of mRNAs was getting translated which might a possible explanation behind the observed hindrance in translation process. Our finding correlates with another study showing abnormal interaction between ribosomal subunits and mRNAs as an explanation behind defective translation where there was no defect in the assembly of mitoribosomes [111].

Our results from identification of CLPP specific substrates helped us to streamline regarding the role of CLPP in regulating ribosomal biogenesis and translation. ERAL1, P32, EF-G1$_{mt}$ appeared to be the promising candidates that were likely to be involved in

this process. In this study we show ERAL1 and EF-G1$_{mt}$ are the substrates of CLPP and P32 likely to be an interactor of CLPP.

ERAL1:

ERAL1 (Era G-protein like 1) is the mammalian orthologue of the *E. coli* Ras-like protein Era [148]. In *E. coli* it has been shown that Era is essential for cell division [149]. In addition, it has been reported that Era binds to the 30S small ribosomal subunit near to the 3' terminus of the 16S rRNA suggesting its direct involvement in the functional assemble of 30S small ribosomal subunit of *E. coli* [150,151]. Our data implies that ERAL1 is preferentially bound to the small subunit of the ribosome and to monosomes to a lesser extent in *Clpp* knockout mice. Previous studies have shown that ERAL1 which is a member of the conserved GTP binding proteins with RNA binding activity, act as a chaperone that protects 12S rRNA on the 28S mitoribosomal subunit during the assembly of small ribosomal subunit. It has been also shown ERAL1 associates with small ribosomal subunits and is involved in its assembly thereby forming functional small ribosomal subunits [116,117]. But unexpectedly we observe that in absence of CLPP, ERAL1 seems to be stuck with the small ribosomal subunit that too in a much higher abundance in *Clpp* knockout mice. It is also unknown about how ERAL1 itself is regulated. ERAL1 being a chaperone of 12S rRNA is expected to leave after assembling the 12S rRNA component along with respective small subunit proteins to form the fully assembled and functional small subunit. Since ERAL1 is still bound to small ribosomal subunit, this can be interpreted as involvement of ERAL1 causing an impairment of 12S rRNA assembly into small ribosomal subunit thereby finally leading to lower loading of mitochondrial mRNAs on monosomes. Moreover, this phenomenon of ERAL1 being bound to small ribosomal subunit arises some open questions regarding what is causing ERAL1 to still hang around with the small ribosomal subunit. It might be possible that either some small ribosomal subunit proteins are missing or if any assembly factor of small ribosomal subunit is absent. Although no assembly factors for small ribosomal subunit has been identified to date, but we can not rule out the presence of any assembly factors since they are required for assembling cytosolic ribosomes in various organisms. There can also be a probability that binding of ERAL1 to the small ribosomal subunit may interfere or block the association of some other proteins thereby impeding the assembly of the small ribosomal subunit or the association of the large subunit to form a fully functional monosome. Hence, it would be interesting to know about the proteins associated with

ERAL1 in the *Clpp* knockout mice since this will give us further insight regarding the binding of ERAL1 to the small ribosomal subunit. In addition, we are currently performing experiments to show if there is any interaction between ERAL1 and CLPX. This may imply that in absence of CLPP, CLPX recognizes and binds ERAL1 but unable to produce to CLPP for subsequent degradation and thereby still bound with the small ribosomal subunit.

On one hand, ERAL1 association to the small ribosomal subunit might be the cause for the decrease translation in *Clpp* knockout mice or the effect of not being able to be turnover or degraded in the absence of CLPP that leads to the series of events or consequences as mentioned above.

P32:

In this study, we report that P32 is likely to be an interactor of CLPP and is preferentially bound to large ribosomal subunit and monosomes. Our result is comparable to previous analysis where P32 was shown to be associated with mitoribosomes [118]. P32 is mainly localized to mitochondrial matrix, but various studies have reported P32 to be present in other subcellular locations [132–135]. P32 has been shown to be multifunctional possessing important roles in mitochondrial translation, correct functioning of mitoribosomes with mRNA, apoptosis, autophagy and regulating mitochondrial bioenergetics [118,136]. It has also been proposed in various studies that P32 may act as a multifunctional chaperone protein [119,137,138]. P32 is a very acidic doughnut shape protein whose one side is much less negatively charged and proposed to bind RNA whereas the acidic side might be involved in protein-protein interactions such as mitoribosome [133]. So far it is not clear about how mRNA is fed into the mRNA entrance gate on the small ribosomal subunit. Few studies have suggested that mRNA 'entry gate' on the small subunit recognizes the unique unstructured 5'sequence of mitochondrial mRNA[47]. It might be possible that P32 mediates the binding of mRNA to the small ribosomal subunit thereby enhancing the formation of monosomes since it has been shown that P32 is essential for association of mRNAs with mitoribosomes. In this same study, P32 was found to significantly bind to RNA and stimulate translation. Hence it was proposed that RNA chaperone activity of P32 might contribute to transport RNAs to mitoribosomes thereby enhancing initiation of translation [118]. Another possibility is P32 might be involved in guiding the 5'leaderless mRNA to mitoribosomes for initiation of translation either by enhancing the formation of mitoribosome or stabilizing mitoribosomes. These proposed roles could also hold true for

Clpp knockout mice since we showed that P32 is bound to mitoribosomes and also interacts with CLPP. Interestingly, ERAL1 and CLPX were among the list of identified proteins in complex with P32 [118]. However, our data suggests that P32 interacts directly with CLPP and not with CLPX and therefore its interaction with CLPX is secondary.

It could be that the complication is initiated at step 1 where ERAL1 is bound to the small ribosomal subunit thereby affecting its assembly and proper function. This event is followed by the subsequent consequences in the next series of events. One of them is P32 being still bound to mitoribosomes, which is essential for association of mRNAs with small ribosomal subunit to enhance initiation of translation. However, since ERAL1 is still bound to ribosomes, the entire system senses some trouble, which instructs P32 to hang around with the mitoribosomes on one side and mRNAs on the other thereby resulting in lower loading of mitochondrial mRNAs on monosomes and decrease in mitochondrial translation.

EF-G1$_{mt}$:

This is a factor involved in the elongation phase of mitochondrial translation. EF-G1$_{mt}$ is required for the translocation of the mitoribosome thereby moving deacylated tRNA out of the P-site and the peptidyl tRNA from the A-site to the P-site of mitoribosome [50]. In this study we have shown EF-G1$_{mt}$ to be a substrate of CLPP and also associates with the mitoribosomes in *Clpp* knockout mice. EF-G1$_{mt}$ association with mitoribosomes in higher abundance is another striking feature since under normal condition of mitochondrial translation, once EF-G1$_{mt}$ and deacylated tRNA are released from the mitoribosomes a new cycle of elongation can begin. This might be another consequence sensing a problem that is initiated at step 1 where ERAL1 is bound to small ribosomal subunit.

CLPX:

In order to carry out protein degradation by CLPXP, it requires the collaboration of CLPX, which binds substrates, adaptors and CLPP. The main function of CLPX is to unfold the stable tertiary structure of the substrate and then translocate the unfolded polypeptide chain into the proteolytic compartment of ClpP for degradation. Previous study have proposed additional role of CLPX as a novel mtDNA regulator. It has been shown that CLPX acts as a chaperone thereby maintaining mtDNA nucleoid distribution through TFAM activity[139]. Trapping and proteomic profiling of ClpP substrates in various organisms have revealed CLPX as one of the identified proteins similar to our analysis[140, 141]. In our study we show that CLPX is also bound to mitoribosomes in higher

abundance in *Clpp* knockout mice. We have also proven ERAL1 and EF-G1$_{mt}$ to be the substrates of CLPP that are recognized, captured, unfolded by CLPX followed by translocation into the proteolytic compartment of CLPP for degradation. One reason behind the association of the CLPX with mitoribosomes could be the consequence of the complication generated at initial step 1 involving ERAL1. Another reason could be that in absence of CLPP, CLPX might have captured CLPP specific substrates ERAL1 and EF-G1$_{mt}$ but unable to produce them for degradation.

To conclude it appears that CLPP exhibits various roles in mammals. In this study we have shown the role of CLPP in regulation of mitochondrial ribosome biogenesis through two of the most promising identified candidates: ERAL1 and P32 where ERAL1 is substrate of CLPP and P32 likely to be an interactor. In addition, we have also presented some interesting preliminary results indicating towards a role of CLPP in mammalian metabolism.

References

1. McBride HM, Neuspiel M, Wasiak S. Mitochondria: More Than Just a Powerhouse. Curr Biol 2006; 16:551–60.
2. Van der Giezen M. Mitochondria and the Rise of Eukaryotes. Bioscience 2011; 61:594–601.
3. Margulis L. Symbiotic theory of the origin of eukaryotic organelles; criteria for proof. Symp Soc Exp Biol 1975; :21–38.
4. Kurland CG, Andersson SG. Origin and evolution of the mitochondrial proteome. Microbiol Mol Biol Rev 2000; 64:786–820.
5. Andersson SGE, Karlberg O, Canbäck B, Kurland CG. On the origin of mitochondria: a genomics perspective. Philos Trans R Soc Lond B Biol Sci 2003; 358:165–77; discussion 177–9.
6. Gray MW. Mitochondrial evolution. Cold Spring Harb Perspect Biol 2012; 4:1–17.
7. Koonin E V. The origin and early evolution of eukaryotes in the light of phylogenomics. Genome Biol 2010; 11:209.
8. Doolittle WF. A paradigm gets shifty. Nature 1998; 392:15–6.
9. Martin W, Müller M. The hydrogen hypothesis for the first eukaryote. Nature 1998; 392:37–41.
10. Navarro A, Boveris A. The mitochondrial energy transduction system and the aging process. 2007; :670–86.
11. Kukat C, Wurm C a, Spåhr H, Falkenberg M, Larsson N-G, Jakobs S. Super-resolution microscopy reveals that mammalian mitochondrial nucleoids have a uniform size and frequently contain a single copy of mtDNA. Proc Natl Acad Sci U S A 2011; 108:13534–9.
12. Chinnery PF, Hudson G. Mitochondrial genetics. Br Med Bull 2013; 106:135–59.
13. Falkenberg M, Larsson N-G, Gustafsson CM. DNA replication and transcription in mammalian mitochondria. Annu Rev Biochem 2007; 76:679–99.
14. Schwartz, , M. and JVi. Paternal inheritance of mito- chondrial DNA. N Engl J Med 2002; 347:576–80.
15. Larsson N-G. Somatic mitochondrial DNA mutations in mammalian aging. Annu Rev

Biochem 2010; 79:683–706.
16. Van den Heuvel L, Smeitink J. The oxidative phosphorylation (OXPHOS) system: nuclear genes and human genetic diseases. Bioessays 2001; 23:518–25.
17. Dudkina N V., Kouřil R, Peters K, Braun HP, Boekema EJ. Structure and function of mitochondrial supercomplexes. Biochim Biophys Acta - Bioenerg 2010; 1797:664–70.
18. Hackenbrock CR, Chazotte B, Gupte SS. The random collision model and a critical assessment of diffusion and collision in mitochondrial electron transport. J Bioenerg Biomembr 1986; 18:331–68.
19. Boekema EJ, Braun H-P. Supramolecular structure of the mitochondrial oxidative phosphorylation system. J Biol Chem 2007; 282:1–4.
20. Schägger H, Pfeiffer K. Supercomplexes in the respiratory chains of yeast and mammalian mitochondria. EMBO J 2000; 19:1777–83.
21. Eubel H, Jänsch L, Braun H-P. New insights into the respiratory chain of plant mitochondria. Supercomplexes and a unique composition of complex II. Plant Physiol 2003; 133:274–86.
22. Dudkina N V, Eubel H, Keegstra W, Boekema EJ, Braun H-P. Structure of a mitochondrial supercomplex formed by respiratory-chain complexes I and III. Proc Natl Acad Sci U S A 2005; 102:3225–9.
23. Schäfer E, Dencher NA, Vonck J, Parcej DN. Three-dimensional structure of the respiratory chain supercomplex I1III2IV1 from bovine heart mitochondria. Biochemistry 2007; 46:12579–85.
24. Heinemeyer J, Braun HP, Boekema EJ, Kouřil R. A structural model of the cytochrome c reductase/oxidase supercomplex from yeast mitochondria. J Biol Chem 2007; 282:12240–8.
25. Acín-Pérez R, Bayona-Bafaluy MP, Fernández-Silva P, Moreno-Loshuertos R, Pérez-Martos A, Bruno C, Moraes CT, Enríquez JA. Respiratory complex III is required to maintain complex I in mammalian mitochondria. Mol Cell 2004; 13:805–15.
26. Boumans H, Grivell LA, Berden JA. The respiratory chain in yeast behaves as a single functional unit. J Biol Chem 1998; 273:4872–7.
27. Blanchi C, Genova ML, Castelli GP, Lenaz G. The mitochondrial respiratory chain is partially organized in a supercomplex assembly: Kinetic evidence using flux control analysis. J Biol Chem 2004; 279:36562–9.
28. Heron C, Ragan CI, Trumpower BL. The interaction between mitochondrial NADH-

ubiquinone oxidoreductase and ubiquinol-cytochrome c oxidoreductase. Restoration of ubiquinone-pool behaviour. Biochem J 1978; 174:791–800.
29. Zhang M, Mileykovskaya E, Dowhan W. Cardiolipin is essential for organization of complexes III and IV into a supercomplex in intact yeast mitochondria. J Biol Chem 2005; 280:29403–8.
30. Pfeiffer K, Gohil V, Stuart RA, Hunte C, Brandt U, Greenberg ML, Schägger H. Cardiolipin Stabilizes Respiratory Chain Supercomplexes. J Biol Chem 2003; 278:52873–80.
31. Acín-Pérez R, Fernández-Silva P, Peleato ML, Pérez-Martos A, Enriquez JA. Respiratory Active Mitochondrial Supercomplexes. Mol Cell 2008; 32:529–39.
32. Gilkerson RW, Schon E a. Nucleoid autonomy. 2008; 1:34–6.
33. Falkenberg M, Gaspari M, Rantanen A, Trifunovic A, Larsson N-G, Gustafsson CM. Mitochondrial transcription factors B1 and B2 activate transcription of human mtDNA. Nat Genet 2002; 31:289–94.
34. Metodiev MD, Lesko N, Park CB, Cámara Y, Shi Y, Wibom R, Hultenby K, Gustafsson CM, Larsson NG. Methylation of 12S rRNA Is Necessary for In Vivo Stability of the Small Subunit of the Mammalian Mitochondrial Ribosome. Cell Metab 2009; 9:386–97.
35. Peralta S, Wang X, Moraes CT. Mitochondrial transcription: Lessons from mouse models. Biochim Biophys Acta - Gene Regul Mech [Internet] 2012; 1819:961–9.
36. Fernandez-Silva P, Martinez-Azorin F, Micol V, Attardi G. The human mitochondrial transcription termination factor (mTERF) is a multizipper protein but binds to DNA as a monomer, with evidence pointing to intramolecular leucine zipper interactions. EMBO J 1997; 16:1066–79.
37. Linder T, Park C, Asin-Cayuela J, Pellegrini M, Larsson N-G, Falkenberg M, Samuelsson T, Gustafsson C. A family of putative transcription termination factors shared amongst metazoans and plants. Curr Genet [Internet] 2005; 48:265–9.
38. Wenz T, Luca C, Torraco A, Moraes CT. mTERF2 Regulates Oxidative Phosphorylation by Modulating mtDNA Transcription. Cell Metab 2009; 9:499–511.
39. Park CB, Asin-Cayuela J, Cámara Y, Shi Y, Pellegrini M, Gaspari M, Wibom R, Hultenby K, Erdjument-Bromage H, Tempst P, et al. MTERF3 Is a Negative Regulator of Mammalian mtDNA Transcription. Cell 2007; 130:273–85.
40. Wredenberg A, Lagouge M, Bratic A, Metodiev MD, Spåhr H, Mourier A, Freyer C,

Ruzzenente B, Tain L, Grönke S, et al. MTERF3 Regulates Mitochondrial Ribosome Biogenesis in Invertebrates and Mammals. PLoS Genet 2013; 9.
41. Cámara Y, Asin-Cayuela J, Park CB, Metodiev MD, Shi Y, Ruzzenente B, Kukat C, Habermann B, Wibom R, Hultenby K, et al. MTERF4 regulates translation by targeting the methyltransferase NSUN4 to the mammalian mitochondrial ribosome. Cell Metab 2011; 13:527–39.
42. Christian BE, Spremulli LL. Mechanism of protein biosynthesis in mammalian mitochondria. Biochim Biophys Acta - Gene Regul Mech 2012; 1819:1035–54.
43. Lightowlers RN, Rozanska A, Chrzanowska-Lightowlers ZM. Mitochondrial protein synthesis: Figuring the fundamentals, complexities and complications, of mammalian mitochondrial translation. FEBS Lett 2014; 588:2496–503.
44. Smirnov A, Entelis N, Martin RP, Tarassov I. Biological significance of 5s rRNA import into human mitochondria: Role of ribosomal protein MRP-L18. Genes Dev 2011; 25:1289–305.
45. Graack HR, Wittmann-Liebold B. Mitochondrial ribosomal proteins (MRPs) of yeast. Biochem J 1998; 329 (Pt 3):433–48.
46. Rorbach J, Soleimanpour-Lichaei R, Lightowlers RN, Chrzanowska-Lightowlers ZM a. How do mammalian mitochondria synthesize proteins? Biochem Soc Trans 2007; 35:1290–1.
47. Sharma MR, Koc EC, Datta PP, Booth TM, Spremulli LL, Agrawal RK. Structure of the mammalian mitochondrial ribosome reveals an expanded functional role for its component proteins. Cell 2003; 115:97–108.
48. Agirrezabala X, Frank J. Elongation in translation as a dynamic interaction among the ribosome, tRNA, and elongation factors EF-G and EF-Tu. Q Rev Biophys 2009; 42:159–200.
49. Temperley RJ, Wydro M, Lightowlers RN, Chrzanowska-Lightowlers ZM. Human mitochondrial mRNAs-like members of all families, similar but different. Biochim. Biophys. Acta - Bioenerg.2010; 1797:1081–5.
50. Tsuboi M1, Morita H, Nozaki Y, Akama K, Ueda T, Ito K, Nierhaus KH, Takeuchi N. EF-G2mt is an exclusive recycling factor in mammalian mitochondrial protein synthesis. Mol Cell. 2009;35(4):502-10.
51. Christian B, Haque E, Spremulli L. Ribosome Shifting or Splitting: It Is All Up To the EF-G. Mol. Cell2009; 35:400–2.

52. Rhee H-W, Zou P, Udeshi ND, Martell JD, Mootha VK, Carr SA, Ting AY. Proteomic Mapping of Mitochondria in Living Cells via Spatially Restricted Enzymatic Tagging. Science (80-) [Internet] 2013; :- – .
53. Herrmann JM, Riemer J. The intermembrane space of mitochondria. Antioxid Redox Signal 2010; 13:1341–58.
54. Vögtle FN, Meisinger C. Sensing Mitochondrial Homeostasis: The Protein Import Machinery Takes Control. Dev Cell 2012; 23:234–6.
55. Bohovych I, Chan SSL, Khalimonchuk O. Mitochondrial Protein Quality Control: The Mechanisms Guarding Mitochondrial Health. Antioxid Redox Signal [Internet] 2015; 22:150211122620008.
56. Figueira TR, Barros MH, Camargo AA, Castilho RF, Ferreira JCB, Kowaltowski AJ, Sluse FE, Souza-Pinto NC, Vercesi AE. Mitochondria as a source of reactive oxygen and nitrogen species: from molecular mechanisms to human health. Antioxid Redox Signal [Internet] 2013; 18:2029–74.
57. Schieber M, Chandel NS. ROS function in redox signaling and oxidative stress. Curr. Biol.2014; 24.
58. Tatsuta T. Protein quality control in mitochondria. J Biochem 2009; 146:455–61.
59. Hammerling BC, Gustafsson ÅB. Mitochondrial Quality Control in the Myocardium: Cooperation between Protein Degradation and Mitophagy. J Mol Cell Cardiol [Internet] 2014; 75:122–30.
60. Pellegrino MW, Nargund AM, Haynes CM. Signaling the mitochondrial unfolded protein response. Biochim Biophys Acta - Mol Cell Res [Internet] 2013; 1833:410–6.
61. Tasaki T, Sriram SM, Park KS, Kwon YT. The N-End Rule Pathway. Annu. Rev. Biochem.2012; 81:261–89.
62. Kremmidiotis G, Gardner AE, Settasatian C, Savoia A, Sutherland GR, Callen DF. Molecular and functional analyses of the human and mouse genes encoding AFG3L1, a mitochondrial metalloprotease homologous to the human spastic paraplegia protein. Genomics 2001; 76:58–65.
63. Tatsuta T, Langer T. Quality control of mitochondria: protection against neurodegeneration and ageing. EMBO J 2008; 27:306–14.
64. Anand R, Wai T, Baker MJ, Kladt N, Schauss AC, Rugarli E, Langer T. The i-AAA protease YME1L and OMA1 cleave OPA1 to balance mitochondrial fusion and fission. J Cell Biol 2014; 204:919–29.

65. Griparic L, Kanazawa T, Van Der Bliek AM. Regulation of the mitochondrial dynamin-like protein Opa1 by proteolytic cleavage. J Cell Biol 2007; 178:757–64.
66. Potting C, Wilmes C, Engmann T, Osman C, Langer T. Regulation of mitochondrial phospholipids by Ups1/PRELI-like proteins depends on proteolysis and Mdm35. EMBO J 2010; 29:2888–98.
67. Dunn CD, Lee MS, Spencer FA, Jensen RE. A genomewide screen for petite-negative yeast strains yields a new subunit of the i-AAA protease complex. Mol Biol Cell 2006; 17:213–26.
68. Dunn CD, Tamura Y, Sesaki H, Jensen RE. Mgr3p and Mgr1p are adaptors for the mitochondrial i-AAA protease complex. Mol Biol Cell 2008; 19:5387–97.
69. Khalimonchuk O, Bird A, Winge DR. Evidence for a pro-oxidant intermediate in the assembly of cytochrome oxidase. J Biol Chem 2007; 282:17442–9.
70. Käser M, Kambacheld M, Kisters-Woike B, Langer T. Oma1, a Novel Membrane-bound Metallopeptidase in Mitochondria with Activities Overlapping with the m-AAA Protease. J Biol Chem 2003; 278:46414–23.
71. Baker MJ, Lampe P a, Stojanovski D, Korwitz A, Anand R, Tatsuta T, Langer T. Stress-induced OMA1 activation and autocatalytic turnover regulate OPA1-dependent mitochondrial dynamics. EMBO J [Internet] 2014; 33:578–93.
72. Ye Y, Shibata Y, Kikkert M, van Voorden S, Wiertz E, Rapoport TA. Recruitment of the p97 ATPase and ubiquitin ligases to the site of retrotranslocation at the endoplasmic reticulum membrane. Proc Natl Acad Sci U S A 2005; 102:14132–8.
73. Kim Y, Park J, Kim S, Song S, Kwon SK, Lee SH, Kitada T, Kim JM, Chung J. PINK1 controls mitochondrial localization of Parkin through direct phosphorylation. Biochem Biophys Res Commun 2008; 377:975–80.
74. Strappazzon F, Cecconi F. The multifaceted mitochondrion: An attractive candidate for therapeutic strategies. Pharmacol Res [Internet] 2015; :1–9.
75. Fischer F, Hamann A, Osiewacz HD. Mitochondrial quality control: An integrated network of pathways. Trends Biochem Sci [Internet] 2012; 37:284–92.
76. Wang X, Winter D, Ashrafi G, Schlehe J, Wong YL, Selkoe D, Rice S, Steen J, Lavoie MJ, Schwarz TL. PINK1 and Parkin target miro for phosphorylation and degradation to arrest mitochondrial motility. Cell 2011; 147:893–906.
77. Narendra D, Tanaka A, Suen DF, Youle RJ. Parkin is recruited selectively to impaired mitochondria and promotes their autophagy. J Cell Biol 2008; 183:795–803.

78. Soubannier V, McLelland GL, Zunino R, Braschi E, Rippstein P, Fon EA, McBride HM. A vesicular transport pathway shuttles cargo from mitochondria to lysosomes. Curr Biol 2012; 22:135–41.
79. Sugiura A, McLelland G-L, Fon E a, McBride HM. A new pathway for mitochondrial quality control: mitochondrial-derived vesicles. EMBO J [Internet] 2014; :1–15.
80. McLelland GL, Soubannier V, Chen CX, McBride HM, Fon EA. Parkin and PINK1 function in a vesicular trafficking pathway regulating mitochondrial quality control. EMBO J 2014; 33:282–95.
81. Wang C, Youle RJ. The role of mitochondria in apoptosis*. Annu Rev Genet 2009; 43:95–118.
82. Igney FH, Krammer PH. Death and anti-death: tumour resistance to apoptosis. Nat Rev Cancer 2002; 2:277–88.
83. Green DR. Apoptotic pathways: paper wraps stone blunts scissors. Cell 2000; 102:1–4.
84. Hanson PI, Whiteheart SW. AAA+ proteins: have engine, will work. Nat Rev Mol Cell Biol 2005; 6:519–29.
85. Sauer RT, Baker TA. AAA+ proteases: ATP-fueled machines of protein destruction. Annu Rev Biochem 2011; 80:587–612.
86. Grimaud R, Toussaint A. Assembly of both the head and tail of bacteriophage Mu is blocked in Escherichia coli groEL and groES mutants. J Bacteriol 1998; 180:1148–53.
87. Yu AYH, Houry WA. ClpP: A distinctive family of cylindrical energy-dependent serine proteases. FEBS Lett.2007; 581:3749–57.
88. Thompson MW, Singh SK, Maurizi MR. Processive degradation of proteins by the ATP-dependent Clp protease from Escherichia coli: Requirement for the multiple array of active sites in ClpP but not ATP hydrolysis. J Biol Chem 1994; 269:18209–15.
89. Neher SB, Villén J, Oakes EC, Bakalarski CE, Sauer RT, Gygi SP, Baker T a. Proteomic Profiling of ClpXP Substrates after DNA Damage Reveals Extensive Instability within SOS Regulon. Mol Cell 2006; 22:193–204.
90. Truscott KN, Bezawork-Geleta A, Dougan D a. Unfolded protein responses in bacteria and mitochondria: A central role for the ClpXP machine. IUBMB Life 2011; 63:955–63.
91. Muffler A, Traulsen DD, Lange R, Hengge-Aronis R. Posttranscriptional osmotic regulation of the sigma(s) subunit of RNA polymerase in Escherichia coli. J Bacteriol

1996; 178:1607–13.
92. Bougdour A, Cunning C, Baptiste PJ, Elliott T, Gottesman S. Multiple pathways for regulation of ??S (RpoS) stability in Escherichia coli via the action of multiple anti-adaptors. Mol Microbiol 2008; 68:298–313.
93. Baraban SC, Taylor MR, Castro P a, Baier H. Pentylenetetrazole induced changes in zebrafish behavior, neural activity and c-fos expression. Neuroscience [Internet] 2005 [cited 2013 Jan 29]; 131:759–68.
94. Bougdour A, Wickner S, Gottesman S. Modulating RssB activity: IraP, a novel regulator of ??S stability in Escherichia coli. Genes Dev 2006; 20:884–97.
95. Bougdour A, Gottesman S. ppGpp regulation of RpoS degradation via anti-adaptor protein IraP. Proc Natl Acad Sci U S A 2007; 104:12896–901.
96. Flynn JM, Levchenko I, Seidel M, Wickner SH, Sauer RT, Baker TA. Overlapping recognition determinants within the ssrA degradation tag allow modulation of proteolysis. Proc Natl Acad Sci U S A 2001; 98:10584–9.
97. Levchenko I, Seidel M, Sauer RT, Baker TA. A specificity-enhancing factor for the ClpXP degradation machine. Science 2000; 289:2354–6.
98. Damerau K, John a. CS. Role of Clp protease subunits in degradation of carbon starvation proteins in Escherichia coli. J Bacteriol 1993; 175:53–63.
99. Msadek T, Dartois V, Kunst F, Herbaud ML, Denizot F, Rapoport G. ClpP of Bacillus subtilis is required for competence development, motility, degradative enzyme synthesis, growth at high temperature and sporulation. Mol Microbiol 1998; 27:899–914.
100. Jenal U, Fuchs T. An essential protease involved in bacterial cell-cycle control. EMBO J 1998; 17:5658–69.
101. Xie F, Zhang Y, Li G, Zhou L, Liu S, Wang C. The ClpP Protease Is Required for the Stress Tolerance and Biofilm Formation in Actinobacillus pleuropneumoniae. PLoS One 2013; 8:1–11.
102. Haynes CM, Ron D. The mitochondrial UPR - protecting organelle protein homeostasis. J Cell Sci 2010; 123:3849–55.
103. Haynes CM, Petrova K, Benedetti C, Yang Y, Ron D. ClpP Mediates Activation of a Mitochondrial Unfolded Protein Response in C. elegans. Dev Cell 2007; 13:467–80.
104. Nargund AM, Pellegrino MW, Fiorese CJ, Baker BM, Haynes CM. Mitochondrial Import Efficiency of ATFS-1 Regulates Mitochondrial UPR Activation. Science (80-.).2012; 337:587–90.

105. Martinus RD, Garth GP, Webster TL, Cartwright P, Naylor DJ, Høj PB, Hoogenraad NJ. Selective induction of mitochondrial chaperones in response to loss of the mitochondrial genome. Eur J Biochem 1996; 240:98–103.
106. Zhao Q, Wang J, Levichkin I V., Stasinopoulos S, Ryan MT, Hoogenraad NJ. A mitochondrial specific stress response in mammalian cells. EMBO J 2002; 21:4411–9.
107. Jenkinson EM, Rehman AU, Walsh T, Clayton-Smith J, Lee K, Morell RJ, Drummond MC, Khan SN, Naeem MA, Rauf B, et al. Perrault syndrome is caused by recessive mutations in CLPP, encoding a mitochondrial ATP-dependent chambered protease. Am J Hum Genet [Internet] 2013; 92:605–13.
108. Wibom R, Hagenfeldt L, Von Döbeln U. Measurement of ATP production and respiratory chain enzyme activities in mitochondria isolated from small muscle biopsy samples. Anal Biochem 2002; 311:139–51.
109. Edgar D, Shabalina I, Camara Y, Wredenberg A, Calvaruso MA, Nijtmans L, Trifunovic A, Nedergaard J, Cannon B. Short Article. 2009; :131–8.
110. Enriquez JA, Chomyn A, Attardi G. MtDNA mutation in MERRF syndrome causes defective aminoacylation of tRNA(Lys) and premature translation termination. Nat Genet 1995; 10:47–55.
111. Ruzzenente B, Metodiev MD, Wredenberg A, Bratic A, Park CB, Cámara Y, Milenkovic D, Zickermann V, Wibom R, Hultenby K, et al. LRPPRC is necessary for polyadenylation and coordination of translation of mitochondrial mRNAs. EMBO J 2011; 31:443–56.
112. Trifunovic A, Hansson A, Wredenberg A, Rovio AT, Dufour E, Khvorostov I, Spelbrink JN, Wibom R, Jacobs HT, Larsson N-G. Somatic mtDNA mutations cause aging phenotypes without affecting reactive oxygen species production. Proc Natl Acad Sci U S A 2005; 102:17993–8.
113. Dogan SA, Pujol C, Maiti P, Kukat A, Wang S, Hermans S, Senft K, Wibom R, Rugarli EI, Trifunovic A. Tissue-specific loss of DARS2 activates stress responses independently of respiratory chain deficiency in the heart. Cell Metab 2014; 19:458–69.
114. Gispert S, Parganlija D, Klinkenberg M, Dröse S, Wittig I, Mittelbronn M, Grzmil P, Koob S, Hamann A, Walter M, et al. Loss of mitochondrial peptidase clpp leads to infertility, hearing loss plus growth retardation via accumulation of CLPX, mtDNA and inflammatory factors. Hum Mol Genet 2013; 22:4871–87.
115. Gottesman S, Roche E, Zhou Y, Sauer RT. The ClpXP and ClpAP proteases

degrade proteins with carboxy-terminal peptide tails added by the SsrA-tagging system. Genes Dev 1998; 12:1338–47.
116. Uchiumi T, Ohgaki K, Yagi M, Aoki Y, Sakai A, Matsumoto S, Kang D. ERAL1 is associated with mitochondrial ribosome and elimination of ERAL1 leads to mitochondrial dysfunction and growth retardation. Nucleic Acids Res 2010; 38:5554–68.
117. Dennerlein S, Rozanska A, Wydro M, Chrzanowska-Lightowlers ZMA, Lightowlers RN. Human ERAL1 is a mitochondrial RNA chaperone involved in the assembly of the 28S small mitochondrial ribosomal subunit. Biochem J 2010; 430:551–8.
118. Yagi M, Uchiumi T, Takazaki S, Okuno B, Nomura M, Yoshida SI, Kanki T, Kang D. P32/gC1qR is indispensable for fetal development and mitochondrial translation: Importance of its RNA-binding ability. Nucleic Acids Res 2012; 40:9717–37.
119. Itahana K, Zhang Y. Mitochondrial p32 Is a Critical Mediator of ARF-Induced Apoptosis. Cancer Cell 2008; 13:542–53.
120. Puranam RS, Attardi G. The RNase P associated with HeLa cell mitochondria contains an essential RNA component identical in sequence to that of the nuclear RNase P. Mol Cell Biol 2001; 21:548–61.
121. Slomovic S, Schuster G. Stable PNPase RNAi silencing: its effect on the processing and adenylation of human mitochondrial RNA. RNA 2008; 14:310–23.
122. Von Ameln S, Wang G, Boulouiz R, Rutherford MA, Smith GM, Li Y, Pogoda HM, Nürnberg G, Stiller B, Volk AE, et al. A mutation in PNPT1, encoding mitochondrial-RNA-import protein PNPase, causes hereditary hearing loss. Am J Hum Genet 2012; 91:919–27.
123. Vedrenne V, Gowher A, De Lonlay P, Nitschke P, Serre V, Boddaert N, Altuzarra C, Mager-Heckel AM, Chretien F, Entelis N, et al. Mutation in PNPT1, which encodes a polyribonucleotide nucleotidyltransferase, impairs RNA import into mitochondria and causes respiratory-chain deficiency. Am J Hum Genet 2012; 91:912–8.
124. Sanchez MI, Mercer TR, Davies SM, Shearwood a M, Nygard KK, Richman TR, Mattick JS, Rackham O, Filipovska a. RNA processing in human mitochondria. Cell Cycle [Internet] 2011; 10:2904–16.
125. Joshi SA, Hersch GL, Baker TA, Sauer RT. Communication between ClpX and ClpP during substrate processing and degradation. Nat Struct Mol Biol 2004; 11:404–11.
126. Jourdain AA, Koppen M, Wydro M, Rodley CD, Lightowlers RN, Chrzanowska-Lightowlers ZM, Martinou JC. GRSF1 regulates RNA processing in mitochondrial RNA

granules. Cell Metab 2013; 17:399–410.
127. Larsson NG, Wang J, Wilhelmsson H, Oldfors a, Rustin P, Lewandoski M, Barsh GS, Clayton D a. 1998 Nature Publishing Group http://www.nature.com/naturegenetics. Nat Genet [Internet] 1998; 18:231–6.
128. Fischer F, Weil A, Hamann A, Osiewacz HD. Human CLPP reverts the longevity phenotype of a fungal ClpP deletion strain. Nat Commun [Internet] 2013; 4:1397.
129. Rattan SI. Principles and practice of hormetic treatment of aging and age-related diseases. Hum Exp Toxicol 2008; 27:151–4.
130. Taylor RW, Turnbull DM. Mitochondrial DNA Transcription: Regulating the Power Supply. Cell 2007; 130:211–3.
131. Almajan ER, Richter R, Paeger L, Martinelli P, Barth E, Decker T, Larsson N, Kloppenburg P, Langer T, Rugarli EI. AFG3L2 supports mitochondrial protein synthesis and Purkinje cell survival. J Clin Invest 2012; 122:4048–58.
132. Matthews DA, Russell WC. Adenovirus core protein V interacts with p32 - a protein which is associated with both the mitochondria and the nucleus. J Gen Virol 1998; 79:1677–85.
133. Jiang J, Zhang Y, Krainer AR, Xu RM. Crystal structure of human p32, a doughnut-shaped acidic mitochondrial matrix protein. Proc Natl Acad Sci U S A 1999; 96:3572–7.
134. Soltys BJ, Kang D, Gupta RS. Localization of P32 protein (gC1q-R) in mitochondria and at specific extramitochondrial locations in normal tissues. Histochem Cell Biol 2000; 114:245–55.
135. Van Leeuwen HC, O'Hare P. Retargeting of the mitochondrial protein p32/gC1Qr to a cytoplasmic compartment and the cell surface. J Cell Sci 2001; 114:2115–23.
136. Fogal V, Richardson AD, Karmali PP, Scheffler IE, Smith JW, Ruoslahti E. Mitochondrial p32 protein is a critical regulator of tumor metabolism via maintenance of oxidative phosphorylation. Mol Cell Biol 2010; 30:1303–18.
137. Sunayama J, Tsuruta F, Masuyama N, Gotoh Y. JNK antagonizes Akt-mediated survival signals by phosphorylating 14-3-3. J Cell Biol 2005; 170:295–304.
138. Storz P, Hausser A, Link G, Dedio J, Ghebrehiwet B, Pfizenmaier K, Johannes FJ. Protein kinase C ?? is regulated by the multifunctional chaperon protein p32. J Biol Chem 2000; 275:24601–7.
139. Kasashima K, Sumitani M, Endo H. Maintenance of mitochondrial genome distribution by mitochondrial AAA+ protein ClpX. Exp Cell Res 2012; 318:2335–43.

140. Feng J, Michalik S, Varming AN, Andersen JH, Albrecht D, Jelsbak L, Krieger S, Ohlsen K, Hecker M, Gerth U, et al. Trapping and proteomic identification of cellular substrates of the ClpP protease in staphylococcus aureus. J Proteome Res 2013; 12:547–58.
141. Flynn JM, Neher SB, Kim YI, Sauer RT, Baker TA. Proteomic discovery of cellular substrates of the ClpXP protease reveals five classes of ClpX-recognition signals. Mol Cell 2003; 11:671–83.
142. Metodi Dimitrov Metodiev, Henrik Spa°hr, Paola Loguercio Polosa, Caroline Meharg, Christian Becker, Janine Altmueller, Bianca Habermann, Nils-Go¨ran Larsson, Benedetta Ruzzenente. Required for Both Methylation of 12S rRNA and Coordination of Mitoribosomal Assembly. PLoS Genet. 2014;10(2):e1004110.
143. Austin CP1, Battey JF, Bradley A, Bucan M, Capecchi M, Collins FS, Dove WF, Duyk G, Dymecki S, Eppig JT, Grieder FB, Heintz N, Hicks G, Insel TR, Joyner A, Koller BH, Lloyd KC, Magnuson T, Moore MW, Nagy A, Pollock JD, Roses AD, Sands AT, Seed B, Skarnes WC, Snoddy J, Soriano P, Stewart DJ, Stewart F, Stillman B, Varmus H, Varticovski L, Verma IM, Vogt TF, von Melchner H, Witkowski J, Woychik RP, Wurst W, Yancopoulos GD, Young SG, Zambrowicz B. The knockout mouse project. Nat Genet. 2004;36(9):921-4.
144. Schnütgen F, Hansen J, De-Zolt S, Horn C, Lutz M, Floss T, Wurst W, Noppinger PR, von Melchner H. Enhanced gene trapping in mouse embryonic stem cells. Nucleic Acids Res. 2008; 36(20)
145. Shigeoka T, Kawaichi M, Ishida Y. Suppression of nonsense-mediated mRNA decay permits unbiased gene trapping in mouse embryonic stem cells. Nucleic Acids Res. 2005; 33(2):e20.
146. Vernochet C1, Mourier A, Bezy O, Macotela Y, Boucher J, Rardin MJ, An D, Lee KY, Ilkayeva OR, Zingaretti CM, Emanuelli B, Smyth G, Cinti S, Newgard CB, Gibson BW, Larsson NG, Kahn CR. Adipose-specific deletion of TFAM increases mitochondrial oxidation and protects mice against obesity and insulin resistance. Cell Metab. 2012; 16(6):765-76.
147. Kim KH, Jeong YT, Oh H, Kim SH, Cho JM, Kim YN, Kim SS, Kim do H, Hur KY, Kim HK, Ko T, Han J, Kim HL, Kim J, Back SH, Komatsu M, Chen H, Chan DC, Konishi M, Itoh N, Choi CS, Lee MS. Autophagy deficiency leads to protection from

obesity and insulin resistance by inducing Fgf21 as a mitokine. Nat Med. 2013;19(1):83-92.
148. Ahnn, J., March, P. E., Takiff, H. E. and Inouye, M. (1986) A GTP-binding protein of Escherichia coli has homology to yeast RAS proteins. Proc. Natl. Acad. Sci. U.S.A. 83, 8849–8853
149. Britton, R. A. (2009) Role of GTPases in bacterial ribosome assembly. Annu. Rev. Microbiol. 63, 155–176
150. Sharma, M. R., Koc, E. C., Datta, P. P., Booth, T. M., Spremulli, L. L. and Agrawal, R. K. (2003) Structure of the mammalian mitochondrial ribosome reveals an expanded functional role for its component proteins. Cell 115, 97–108
151. Tu, C., Zhou, X., Tropea, J. E., Austin, B. P., Waugh, D. S., Court, D. L. and Ji, X. (2009) Structure of ERA in complex with the 3_ end of 16S rRNA: implications for ribosome biogenesis. Proc. Natl. Acad. Sci. U.S.A. 106, 14843–14848

Acknowledgements

"You have to dream before your dreams can come true"

– Dr. A.P.J. Abdul Kalam

My PhD journey officially started from October 2010, but my dream of pursuing PhD began since my engineering days. It has been a long and wonderful journey with lot of valuable experiences and I want to take this opportunity to thank the important people of my life and career who have contributed in the journey of fulfilling my dream.

First of all, I would like to thank my boss, my mentor and my supervisor Prof. Aleksandra Trifunovic for her immense support throughout my PhD. I want to thank you Sandra for giving me the platform to fulfill my dream. I want to express my gratitude to you for having your faith in me and be with me irrespective of the situation. I thoroughly enjoyed all these years working with you and conduct my studies under your valuable guidance. I am very happy and honored that my dream is getting fulfilled having you as PhD supervisor.

I still remember Sandra when I contacted you for the very first time and you suggested me to apply through CECAD since you were looking for PhD students. Once I came to Cologne for the interview I knew this is the place where I wanted to be. I remember every moment of those interview days; coming to Cologne, meeting Melek, Doris, writing my exam, interviews, going to Mensa, meeting our CECAD seniors, getting the opportunity to talk to you during CECAD barbecue. Those were indeed some special moments. During the interview, I was tensed inside since you were not asking me questions in the beginning. I thought I might have lost the opportunity. Prof. Björn Schumacher and Prof. Carien Niessen were doing the rounds of questions and deep down I was wondering when you would ask me. This was the first time in my life when I badly wanted a Professor to ask me any question. I remember each and every question of yours and even my answers. I kept praying throughout my interview days to be able to get this opportunity. I am thankful to God that my prayers were answered in two days and I got selected even before leaving for Texas. I immediately said Yes! I think I gave the fastest confirmation to Doris.

Thank you Sandra for everything! It was truly a wonderful journey and I am blessed to have you as my boss. You are the best boss of my life Sandra and I know I will never find another boss like you. I will definitely miss you and working with you. I will also miss your delicious food especially during Christmas party!

I am grateful to you Sandra, for giving me the liberty to convey my ideas through all the scientific discussions. These sessions with you gave me lot of confidence and motivation where I could grow and develop my job skills and interpersonal skills. Thank you Sandra for giving me the freedom to express myself without any hesitation and for being a great listener. I am obliged to you for giving me CLPP along with opportunities to be involved in other projects. During this PhD phase I got the ample scope to learn and grow since you are open to any scientific ideas and experiments and never said NO to innumerable trials. I express my deepest gratitude for your patience and constant trust in me. I am indebted to you for accepting me the way I am and helping me to strengthen my key areas. I will be completing 5 years on 10th November 2015 in your group and I want to thank you Sandra for guiding me through the path of my scientific career. I am thankful to you for being so approachable and giving me the privilege of pouring my heart out without any inhibition. I am grateful to you for providing me this comfort that is very rare to have. Thank you Sandra for n number of times, for every single moment and opportunity, for your understanding, your patience, your trust, your valuable guidance, your enormous support, your kindness, for introducing me to this awesome field of Mitochondria. I am grateful to God and equally thankful to you for having you as my boss during an important phase of my life and career. Thank you Sandra for the priceless moments!

I want to express my deepest gratitude to my supervisor during my Master studies Prof. Michael San Francisco for nurturing the habit of independent thinking and working. His teachings and guidance have inspired me throughout my career and helped me to develop the skills of connecting dots together and see the bigger picture.

I want to thank Prof. Khris Mahanty (Khris Uncle) for guiding me throughout my academic career. Thank you Uncle for all your valuable suggestions, kind help and your blessings.

I want to acknowledge all the unconditional love, immense hard work and sacrifices done by my parents in order to give us the best in life. I am truly blessed to have such an amazing and supportive family. I want to pay my regards to the entire family: my mother Anima Maiti, my father Sanchindranath Maiti, my sister Payal Gore, my brother in law Syamal Kumar Gore and my awesome niece Subhangi Gore. Especially my mother, who is my pillar of strength, who never gave up in the journey of pursuing my dreams, who kept believing in me and stood beside me through my thick and thin. Thank you "Maa" for being with me, without you it was impossible for me to succeed. I know on 3rd July 2015 you will be the happiest and proudest Maa on earth since our dream will come true.

I am indebted to my Dearest Guruji, Sri Sri Ravi Shankar for guiding me through the spiritual path, for showing me the beauty and power of meditation and yoga, for helping me to experience freedom and the innermost experience of my being. Thank you Guruji for introducing me to the family of Art of Living Foundation. Thank you for being there with me and for always bringing me back to the right path. Thank you for bringing happiness and making my life a celebration!

The Almighty has truly blessed me for not only giving me a wonderful family but also filling my life with some great friends. My life would have been incomplete without all of them. My family in Cologne and for life: Sayantani Basu, Gaurav Ahuja, Tripti Mishra Ahuja and Oindrilla Mukherjee (Mukhujye). I don't know how would I have managed and survived without you. I will always be grateful to Cologne since it not only gave me a wonderful boss, an exciting project - CLPP but also such gem of friends. Thank you all for giving everything of yours to help me overcome the lowest point of my life and keeping me alive. Thank you for bringing me back to life and filling it with lot of love, happiness, dreams, strength, courage and a new direction. I wouldn't have made it for sure without all of you. Anything I would write here will fall short in comparison to the way you all have helped me in every aspect of my life and career, became my strength and the reason behind my smile. Thank you for your true love and friendship and being the most important part of my life.

My great friends who were/are always there for me throughout different phases of my life irrespective of time, distance and situation: Ritankar Majumdar, Pramod Singh, Amanjot

Riar, Sharanya Murali, Jhuma Sen and Lizette Siles: thank you guys for being there through out and becoming my extended family. Thank you for everything that we have shared so far and will continue to share much more.

I want to take this opportunity to specially thank Ritankar Majumdar for giving a direction to my life, for showing me the beauty of Biotechnology, for bringing the best out of me. I wouldn't have considered doing Science if I didn't meet you during my engineering days. Thank you Rito for not only teaching me Science but also showing me true friendship and love. I thank God every moment for sending you to me since it changed me along with my views and values towards life and relations.

I want to thank my wonderful Aachen gang: Sayantani Basu, Oindrilla Mukherjee, Mitrajit Ghosh, Paramita Das and Subrata Chattopadhyay for all the support, fun filled and crazy moments during these years. I thoroughly cherished each moment we spent including the trips around Europe, short weekend trips around Aachen, playing cards, watching movies, dumb charades session, singing, dancing, long walks within Aachen and most importantly having the mouth watering Desi and traditional Bengali food cooked mostly by Mukhujye and Mitrajit.

I want to acknowledge Manuela Rehnelt (Manu) for all her support, friendship and being a part of my life. She was the first person I spoke to in the University hostel and since then we have shared so many wonderful and absolutely crazy moments. Thank you Manu for this amazing friendship!

I want to thank Tran (Dr. H. T. Horning), Betty (Dr. Benedetta Ruzzenente), Claire (Dr. Claire Pujol), Roza (Dr. Rozina Kardakaris) and Maria Bust for helping me to walk through the tough times during my PhD especially during the last phase of PhD. I am obliged to you for your support, guidance and friendship. Thank you Tran and Betty for sharing your scientific knowledge with me, giving valuable inputs to my research and for teaching me two great experimental techniques. Thank you all for being in my life and keeping my faith that one can be a great friend in Science keeping personal scientific interests and gains aside. I wouldn't be able to see the end if I didn't get this immense support and motivation from all of you.

A big thank you to the entire CLPP team: Dr. Alexandra Kukat, Dr. Karolina Szczepanowska, Katharina Senft, Steffen Hermans, Dr. Anil Sukru Dogan and Dr. Claire Pujol for such a great team work. It was really a nice experience to be able to work with you. I want to thank our collaborators Dr. Benedetta Ruzzenente, Dr. H. T. Horning, Dr. Rolf Wibom (Karolinska Institute) and Prof. Leo Nijtmans (NCLMS) for being a part of the CLPP project.

I want to especially thank Dr. Alexandra Kukat for her supervision, guidance and teachings, for helping me with a smooth transition from Microbiology to Mitochondrial Genetics. Thank you Alex for sharing your knowledge and experience with me. I am obliged to you for helping me to settle down in a new country and working environment, for all your understanding, support, generosity and kindness. I want to thank you for all the wonderful moments we shared.

My other lab mates Dr. Marija Herholz, Victor Pavlenko, Estela Cepeda, Christina Becker, Dominic Seiferling, Marijana Aradjanski, Linda Bauman and Eduard Hofsetz: thank you for all your kind support especially for providing me your endless help with all the official documents in German!

I would like to thank my wonderful CECAD batch mates especially Hui-Ling Ou (Joan) for her friendship. I am grateful to Dr. Doris Birker for selecting me over many other candidates and giving me the wonderful opportunity to come to Cologne and be part of Sandra's team. Thank you Doris for providing me your extended help all these years.

I would like to thank Prof. Thomas Langer, Prof. Peter Kloppenburg, Prof. Nils-Göran Larsson, Prof. Elena Rugarli, Prof. Rudolf J. Weisner, Prof. Jens Brüning, Dr. Tina Wenz and their amazing group members for great help, valuable inputs, discussions and friendship throughout my PhD.

"All our dreams come true, if we have the courage to pursue them"

- Walt Disney

I know it is just the beginning ……

"Miles to go before I sleep" – Robert Frost

Erklärung

Ich versichere, dass ich die von mir vorgelegte Dissertation selbständig angefertigt, die benutzten Quellen und Hilfsmittel vollständig angegeben und die Stellen der Arbeit - einschließlich Tabellen, Karten und Abbildungen -, die anderen Werken im Wortlaut oder dem Sinn nach entnommen sind, in jedem Einzelfall als Entlehnung kenntlich gemacht habe; dass diese Dissertation noch keiner anderen Fakultät oder Universität zur Prüfung vorgelegen hat; dass sie - abgesehen von unten angegebenen Teilpublikationen - noch nicht veröffentlicht worden ist sowie, dass ich eine solche Veröffentlichung vor Abschluss des Promotionsverfahrens nicht vornehmen werde.

Die Bestimmungen der Promotionsordnung sind mir bekannt. Die von mir vorgelegte Dissertation ist von Prof. Aleksandra Trifunovic betreut worden.

Köln, den 08.05.2015

_____

(Priyanka Maiti)